A Port Hamiltonian model of the human outer, middle and inner ear, and its application

Milka C. I. Madahana

A dissertation submitted to the Faculty of Engineering and the Built Environment, University of the Witwatersrand, Johannesburg, in fulfilment of the requirements for the degree of Master of Science in Engineering.

Johannesburg, September 2019

Declaration

I declare that this dissertation is my own, unaided work, except where otherwise acknowledged. It is being submitted for the degree of Master of Science in Engineering to the University of the Witwatersrand, Johannesburg. It has not been submitted before for any degree or examination to any other university.

Signed this ____ day of ______________ 20___

____

Milka C. I. Madahana

Abstract

The objective of this research was to develop an integrated Port Hamiltonian model of the human outer, middle and inner ear. The developed Port Hamiltonian model of the human ear is based on the Dirac structure. The outer, middle and inner ear are developed in segments, tested and validated prior to the system being coupled. The outer, middle and inner ear are validated against existing literature and the results are found to be comparable. The application of the developed Port Hamiltonian model is illustrated using a developed feedback based noise policy management model for mine workers. This feedback based measurement system can be used to monitor mine workers in the mines hence provide the mine administrators with the current state of hearing of the individual worker. The information obtained from the system may be used by the administration to provide an early intervention and as a result the mine workers are protected from experiencing significant hearing threshold shifts. A control engineering approach is then used to formulate the mining noise occupational policies as a control law. Both social and measurements aspects of this system are explored. The International Standard Organization guide ISO:1999 is used to generate data and develop a basic feedback model. The basic feedback model is further refined into a dynamic model which includes a Port Hamiltonian integrated ear model and the mining policies. The feedback based noise policy management model is validated using real data from the mine documented in open source literature. The models are implemented using MATLAB as a modelling platform and the results are generated using the Simulink model. This research work has been given an ethical clearance certificate by the Human Research Ethics Committee (Medical), therefore, allowing for the findings of the investigations to be published. In conclusion,to be developed is an integrated Port Hamiltonian model of the Human outer, middle and inner ear to be used for estimation of Noise induced hearing loss. The use of this model is then illustrated using a feedback based noise policy monitoring system for mine workers.

To my father and mother, John and Pauline.

Acknowledgements

I would like to thank my supervisor Dr Otis Nyandoro for the guidance, support, advise and extraordinary patience throughout the research period. I would also like to thank Prof Brian Wigdorowitz and Prof Anton Van Wyk for their valuable guidance, input and support. John Ekoru and Tinashe Chigodzha for their support and always being there to assist me. I would like to thank my family and friends, for their love, support and understanding. To God Almighty, I am grateful for the provision, strength, sanity and the finishing grace.

Contents

List of Figures

List of Tables

Nomenclature

NIOSH National Institute for Occupational Safety and Health

ONIHL Occupational Noise Induced Hearing Loss

HCP Hearing Conservation Programme

DMR Department Of Minerals and Energy

MHSC The Mine Health and Safety Council

STS Standard Threshold Shift

NDP Net Domestic Product

PPE Personal Protective Equipment

IHC Inner Hair Cells

OHC Outer Hair Cells

TTS Temporal Threshold Shift

PTS Permanent Threshold Shift

GDHL Gradually Developing Hearing Loss

S.V Scala Vestibula

S.T Scala Tympani

N.S Navier Stokes

C.P Cochlear Partition

SPL Sound Pressure Level

PID Proportional Integral Derivative

LQR Linear Quadratic Regulator

THS Threshold Shift

ME Mining Engineer

Chapter 1

Introduction

Occupational Noise Induced Hearing Loss (ONIHL) is a permanent hearing impairment that progresses gradually for an extended period of time (several years) as a consequence of predisposition to high levels of incessant or interment noise [1]. Irrespective of the Hearing Conservation Programmes (HCP), ONIHL has continued to upsurge over the years in the South African mines. The average exposure in South African mines is observed to be between $63.9dBA$ and $113dBA$ with roughly 73.2% of the mine workers in the industry being subjected to noise intensity levels above the legislated occupational exposure limit of $85dBA$ [2]. 1820 cases of ONIHL were reported in 2007 by the department of mineral resources in South Africa [3]. The same report [3] which is released annually shows an increase in the number of reported cases of ONIHL from 2007 to 2019. The National Institute for Occupational Safety and Health (NIOSH) reported that roughly 50% of mine workers will have hearing loss when they are 50 years old, and 70% will have hearing loss by the age of 60 [4]. ONIHL significantly reduces the quality of an individuals life. Individuals with ONIHL characteristically suffer from communication interference, dejection, anxiety, humiliation, friction in relationships and shame. Hearing loss has a ripple effect of not only affecting the miner but their families and the entire community [5]. The characteristic of ONIHL are; firstly, the hearing loss increases with increase in noise intensity and also the period of exposure. Secondly, individual susceptibility to ONIHL varies greatly but the variation is not well understood. Some of the factors that have been implicated in the variations are: age, cigarette smoking, use of ototoxic medication, type 2 diabetes and previous sensorineural hearing loss [6].

1.1 Background

1.1.1 Noise and its effects on human health

Noise may be defined as undesirable sound lacking musical quality. The source from which noise is generated may be used to classify noise as:

- Intermitent
- Impact or impulsive noise
- Repetive impact noise
- Continous narrow band noise
- Continous wide band noise

  The listed classifications of noise are emitted in the mines at varying frequencies and intensities. Exposure to occupational noise may cause hearing impairment, ONIHL tinnitus, disturbance in speech communication and increased risks of accidents. ONIHL is one of the most prevalent occupational diseases caused by extended exposure to loud noise [7]. A direct correlation exists between the capacity of a machine and the amount of noise it produces. Large machines with greater capacity produce more noise[8].

1.1.2 Noise policies in the mine

The South African mines have rules and regulation for occupational noise in the mines, summed up into policies that assist administrators in decision making. The Department of Minerals and Energy (DMR) has well documented compilation of a mandatory code of practice for occupational health programme for noise. The main aim of the guideline is to enable the mine employers to include all the guidelines in their implementation of policies hence ensuring zero harm to the mines. The Mine Healthy and Safety Council (MHSC), 2014 occupational and health safety summit milestones states that by December 2024, the total operational or process noise emitted by any equipment must not exceed a sound pressure level of 107 dB and by December 2016, no employee's Standard Threshold shift (STS) should exceed 25 dB from the baseline when averaged at 2000, 3000 and 4000 HZ in one or both ears. These rules and regulations have been incorporated into the Hearing

Conservation programmes (HCP) in the mines. However, literature still shows that the implementation of the programmes have not been effective [5].

1.1.3 Stakeholders in the mines

The mine stakeholders are: the government, political parties, business and investors, non governmental organizations, opinion makers, organized labour, communities and the media [9]. All the stakeholders play a role in policy formulation, implementation and monitoring. The government creates a politically stable environment and business-friendly policies and legislations that ensure the country experiences economic growth. The main objective of the government is to meet its target for Net Domestic Product (NDP) using the mining industry as one of the target areas. The Chamber of Mines acts as an intermediary body between the government and the mines. Currently, the chamber of mines is negotiating with the Department of Mineral Resources (DMR) on reviewing the charter that was established in 2004 to 2014 and set up new targets.

Political parties represented in parliament are one of the main stakeholders. They are mainly concerned with the socio-economic health of the mine workers, the future plans of the mining industry in South Africa, strategies and policies that would affect the well-being of the workers. The political parties play various roles in the mining industry: for instance they hold the government, chamber and unions accountable to providing updates on progress made with regards to occupational health issues and compensation. The business investors main goal is to make profits from the mines. The structure and policies presented in the charter have to ensure that they make profits from their investment. Non governmental organization and opinion makers ensure that there is a compliance and implementation of policies discussed in the mining charter. The organized labour are concerned with job preservation as well as having a safe and sustainable mining industry. Communities around the mines are stake holders whose main interest is creation of jobs for community members, community development by the mining company, compensation for injuries/deaths and the legacy issues [10].

1.1.4 Hearing Loss myths among mine workers

Hearing myths among the mine workers affect current policy implementation and reduction of ONIHL. Witt, [11], documents hearing myths among workers with regards to wearing of the hearing protection. Similar beliefs are also held by the mining workers in the South African mines. For instance it is believed that ear plugs are a source of ear infection. There is no research that substantiates this claim. It is also believed that the eardrum can be hurt if the ear protection is pushed too far. Liberman et al, [12], states that the eardrum canal is approximately 35 millimetres long ending at the eardrum. Ear protection designers pay attention to the anatomy of the ear and therefore, their designs meet the required specifications of being shorter than the length of the ear canal. The soft cartilage structure at the opening of the ear canal transforms into a bony structure when any solid object moves to close proximity of the ear drum. The miners also claim that they cannot hear their co-workers, machine noise or alarms when wearing ear plugs. [11] This then affects their job performance since communication will be in jeopardy. Manufacturers have since responded by designing better ear plugs. Attenuation of frequencies across all frequencies, including use of amplification circuits and electronic suppression of background noise are some of the techniques currently being employed. Miners also claim that they need to prove their strength by claiming, that the deafer you are, the more you have worked at the mines and therefore deserve respect. This myth encourages the younger miners to avoid ear protection so as to increase their level of respect over time.

1.1.5 Problem contextualization

As a result of the sophisticated and efficient equipment currently being designed, the mining industry has experienced evolution and tremendous increase in production. In addition to that, there is depletion in minerals at the reserves that are shallow in the South African mines, therefore reefs that are at a much deeper level are being exploited. This has resulted in an increase in noise level coming from the rocks and the machinery. Deep mines can become very warm hence making it very uncomfortable for the mine workers to wear protection devices for longer work shifts. Both the ageing and the new work force needs to be protected to ensure that there is no further hearing loss and that communication among mine workers during work is not compromised. South African mines have Hearing Conservation Programs (HCP). However, these have not been successful due to the following:

- Fragmented and poorly implemented HCP [5].
- Longer intervals between the testing periods (Annual or Biannual testing period for workers).

- Longer waiting periods before change in policies (Currently they are changed after 10 years).
- Focusing on hearing protection than noise monitoring.
- Lack of sufficient legislation and insufficient universal standards [5].
- Lack of knowledge by health and safety practitioners on impact and effects of noise and risk perception [5].
- Reliance on the use of Personal Protective Equipment (PPE) as a trusted mode of protection against occupational noise induced hearing loss. PPE should only be employed in cases where engineering controls have failed [13].
- Lack of efficient noise monitoring and administrative system.

In order for noise induced hearing loss to be dealt with at an early stage, there is a need for development of integrated models of the human outer, middle and inner ear. These models can then be used in estimation of noise induced hearing loss under a real work environment.

1.1.6 Models for estimation of noise induced hearing loss

There are several models that are used to model the human ear. This section summaries current ear models in the literature. For references purposes a summary of the models is provided. Further details are given in chapter two of this dissertation. These models may be probabilistic [14] or time based [15]. The probabilistic models usually demonstrate how fatigue occurs to the inner and outer hair cells while the time based models demonstrate damage to the cochlear as a result of exposure to occupational noise. One of the demerits of the probabilistic model is that they are empirically derived hence excluding the actual human ear [15]. Dynamic ear models include electrical circuit models whose parameters are not closely linked to the anatomical data and are independent of the behaviour being modelled. Lumped and distributed parameter models are easier to compute than finite element models, however, their derivations rely on assumptions made, this makes it difficult to model the complexities of realistic geometries. The finite element models provide insight into vibration shapes, stress distribution and dynamic behaviour and are suited for models that are detailed and require accuracy[16], however, the simulations for the finite element model take a very long time and its not always easy to find a suitable mesh [17].

1.2 Research question

From the problem contextualization and research literature, two main questions arise:

- Can an integrated Port Hamiltonian model of the human outer, middle and inner ear be developed and used to estimate noise induced hearing loss?
- Can this developed Port Hamiltonian model be used to estimate noise induced hearing loss in a feedback system and hence provide a noise policy management system?

1.3 Research contribution

The main contribution to knowledge in this research is:

- Development of a comprehensive integrated Port Hamiltonian model of the human outer, middle and inner ear that may be used for estimation and assessment of noise induced hearing loss.
- Unique application of this Port Hamiltonian model to a noise policy management feedback model.

  The significance of the developed Port Hamiltonian model is that it may be used for monitoring and providing early intervention for Noise Induced Hearing Loss for the South African mines.

1.4 Scope and Limitations

This study is limited by the following conditions:

1. The developed Port Hamiltonian Model of the Human outer, middle and inner ear is for humans only.
2. The auditory system of human beings extends from the pinna to the auditory nerve. Since cochlea degeneration with outer hair cells can still provide reasonable results to indicate ONIHL, the inner hair cells and the auditory nerve are excluded.

3. Measurement of the ear dimensions of the auditory system would involve surgery on a living subject which would be invasive. Parameters for validation of the models are therefore obtained from existing literature.

1.5 Methodology

An overview of the methodology to be followed is presented, a detailed methodology is presented in chapter 3 of this research work. In order to estimate ONIHL, it is

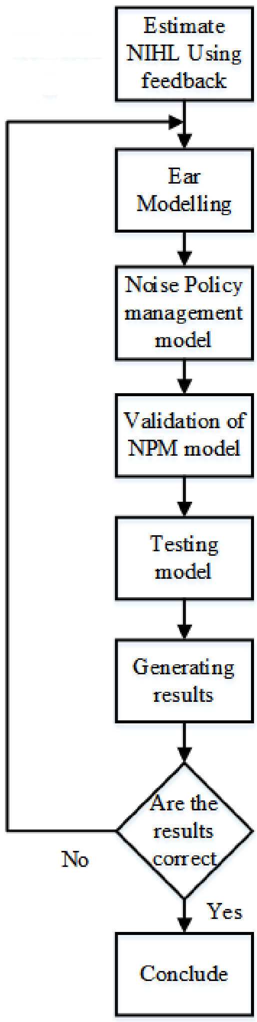

Figure 1.1: Methodology for the design of the feedback based model

essential that an integrated model of the human outer, middle and inner ear has to be developed. To test the usefulness of this model, a unique mining context is used, The methodology provided shows the significance of developing the model and hence answering of the key research question in section 1.2.

1.6 Published work

Aspects of this dissertation have been published or submitted in the following references:

- Madahana M. C. I .,Ekoru, J. E. D. and Nyandoro, O. T. C. , Smart noise policy monitoring and feedback control system for mining application, IFAC - Journal Papers online ”Accepted”
- Madahana M. C. I.,Ekoru, J. E. D., Mashinini and Nyandoro, O. T. C. , Noise level policy advising system, IFAC - Papers online 2019
- Madahana M. C. I.,Ekoru, J. E. D., Mashinini and Nyandoro, O. T. C. , Mine worker Threshold shift estimation via optimization algorithms for deep current neural networks, IFAC - Papers Journal online 2019
- Madahana M. C. I., Nyandoro, O. T. C. and Ekoru, J. E. D., Sliding mode controller for a feedback accelerometer with a distributed Mass, IFAC- Journal PapersOnLine, vol. 50, No 2, pp 295 - 300,2017
- Moroe F M,Shangase K K, Madahana M C I, Nyandoro O T C ,A feedback-based noise monitoring model: A proposed model of managing occupational noise induced hearing loss in the mining sector in South Africa” Journal of the Southern African Institute of Mining and Metallurgy, January 2018.
- Madahana M. C. I .,Ekoru, J. E. D. and Nyandoro, O. T. C. , A port Hamiltonian Model of the Outer and Middle ear for assesment of middle ear bone conduction diseases , IFAC - Journal Papers online ”Under review”
- Madahana M. C. I .,Ekoru, J. E. D. and Nyandoro, O. T. C. , Integrated Port Hamiltonian model of the human outer, middle and inner ear for hearing loss assesment, IFAC - Journal Papers online ”Under review”
- Madahana M. C. I .,Ekoru, J. E. D. and Nyandoro, O. T. C. , Development of a feedback based prototype for noise level policy monitoring, IFAC - Journal Papers online ”Under review”
- Ngwako T, Madahana M. C. I.and Nyandoro, O. T. C. , Modeling and control of an autonomous Linear DC Machine based Mine Locomotive, IFAC - Journal Papers online ”Accepted”

- Ngwako T, Madahana M. C. I.and Nyandoro, O. T. C. ,A condition for a singular Optimal control Formulation for a tandem Pair of Gravity Fed Linear DC Machine Powered Mine Locomotives, IFAC - Journal Papers online ”Accepted”

1.7 Dissertation structure and reading guide

This dissertation is structured as follows:

An extensive theoretical background of the work done is provided in the literature review in chapter 2. In this chapter, the acoustics of hearing which includes the human ear anatomy and the role of the outer, middle and inner ear with respect to sound transmission is discussed. Ear models for instance; probabilistic, electrical, finite element, lumped, distributed and energy based models (Lagrangian and Port Hamiltonian) are also presented in this chapter.

A detailed methodology showing the development of the overall system and subsystems is provided in chapter 3. Through this chapter, the steps followed to answer the research question and sub questions are presented. Data collection and ethical issues that could arise from this research are also discussed.

The dynamic model of the ear is presented in chapter 4. This chapter includes the mathematical preliminaries followed by a comprehensive modelling of the outer, middle and inner ear using the Port Hamiltonian approach. The validation, results and analysis of the results are also provided in this chapter.

A Noise policy management model is proposed in chapter 5. The modified ISO:1999 together with the developed dynamic ear model is used in the development of a feedback model. The results of the model and the analysis are also presented.

The recommendations and conclusion are summarised in chapter 6 of this research dissertation.

1.8 Conclusion

Ability to hear drastically influences the quality of life for a human being. Numerous researchers all over the world have developed models to asses different pathological conditions that can affect one’s ability to hear. Most of these models are segmented and only address pathological conditions found in a certain section of the ear. There is still a lot that has to be done in order to easily and accurately detect this condition. The work that is presented in this dissertation is focused on the development of an integrated Port Hamiltonian model of the outer, middle and inner ear to be applied particularly in the assessment of hearing loss.

Chapter 2

Literature review

2.1 Chapter overview

The purpose of this chapter is to provide an extensive summary of the ear anatomy, the mechanism of hearing and human ear modelling techniques. The literature will also serve as motivation for the research area that this work is based on. Some of the points raised in this chapter are presented in detail in the subsequent chapters.

2.2 The acoustics of hearing

2.2.1 Summary of the human hearing mechanism

The human auditory system consists of the outer, middle, inner ear and the acoustic nerve. Sound energy is gathered by the outer ear and transferred to the middle ear via the concha also known as the ear canal to the middle ear. The incoming sound energy causes the ear drum to vibrate, these vibrations are then transferred to the inner ear via the ossicles. The inner ear is composed of two parts, The cochlea and the vestibule system which is an organ of balance [19]. The snail shaped cochlea comprises of thousands of hair cells named Inner Hair Cells (IHC) and Outer Hair Cells (OHC). One of the roles of the OHC is to aid in sound vibration amplification from the middle ear while the IHC converts these vibrations into electrical signals which are then sent to the brain via the auditory nerve. Translation of the signals in the brain makes them distinguishable and comprehensible to the human. Damages may occur to the organ of corti through various ways like aging, loud noise, ototoxic

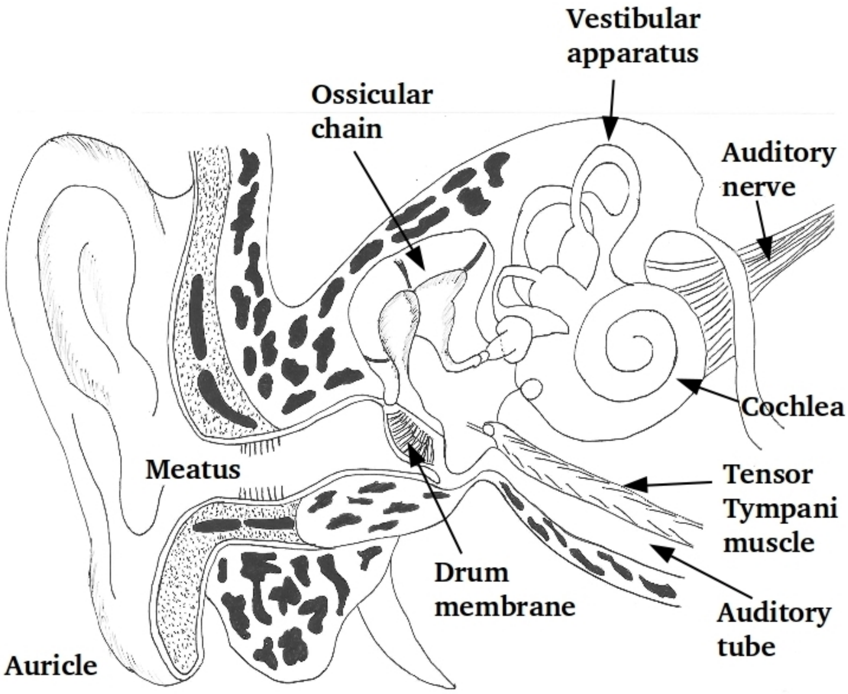

Figure 2.1: Human ear anatomy [18].

chemicals and medication. Damage to the hair cells (Both OHC and IHC) caused by exposure to loud noise results in irreversible hearing loss known as sensorineural hearing loss [20].

2.2.2 Sound and hearing

Sound is an auditory brain sensation caused by disturbance in a medium[21]. Hearing occurs when the ear transforms sound vibrations into nerve impulses and they are interpreted as sound by the brain. The auditory system has the ability to distinguish different aspects of a sound for instance pitch and loudness. Pitch is the biased view of frequency measured in cycles per second with the unit of Hertz. The normal audible range of frequencies is 20 Hertz to 20 Kilohertz with sensitive frequencies occurring between 1000 to 4000 Hertz. The perception of sound intensity is referred to as loudness and it is measured in decibels. With respect to the ear, it is referred to as the pressure produced by sound on the tympanic membrane. The human hearing range on the decibel scale ranges from 0dB to 130 dB.

2.2.3 The outer ear

The outer ear is made up of the pinna also referred to as the auricle and the ear canal. The outer ear is made of cartilage and acts as a sound reflector. Sound waves below 1 KHz are not affected by the pinna. However, the effect of the pinna becomes significant at those speech frequencies which occur between 2 - 3 KHz[22]. At the speech frequencies, the sound pressure is boosted significantly. The pinna has a behaviour similar to the reflecting dish and directs sound towards the ear canal. Both the reflected signal and direct signal enter the ear canal in phase. There is a slight delay in the entry of the reflected wave at higher frequencies resulting in destructive interference. When the entire path length is a half wavelength then the greatest interference occurs. Effects of boosting are noticeable above 1 KHz since the size of the pinna becomes significant when the wavelength approaches four times the size of the pinna. The outer ear influences the spectral shaping of sound. Every human being has a unique ear pinna and canal, which implies the sound pressure at each individual's ear drum varies in the way it is distributed in the frequency domain. Sound spectral and shaping to the ear is therefore affected by the whole outer ear.

The ear canal extends from the concha (the bowl) to the ear drum. It has a behaviour similar to a quarter-wave resonator and hence amplifies the resonance frequencies. The ear canal's length determines the resonance frequencies position. The average size of a human canal is 26 mm in length and 7 mm in diameter. The ear canal connects or terminates at the ear drum. The Pinna's size and shape together with the curvature of the ear canal have an effect on the pressure frequency response at the tympanic membrane [23].

2.2.4 The ear drum

The ear drum is known as the tympanic membrane, tympanum or myrinx. It transmits incoming sound from the ear canal to the ossicles. The malleus bone is between the tympanic membrane. The ear drum is concave shaped and terminates the ear canal at approximately a 40 degree slanted angle. The ear drum is a thin robust layer consisting of the outer cutaneous layer, fibrous layer (lamina propria) and the inner layer (Serous membrane). Rupture of the ear drum may result in conductive hearing loss [24].

Transmission of sound at high pressure level to the ossicles can be influenced by the middle ear muscles, the tensor tympani and the stapedius. The tympanic membrane tenses when the malleus pulls inward due to the tensor tympani contractions. The intensity of sound reaching the cochlea is reduced by the footplate of the oval window pulling outward due to the contractions of the stapedius. For high intensity sounds applied to the left or the right ear, the stapidius responds reflexly with fast contractions. The effect is observed from 90 to 95 dB for a sinusoidal input [24].

2.2.5 Middle ear

The middle ear is constrained by the tympanic membrane and the oval window of the cochlea. It consists of three small bones, namely; the malleus, the incus and the stapes. The role of these bones is to couple the vibrations of the tympanic membrane into waves of the inner ear fluid membrane. The cavity in the middle ear is filled with air and it is also known as Cavum tympani or tympanic cavity. The stapes is attached to the ear drum and to the incus while the stapes is connected to the inner ear. The tympanic membrane experiences a small pressure by a sound wave. This pressure is boosted by a factor of thirty by the three bones prior to being passed on to the oval window. This boost is brought about by the difference in the area of the ear drum, oval window and the level action of the ossciles [25].

When the ear drum vibrates, it sets the malleus into vibration which inturn vibrates in sync with the sound. The vibrations are then transferred to the incus. The stapes together with the plate at its tip that lies on the oval window also begin to vibrate. This vibration initiates pressure waves in the cochlear fluid [25].

2.2.6 Inner ear

The inner ear is made up of a cochlea which has approximately 8000 hair cells with ostereocilia. When elongated, the cochlea is 30mm long with 0.2 ml cochlea fluid. The fluid's motion in the cochlea is converted to electrical energy. The cochlea has three parallel canals namely: scala vestibuli, tympani and media. The scala vestibuli is seperated from the cochlear duct by the vestibular (Reissner's membrane). The basilar membrane separates the cochlear duct from the scala tympani. Corti is found in the cochlear duct on the basilar membrane while the tectorial membrane is attached to the roof of organ of corti. The mechanical sound vibrations in the organ of corti are converted into nerve impulses by the hair cells. For a given tonal stimuli, the outer cells respond by contracting rhythmically. The mechanical resonance and the location of an outer hair cell on the basilar membrane determines its response. Inner hair cells have approximately the same length. Enhanced and modified mechano-electrical discriminatory responses of the inner hair cells are due to the outer hair cells. The total number of outer hair cells is approximately 12,000 and inner hair cells is 3500 [26].

The inner ear functioning is observed when the stapes vibrate and send waves of fluids into scala vestibuli. The waves move through to the apex of the cochlea to the scala tympani and eventually to the round window. The waves are then transmitted through the vestibular membrane to the scala media where travelling waves are generated along the basilar membrane. There is a variation in width, tension and frequency response of the basilar membrane from base to apex. High frequencies affect the oval window while low frequencies resonate with the Helicotrema. The hair cell receptors are stimulated by the displacement of the basilar membrane. The ion channels are opened due to the bending of the stereocilia as they vibrate. A potential is generated within the hair cell. When the hair cells are activated, a neuro transmitter to synaptic is released. The generated neural spike propagates to the auditory cortex causing any individual to interpret and recognize sound [27].

2.2.7 Types of hearing losses

There are three types of hearing losses namely sensorineural (auditory and sensory) conductive and mixed hearing losses. The outer and the middle ear are typically affected by conductive hearing losses. Surgical techniques or medication can correct this type of hearing loss [28]. Sensorineural hearing loss has an effect on the inner ear (sensory) that links the inner ear to the source of the nerve in the brain. Conductive and sensorineural hearing loss may happen simultaneously thus affecting the outer, middle and inner ear. Such a loss is called mixed hearing loss [10].

2.2.8 Hearing loss mechanism

Intensity and the period of exposure to loud noise determines whether Temporal Threshold Shift (TTS) or Permanent Threshold Shift (PTS) which is irreversible will occur. Over time, continuous exposure to immoderate noise may result in damaged transmission of sounds to the brain for low and high frequencies. An increase in intensity and duration of exposure of noise results in irreversible damage of the sensory organ. When the blood flow into the cochlear ceases or decreases, the hair cells are affected and end up fusing into a massive cilia or disappearing. Noise therefore acts as an agent in accelerating disintegration of the supporting structure for the hair cells [12].

In this research, the hearing loss is based on a group of people working under similar mining conditions. This implies that they are exposed to the same noise intensity and at the same frequency. Their ethnicity, social economic background and previous exposure to ONIHL is not considered.

2.2.9 Audiometric characteristics of ONIHL

Occupational noise exposure affects the inner hair cells associated with discrimination of speech and perception of frequencies. A sharp depression (V shape or a notch) shows at high frequencies (3 kHz and 6 kHz). On the other hand, lower frequencies (0.5 kHz to 2 kHz) remains normal. With an increase in hearing loss at higher frequency, there is also a deterioration of hearing loss at lower frequencies. It takes a longer time for the lower frequencies to be affected; however, there is a gradual flattening out after long period of exposure [29].

2.3 Modelling the ear

Ear models of ONIHL can either be probabilistic, demonstrating how fatigue occurs to the inner and outer hair cells resulting in their ultimate damage, or they may be time based models showing the damage of the cochlear as a result of exposure to occupational noise. In this literature review, a summary of both models is given. However, the research will focus in dealing with cohorts of mine workers exposed to the same noise intensity and at the same frequency. Individual ears will not be considered, but it is imperative to understand how the loss occurs in one person before grouping all the individuals.

2.3.1 Probabilistic models

Equal Velocity Level (EVL) and Complex Velocity Level (CVL)

To discuss Noise Induced Hearing Loss ONIHL model from a probabilistic view point, ONIHL can be subdivided into acoustic trauma and Gradually Developing Hearing Loss (GDHL). Acoustic trauma happens quickly resulting in an immediate and permanent hearing loss. GDHL hearing loss develops over time and can be caused by occupational noise exposure. Various regulations and standards have been developed over years for example; ISO 1999:2013, CHABA, MIL STD -1474D, NOISH98, ANSI - S3.44 - 1996. These standards are either derived empirically or using waveforms. These noise metrics estimate acoustic energy and also characterize the noise exposure. However, they are limited in their ability to give physical insight into the processes that result in ONIHL [30]. Price [14] developed a highly accurate model suitable for investigating mechanical damage caused by impulse noise in human beings. This model however, is unable to estimate GDHL produced by occupational noise. Song [31] applied an analog based model to predict ONIHL in the human auditory system. There was lack of consistency of the results produced with Chinchilla data. Numerous functional and analog models for the auditory system have been produced [14]. In functional auditory models, three families of auditory filters have been developed so far, namely: the rounded exponential, the gammatone and the filter cascades [14]. The Basilar Membrane (BM) repeatedly flexes under noise exposure therefore it is assumed that ONIHL is caused by auditory fatigue. The intensity, frequency, duration, recovery interval of the noise and auditory systems own fatigue frequency influence auditory fatigue [14].

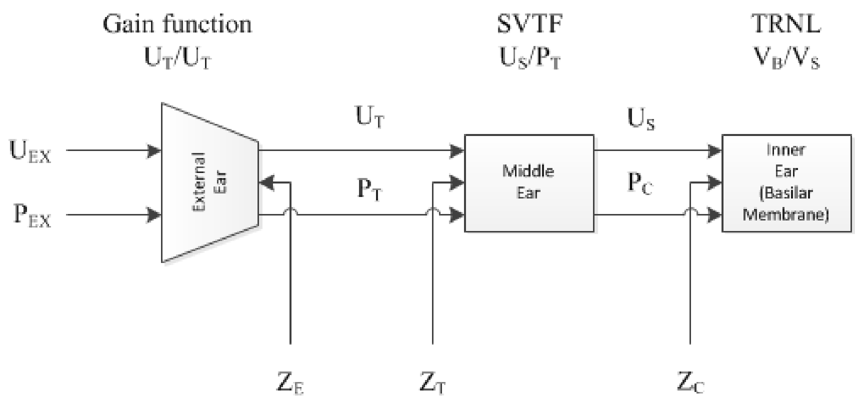

Figure 2.2: Modelling the auditory system [14].

The external and middle ear collect sound energy and transmit it into the inner ear. The middle ear behaves like an impedance matching device by transmitting cochlea, acoustic power from the stimulus [14].

2.3.2 Dynamic ear models

Electrical circuits model

This model is usually designed as mechano-acoustical circuits. Three types of idealized circuit elements namely point mass, ideal spring and damper are used to represent the behaviour of the anatomical structure [32]. This model may also be categorized under the lumped parameter model which has a merit of being able to replicate specified experimental data [32]. However, this model's parameters are not closely linked to the physiological or anatomical data independently of the behaviour being modelled [32].

Lumped and distributed (non lumped parameter) models

The non-lumped parameter models are made up of a plane distributed representation of the ear drum coupled to the middle ear's linear lumped model. Other non-lumped parameter models consist of a representation of the ear mechanics using an asymptotic method for a formulation of an approximation of analytical models [33]. The merit of this modelling approach is that it leads to models that are easier to compute than finite element models. However, their whole derivations rely on each assumption made and estimations done in the course of the analysis hence making it difficult to model the complexities of realistic geometries [32].

Finite element model

Finite element models divides the structure under investigation into elements with finite size, allowing for detailed examination of mechanical performance of complex structures. The elements may have mixed shapes and forms such as triangles and beams. Mesh generation is a terminology used when dividing a region into elements. After the structure of interest is divided into simple elements, the mechanical behaviour of each element is then analysed and its response to specific applied loads is expressed in terms of the displacement of its edges. The mechanical response of each element is analysed based on the Ritz-Rayleigh procedure [32]. The finite element model is used in modelling complex biological systems with elaborate geometry ultra-structural behavior with non-homogeneous, anisotropic materials. This modelling technique can also provide insight into vibration shapes, stress distributions and dynamic behavior at any point in a system which is not possible with analytical solutions. This method is hence suitable for modelling detailed and accurate human auditory system. It is typically used to investigate sound transmission, conduct ear assessment or assist in disease diagnostic and treatments of hearing losses [16].

2.3.3 Outer, middle and inner ear dynamic models

Outer ear model

Research has been carried out over several decades to investigate the overall effect of sound transmission to the tympanic membrane through the ear canal. When investigated at low frequencies, the ear canal exhibits the behaviour of a simple rigid wall which can be represented in circuits by a single capacitor [15], [34]. At high frequency, the ear canals length becomes comparable to the wavelength as standing waves patterns form. The ear canal may also be modelled as a combination of a single mass-spring system [35]. Analytically, the ear canal can be modelled as a homogeneous transmission line [36]. The non-homogeneous effect of the transverse canal can be modelled using a one dimensional modified horn equation [37]. Hiipakka et al [38] models reports that an ear canal may also be modelled as a lossless acoustic transmission line with a sound source whose pressure is external with internal acoustic impedance. Giguare [39]models the auditory canal as approximately cylindrical resonator and for frequencies up to the normal mode as it is assumed that the concha is a uniform transmission line. This model, however does not put into consideration the variation of the radius of the auditory canal along its length [17].

Middle ear

Feng et al [40] presents a middle ear simulator used mainly to provide quantitative information to be used in the physical model construction (mainly middle ear) for sound transmission. This model was developed to address the short coming of most physical middle ear models documented in literature that are short of robust theoretical basis and correlations with the geometry of the real ear. Daniel et al [32], developed a three dimensional finite element model of the human ear drum and middle ear. The phase-shift Moire shape measurements was used to precisely define the shape of the ear drum. The geometry of the middle ear was from histological serial sections and high resolution human ear magnetic resonance microscopy. This model allows for a better comprehension of the human middle ear mechanics. It may also be used in design of ossicular protheses and can simulate different pathological conditions [41].

Inner ear model

There have been several model developments of the cochlea to aid in investigating the aspects of the hearing functions that are complex to study in vivo because of the cochlea's inaccessibility. Some of the lumped parameter models of the organ of Corti include an active nonlinear physiologically based cochlear model by [42]. The three dimensional model presented incooperates the viscous fluid effects with an organ of Corti that has a nonlinear active feed forward mechanism. Ramamoorty et al [43] designed a three dimensional finite element cochlea model consisting of electrical, acoustic and mechanical elements. Zhang et al [44] developed a finite element model of the human ear and used it to research the purpose of the middle ear and the cochlea with respect to the ear structure. Research carried out by Elliot et al [45] illustrates the use of the wave finite element method in decomposing the results of a finite element calculation in terms of components. This permits the application of the wave approach using complex numerical methods. Analytical models with an in-depth of the cochlea hydrodynamics have also been provided [46]. There has been a tremendous change and improvement to the physical models built from [47], Tonndorf in 1959 to [48] MEMs based organ of Corti or parts of organ of Corti. Modern advanced technology in measurement systems technology has resulted in micro-mechanical models thus providing evidence that the cochlea is nonlinear and active [49].

2.3.4 Integrated models of the auditory system

Integrated models of the human auditory system, though currently very few, have been designed mainly to understand the mechanism of sound transmission, evaluate hearing loss and simulate pathological conditions [15]. A one dimensional vibration network model was developed to predict empirical data measured on human temporal bone [50]. A three dimensional model of the human ear which included both the internal and the external ear was presented by Gan et al [44] used to predict the impacts of the ear drum thickness and stiffness. The results showed that peak responses of both tympanic membranes and the stapes footplate occurred between 3000Hz and 4000Hz. Gan et al [44] further modified this model to include coupled structural acoustic interfaces analysis from the outer ear to the middle ear. Input sound pressure was applied at different frequencies and the pressure distribution in the canal and the middle ear was deduced. Gan et al [51], developed a complete human auditory finite element model and used it to predict the effects of perforations of the tympanic membrane on sound transmission via the middle ear. The finite element model developed gives sufficient predictions on impacts of perforation location and size on the middle ear transfer function. Gan et al [52] made progress towards developing an entire model for the human ear to be used for acoustic-mechanical analysis. The basilar membrane motion frequency sensitivity and the pressure induced by sound pressure from the intra cochlear ear canal was predicted. Kim et al [53] developed a three dimensional finite element model of the human middle and inner ear to be used in gaining insight into the basics mechanism of bone conduction and hearing. Gan et al [54] developed a three dimensional finite element model for sound transmission simulation through the human outer, middle and inner ear. A feed forward mechanism that is active was added to the passive cochlear model to demonstrate the dynamics of the outer hair cells. A finite element model of the human ear consisting of the ear canal, middle ear and a spiral cochlea was developed. The novelty of this model lies in its ability to be used as a computational visualization tool. In 2014, Zhang et el [55] further developed a finite element modelling of abnormal and normal ear energy absorbance. The work presented was a first attempt to simulate the clinical audiology tests using a finite element mode. The results presented were essential in gaining insight about the relationship between the middle ear structure and energy transmission. Other novel models that have been presented are found in [56],[57],[58],[59].

2.3.5 Energy based models

Lagragian model

A refined time averaged lagrangian cochlear model is developed by Yoon et al [60]. This model use a push pull mechanism in the organ of corti. This models uses the time averaged Langragian for the conservative system to resolve the phase excursion issues. Using the micromechanical model developed by Hernandez, [61] presents a new solution to it using Lagranges equations. The main advantage of this new model is that it allows for a mathematical model for the displacement on the outer hair cells found in the organ of corti. The comprehensive Lagrangian model of the middle ear proposed in [62] is to be used in the design of audiometers.

Motivation for the Port Hamiltonian Approach

The Port-Hamiltonian description allows for a more systematic framework for analysing, controlling and simulating intricate physical systems for both distributed parameter and lumped parameter models. The Hamiltonian equations of motions have their foundation in analytical mechanics and Euler Lagrange equations. Hamiltonian dynamics are defined by the Dirac structures and the Hamiltonian is termed as the total stored energy. Port Hamiltonian systems can therefore be defined as open dynamical systems which interact with their environment through ports [63]. The Port-Hamiltonian method can be used to model complex and atomically based interconnected systems for instance inertias, springs and dampers [63]. A Port-Hamiltonian model of a vocal fold fluid structure interaction was reported by Mora et al [64]. The focus of the research carried out by Mora et al [64] was to understand the energy transfer between the moving fluid and the mechanical structure. Vocal fields can be categorized under mechanical structure which can easily be modelled as a spring-damper system. Approximation of the collision forces of the vocal folds assists in the diagnosis of phono traumatic voice pathologies. In summary, the research was about the interacting forces and the energy flux in the model. Angerer et al [65] proposed a passivity based control approach in Port-Hamiltonian framework for the cooperative manipulation system guided by the human being. Seslija [66] used a Port-Hamiltonian based model for reaction diffusion systems. A clear geometric interpretation formalized by a stokes Dirac structure allows for the dissipative systems to be treated as interconnected.

A Port-Hamiltonian modelling for a soft finger manipulation is presented by Ficuciello [67]. In this system, the algebraic constraints of the interconnected system are represented by a Dirac structure. The idea of energy flow and power preservation through interconnected systems is used. Other biomedical system developed using the Port Hamiltonian technique can be found in [68]. From the literature review it is quite evident that P-H models can be applied to biomedical systems. Impact of noise on an individual that results to noise induced hearing loss is characterized mainly by energy intensity, frequency level and exposure time. The Port-Hamiltonian method allows for interconnected systems to be modelled in terms of energy in a mathematically correct way. This facilitates for the development of an alternative efficient, less complicated and more accurate model to be used in the assessment of noise induced hearing loss in the human ear. One of the main contributions in this research is the development of an integrated comprehensive dynamic model of the human outer, middle and inner ear using the Port-Hamiltonian method. From the literature survey, to the best of the researchers knowledge, there is currently no integrated Port-Hamiltonian model of the human outer, middle and inner ear for assessment of different pathological conditions which includes, ONIHL.

Extended literature review

To improve on readability and easy flow of this document, further literature review is found in the relevant sections and subsections as indicated below.

- Motivation for the Port Hamiltonian model is in section 2.3.5
- Port Hamiltonian modelling approach literature review is in section 4.2 presented as the mathematical preliminaries and Appendix B
- Noise policy management model is in section 5.2

2.3.6 Conclusion

In order for a proper diagnosis and assessment of the human outer, middle and inner ear to be done accurately and efficiently, there is a need for a suitable model to be developed. Several segmented dynamic models that target other particular conditions rather than ONIHL have been developed. ONIHL continues to be one of the critical challenges that adversely affects people exposed to loud continuous noise at work, for example mine workers. Port-Hamiltonian model of the ear can be used in assessment and diagnosis of ONIHL among mine workers.

Chapter 3

Research methodology

3.1 Research methodology

3.2 Chapter overview

This chapter shows the steps followed in answering the research question. These includes the development of a Port-Hamiltonian model of the human outer, middle and inner ear. The applications of the developed model is shown by applying it to a unique feedback noise policy management model for mine workers. Data collection and ethical clearance issues are also discussed in this chapter.

3.2.1 Research Approach

The objective of the research is to develop a unique Port-Hamiltonian model of the outer, middle and inner ear then use it in a feedback model that is used to monitor mine workers in the mine with given noise policies. Quantitative data obtained from existing literature is used to validate both the developed ear model and the noise policy management model. Qualitative data from the literature is also used to discuss, analyse and explain the results.

3.2.2 Data collection

The data used to answer the research question was obtained from journal papers with particular emphasis on the paper titled, Rock drills used in south African mines:

a comparative study of noise and vibration levels , ISO:1999 standard [69], mining machinery in South Africa specification sheet and books. Both the literature review and analysis were carried out to extract important information. The parameters used for the ear were also obtained from existing literature. Simulations were carried out using Matlab with the signals and system processing tool box.

3.2.3 Explanation of how the methodology answers the research question

Figures 3.1 , 3.2 and 3.3 shows the overall ONIHL dynamic ear modeling and the noise policy management model.

To understand the mechanism of hearing and the process that results in ONIHL, a dynamic ear model is developed. ONIHL is characterized by the amount of energy in decibels, frequency and time of exposure. There are very few numerical, analytical and energy based models in the literature that focus on hearing loss due to ONIHL. There is therefore a need to employ an energy based method that can model complex and interconnected systems. A comprehensive integrated Port-Hamiltonian model incorporating energy and momentum is used to model the outer, middle and inner ear. The noise policy management model is used to address the limitations of the existing models that do not include the mining policies.

3.2.4 Ethical clearance

Historical data from mines that has been published in books, journal papers or conference papers is used to verify the built models. All sources of data used for this research are acknowledged. The ISO: 1999 standard was purchased and is used as a source of historical data as well. The other main source of historical data is a journal paper titled:"Rock drills used in South African mines: a comparative study of noise and vibration levels" [70] . The ISO: 1999 standard [69] provides statistical information of behaviour of groups of individual and not for single individuals. Whilst the rock drills papers provide machinery used and the operating conditions, extra information used was obtained using data sheets for machinery used in the South African mine. Specifications for this machinery was obtained directly from the supplying companies. This research will not involve the use of data from individual miners. The information to be used for validation will be the noise intensity and frequency of exposures for different cohorts at the mine. Therefore, there is no

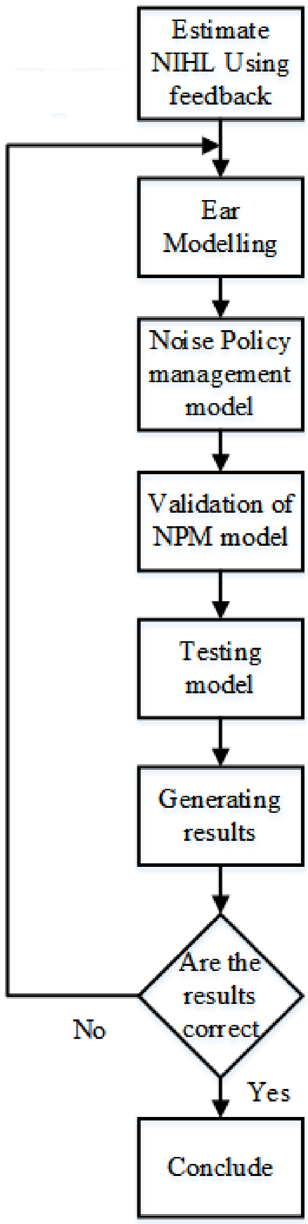

Figure 3.1: Methodology for the design of the feedback based model

need for permission from any mine to use their data. The information used has already been published and is in the public domain. Obtaining information from the mine is not part of this research project. This research work has a medical ethical clearance certificate that allows for the research of the findings to be published. These documents are in Appendix A.

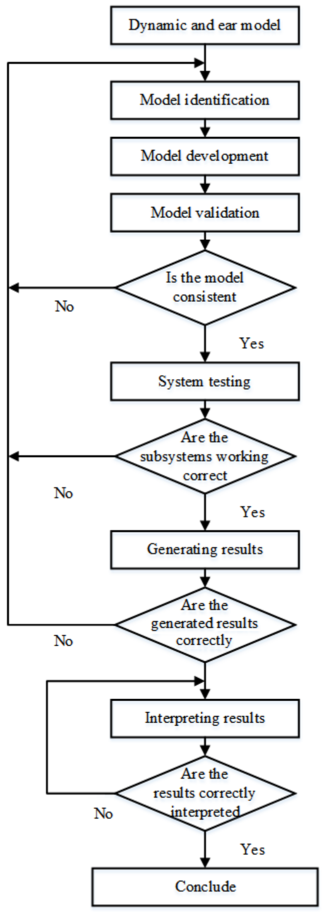

Figure 3.2: Ear modelling methodology

3.2.5 Conclusion

Research methodology has been presented to show how the research questions will be answered. The Research approach, data collection process and ethical clearance are all aspects of the methodology that have been discussed.

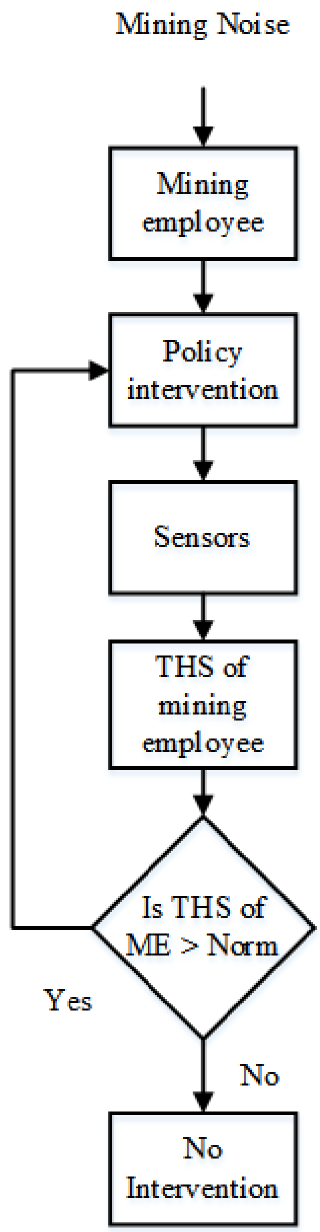

Figure 3.3: Noise management policy model

Chapter 4

Dynamic ear model

4.1 Chapter overview

This chapter presents the development of the Port-Hamiltonian model of the outer, middle and inner ear. The mathematical preliminaries of the Port-Hamiltonian method used to model the outer, middle and inner ear is presented. The Port-Hamiltonian models of the respective segments (outer, middle and inner ear) are provided, as well as the integrated coupled model of the human ear. The parameters used and assumptions made to simplify the complexity of the system are also given in detail. The developed model is validated using parameters and data from existing literature. The results and discussion for each segment is provided in the relevant sections. This section also includes model discretization and coupling. The results of the integrated model are also provided.

4.2 Mathematical preliminaries of the Port Hamiltonian model of the human ear

In this section, the mathematical preliminaries of the Port Hamiltonian model necessary to model the ear is given. From the point of view of Port-Hamiltonian systems, the ear model is a mixed-port Hamiltonian system.

Definition 1. *[71, 72] The i^{th} bond space, $\mathcal{B}^i$, is defined as the product of the efforts $\mathcal{F}^i$ and flows $\mathcal{E}^i$*

$$\mathcal{B}^i = \mathcal{F}^i \times \mathcal{E}^i \tag{4.1}$$

where

$$\begin{aligned} \mathcal{F}^i &= \mathcal{F}_h^i \times \mathcal{F}_r^i \times \mathcal{F}_I^i \times \mathcal{F}_\partial^i && (4.2) \\ \mathcal{E}^i &= \mathcal{E}_h^i \times \mathcal{E}_r^i \times \mathcal{E}_I^i \times \mathcal{E}_\partial^i && (4.3) \end{aligned}$$

The subscripts on the flow and effort variables are defined as follows: h *=Hamiltonian,* r *=dissipative/resistive,* I *=distributed input and* ∂ *=boundary. The flows and efforts belong to the following spaces*

$$\mathcal{F}_h^i = L_2(a,b)^{n^i}, \quad \mathcal{E}_h^i = L_2(a,b)^{n^i}, \quad \mathcal{F}_r^i = L_2(a,b)^{m_1^i}, \quad \mathcal{E}_r^i = L_2(a,b)^{m_1^i}, \tag{4.4}$$

$$\mathcal{F}_\partial = \mathbb{R}^{r^i}, \qquad \mathcal{E}_\partial = \mathbb{R}^{r^i} \tag{4.5}$$

on the interval $z \in [a,b]$*, where the parameters* $n^i > 0$*,* $m_1^i \geq 0$*,* $m_2^i \geq 0$ *and* $r^i > 0$*.*

Definition 2. *[71, 72] The formally skew-symmetric operator,* $\mathcal{J}_{h,r}^i$*, is expressed as*

$$\mathcal{J}_{h,r}^i = \begin{bmatrix} \mathcal{J}^i & G_R^i \\ -G_R^{*i} & 0 \end{bmatrix} = \sum_{\forall k^i} \tilde{P}_{k^i} \partial_z^{k^i} = \sum_{\forall k^i} \begin{bmatrix} P_{k^i} & G_{k^i} \\ (-1)^{k^i+1} G_{k^i}^T & 0 \end{bmatrix} \partial_z^{k^i} \tag{4.6}$$

where $i = 1, 2, \ldots, N$ *and* $k^i = 0, 1, \ldots, N^i$*, the matrices* $P_{k^i} \in \mathbb{R}^{n^i \times n^i}$ *and* $G_{k^i} \in \mathbb{R}^{n^i \times m_1^i}$ *are real. The operators* $\mathcal{J}^i$*,* $\mathcal{G}_R^i$*,* $\mathcal{G}_R^{*i}$ *and* $\mathcal{G}_I$ *are also formally skew-symmetric and are defined as*

$$\begin{aligned} \mathcal{J}^i &= \sum_{\forall k^i} P_{k^i} \partial_z^{k^i} \\ \mathcal{G}_R^i &= \sum_{\forall k^i} G_{k^i} \partial_z^{k^i} \\ \mathcal{G}_R^{*i} &= \sum_{\forall k} (-1)^{k^i} G_{k^i}^T \partial_z^{k^i} \\ \mathcal{G}_I &\in \mathcal{L}(L_2(a,b)^{m_2^i}, L_2(a,b)^{n^i}) && (4.7) \end{aligned}$$

where $\partial_z^{k^i} = \partial^{k^i} / \partial_z^{k^i}$ *is the* $(k^i)^{th}$ *order partial derivative with respect to* $z \in (a,b)$*. The skew-symmetric property, that is,* $\mathcal{J}^i = -\mathcal{J}^{*i}$*,* $\mathcal{G}_R^i = -\mathcal{G}_R^{*i}$ *and* $\mathcal{G}_I^i = -\mathcal{G}_I^{*i}$ *is due to the property*

$$P_{k^i} = (-1)^{k^i+1} P_{k^i}^T \tag{4.8}$$

$$\tilde{P}_{k^i} = (-1)^{k^i+1} \tilde{P}_{k^i}^T \tag{4.9}$$

$$G_{k^i} = (-1)^{k^i+1} G_{k^i}^T \tag{4.10}$$

Definition 3. *[71, 72] The formally skew-symmetric operator,* $\mathcal{J}_{h,r,I}$ *is expressed as*

$$\mathcal{J}_{h,r,I}^i = \begin{bmatrix} \mathcal{J}^i & G_R^i & G_I^i \\ -G_R^{*i} & 0 & 0 \\ -G_I^{*i} & 0 & 0 \end{bmatrix} = \begin{bmatrix} P_0^i & G_0^i & G_I^i \\ -G_0^{Ti} & 0 & 0 \\ -G_I^{*i} & 0 & 0 \end{bmatrix} + \sum_{k^i=1}^{N^i} \tilde{P}_{k^i} \partial_z^{k^i} \tag{4.11}$$

where $\tilde{P}_{k^i}$ *is defined in equation 4.9.*

Theorem 4.2.1. *[71, 72] For any two functions $e_1^i = [e_{h,1}^i, e_{r,1}^i]^T$ and $e_2^i = [e_{h,2}^i, e_{r,2}^i]^T$ of the N^i order Sobolev space $H^{N^i}(a,b)^{n^i+m_1^i}$ and the operator, $\mathcal{J}_e^i$ in equation 4.6,*

$$\begin{aligned} &\textstyle\int_a^b (\mathcal{J}_{h,r}^i e_1^i)^T(z)\,dz + \int_a^b (\mathcal{J}_{h,r}^i e_1^i)^T(z)\,dz \\ &= \left[\begin{pmatrix} e_1^i(z) & \partial_z e_1^i(z) & \cdots & \partial_z^{N^i-1} e_1^i(z) \end{pmatrix} Q^i \begin{pmatrix} e_2^i(z) \\ \partial_z e_2^i(z) \\ \vdots \\ \partial_z^{N^i-1} e_2^i(z) \end{pmatrix} \right]_a^b \end{aligned} \tag{4.12}$$

where the symmetric non-singular matrix, $Q^{N^i(n^i+m_1^i)\times N^i(n^i+m_1^i)}$ is expressed as:

$$Q^i = \begin{bmatrix} \tilde{P}_1^i & \tilde{P}_2^i & \cdots & \tilde{P}_{N^i-1}^i & \tilde{P}_{N^i}^i \\ -\tilde{P}_2^i & -\tilde{P}_3^i & \cdots & -\tilde{P}_{N^i}^i & 0 \\ \tilde{P}_3^i & \tilde{P}_4^i & \cdots & 0 & 0 \\ \vdots & \vdots & \vdots & \vdots & \\ (-1)^{N^i-1}\tilde{P}_{N^i}^i & 0 & \cdots & 0 & 0 \end{bmatrix} \tag{4.13}$$

where $\tilde{P}_{N^i}^i$ is given in equation 4.9.

Definition 4. *[71, 72] The boundary trace map, $\tau : H^{N^i}(a,b;\mathbb{R}^{n^i}) \to \mathbb{R}^{2n^iN^i}$ is given by*

$$\tau(e^i) \quad = \quad \begin{bmatrix} e^i(b) \\ \partial_z e^i(b) \\ \vdots \\ \partial_z^{N^i-1} e^i(b) \\ e^i(a) \\ \partial_z e^i(a) \\ \vdots \\ \partial_z^{N^i-1} e^i(a) \end{bmatrix} \tag{4.14}$$

where $H^{N^i}(a,b;\mathbb{R}^{n^i})$ is an N^i order Sobolev space.

Theorem 4.2.2. *[71, 72] Given any two functions $e_1^i = [e_{h,1}^i, e_{r,1}^i, e_{I,1}^i]^T$ and $e_2^i = [e_{h,2}^i, e_{r,2}^i, e_{I,2}^i]^T$, that are elements of the N^i order Sobolev space $H^{N^i}(a,b)^{n^i+m_1^i+m_2^i}$ and the operator, $\mathcal{J}_{h,r,I}^i$ in equation 4.7 then*

$$\begin{aligned} &\textstyle\int_a^b (\mathcal{J}_{h,r,I}^i e_1^i)^T(z)\,dz + \int_a^b (\mathcal{J}_{h,r,I}^i e_1^i)^T(z)\,dz \\ &= \left\langle \begin{bmatrix} M_Q^i & 0 \\ 0 & M_Q^i \end{bmatrix} \tau\left(\begin{bmatrix} e_{h,1}^i \\ e_{r,1}^i \end{bmatrix}\right), \begin{bmatrix} \tilde{Q}^i & 0 \\ 0 & -\tilde{Q}^i \end{bmatrix} \begin{bmatrix} M_Q^i & 0 \\ 0 & M_Q^i \end{bmatrix} \tau\left(\begin{bmatrix} e_{h,1}^i \\ e_{r,1}^i \end{bmatrix}\right) \right\rangle_{\mathbb{R}^{2r}} \end{aligned} \tag{4.15}$$

where $\tilde{Q} = M^TQM$ and $M_Q = (M^TM)^{-1}M^T$ (the index i has been dropped for simplicity). The columns of the matrix $M \in \mathbb{R}^{N^i(n^i+m_1^i)\times r^i}$ are spanned by the range of Q.

Definition 5. *The boundary port is given by the vector* $\begin{bmatrix} f_{\partial,e^i} \\ e_{\partial,e^i} \end{bmatrix}$ *is expressed as*

$$\begin{aligned}
\begin{bmatrix} f_{\partial,e^i} \\ e_{\partial,e^i} \end{bmatrix} &= R^i_{ext} \begin{bmatrix} M^i_Q & 0 \\ 0 & M^i_Q \end{bmatrix} \tau\left(e^i\right) \\
&= \frac{1}{\sqrt{2}} \begin{bmatrix} Q^i & -Q^i \\ I & I \end{bmatrix} \begin{bmatrix} M^i_Q & 0 \\ 0 & M^i_Q \end{bmatrix} \tau\left(e^i\right) \qquad (4.16)
\end{aligned}$$

where the vectors $f_{\partial,e^i} \in \mathbb{R}^r$ *and* $e_{\partial,e^i} \in \mathbb{R}^r$ *and the matrix* $R_{ext} \in \mathbb{R}^{2r\times 2r}$ *are real.*

Theorem 4.2.3. *[71, 72] A Dirac structure,* $\mathcal{D}^i_{\mathcal{J}_e}$*, (in relation to the symmetric pairing given by equation 4.12) is a subspace of the bond space* $\mathcal{B}^i$ *given by the set*

$$\mathcal{D}^i_{\mathcal{J}_e} = \left\{ \begin{bmatrix} f^i \\ f^i_\partial \\ e^i \\ e^i_\partial \end{bmatrix} \in \mathcal{B}^i \;\middle|\; \begin{array}{l} \mathcal{J}^i_e e^i = f^i, \\ f^i = \begin{bmatrix} f^i_h \\ f^i_r \\ f^i_I \end{bmatrix}, e^i = \begin{bmatrix} e^i_h \\ e^i_r \\ e^i_I \end{bmatrix}, \\ \begin{bmatrix} f_{\partial,e^i} \\ e_{\partial,e^i} \end{bmatrix}_{|D(\mathcal{J}^i_e)} = R^i_{ext} \begin{bmatrix} M^i_Q & 0 \\ 0 & M^i_Q \end{bmatrix} \tau\left(\begin{bmatrix} e^i_h \\ e^i_r \end{bmatrix}\right), \\ e^i \in H(J^i_e, (a,b))^{n^i+m^i_1+m^i_2} \end{array} \right\} \qquad (4.17)$$

where

$$D(\mathcal{J}^i_e) = \begin{bmatrix} H^{N^i}(a,b,R^{n^i}) \\ H^{N^i}(a,b,R^{m^i_1}) \\ H^{N^i}(a,b,R^{m^i_2}) \end{bmatrix} \qquad (4.18)$$

Theorem 4.2.4. *[71, 72] A Dirac structure,* $\mathcal{D}_{\widetilde{\mathcal{J}}_{\widetilde{e}}}$*, (in relation to the canonical symmetric pairing given by equation 4.12), is a subspace of the* $N-$*dimensional bond space* $\widetilde{\mathcal{B}} \triangleq \mathcal{B}^1 \times \mathcal{B}^2 \times \cdots \times \mathcal{B}^N$ *given by the set*

$$\mathcal{D}_{\widetilde{\mathcal{J}}_{\widetilde{e}}} = \left\{ \begin{bmatrix} \widetilde{f} \\ \widetilde{f}_\partial \\ \widetilde{e} \\ \widetilde{e}_\partial \end{bmatrix} \in \widetilde{\mathcal{B}} \;\middle|\; \begin{array}{l} \widetilde{\mathcal{J}}_e \widetilde{e} = \widetilde{f}, \\ \widetilde{f} = \begin{bmatrix} f^1 \\ f^2 \\ \vdots \\ f^N \end{bmatrix}, \widetilde{e} = \begin{bmatrix} e_1 \\ e^2 \\ \vdots \\ e^N \end{bmatrix}, \\ \begin{bmatrix} \widetilde{f}_{\partial,\widetilde{e}} \\ \widetilde{e}_{\partial,\widetilde{e}} \end{bmatrix}_{|D(\widetilde{\mathcal{J}}_e)} = \widetilde{R}_{ext} \begin{bmatrix} M_Q & 0 \\ 0 & M_Q \end{bmatrix} \tau\left(\widetilde{e}\right), \\ \widetilde{e} \in H(\widetilde{\mathcal{J}}_e, (a,b))^{\sum_{\forall i}(n^i+m^i_1+m^i_2)}, \quad i = 1,2,\ldots,N \end{array} \right\} \qquad (4.19)$$

4.3 System modelling

Modelling parameters and assumptions taken while developing the Port Hamiltonian model of the human ear are provided in the subsections that follow.

4.3.1 Modelling Parameters

Table 4.1: Air at 20° Celcius, [73]

Parameter	**Symbol**	**Value**
Density	ρ_{a}	$1.204 \times 10^{-3} g/cm^3$
Speed of sound	c_{a}	$3.43 \times 10^{4} cm/s$
kinematic viscosity	ν_{a}	$0.1516 cm^2/s$

Table 4.2: Tympanic Membrane [74, 75]

Parameter	**Symbol**	**Value**
Density	ρ_{TM}	$1.2 g/cm^3$
Young's Modulus	EI_{TM}	$3.5 \times 10^{8} cm/s$
Damping	β_{TM}	$1.2 \times 10^{-5} s^{-1}$

Table 4.3: Middle ear parameters [76]

Parameter	**Symbol**	**Value**
Mass of the Malleus	M_3	$4.00 \times 10^{-3} g$
Mass of the Incus	M_4	$4.00 \times 10^{-3} g$
Mass of the Stapes	M_5	$1.78 \times 10^{-3} g$
Spring stiffnesses	K_3	$9.474 \times 10^{6} g/s^2$
	K_5	$1.000017 \times 10^{9} g/s^2$
	K_6	$1.67 \times 10^{5} g/s^2$
Coefficient of damping	B_3	$1.74 \times 10^{3} g/s$
	B_4	$1.22 \times 10^{2} g/s$
	B_5	$2.16 \times 10^{1} g/s$
	B_6	$3.6 \times 10^{-1} g/s$
	B_7	$2.0 \times 10^{1} g/s$

Table 4.4: Basilar Membrane [74, 75]

Parameter	**Symbol**	**Value**
Density	ρ_{BM}	$1.2g/cm^3$
Young's Modulus (base to middle)	EI_{BM}	$[50 \times 10^{11}, 15 \times 10^{11}]g \cdot cm/s^2$
Young's Modulus (middle to apex)	EI_{BM}	$[15 \times 10^{11}, 3 \times 10^{11}]g \cdot cm/s^2$
Damping (base to apex)	β_{BM}	$[0.2 \times 10^{-3}, 0.1 \times 10^{-2}]g \cdot cm/s^2$

Table 4.5: Scala Vestibula Fluid (Water at 20° Celcius)[74, 75]

Parameter	**Symbol**	**Value**
Density	ρ_{SV}	$9.982 \times 10^{-1}g/cm^3$
Speed of sound	c_{SV}	$1.45 \times 10^5 cm/s$
Kinematic viscosity	ν_{SV}	$1.003 \times 10^{-5}cm^2/s$

Table 4.6: Scala Tympani Fluid (Water at 20° Celcius)[74, 75]

Parameter	**Symbol**	**Value**
Density	ρ_{ST}	$9.982 \times 10^{-1}g/cm^3$
Speed of sound	c_{ST}	$1.45 \times 10^5 cm/s$
Kinematic viscosity	ν_{ST}	$1.003 \times 10^{-5}cm^2/s$

Table 4.7: Outer Hair Cells[77, 78]

Parameter	**Symbol**	**Value**
Peak to peak electromotile deflection	α_{s}	$1 \times 10^{-6}cm$
Reference electromotile voltage	α_{l}	$2 \times 10^{-6}V$
Cut-off frequency	ω_{ohc}	$2\pi \times 10^3 rad/s$
Resting potential of Periylymph	$\psi_{5_{d0}}$	$-7 \times 10^{-2}V$

4.3.2 Modelling assumptions

The assumptions taken during modelling are stated in this section and repeated in the relevant sections for reference purposes

1. Assumptions Ear canal:

   - The ear canal is modelled as a straight rectangular passage (the ear canal is curved).
   - The effect of the Pinna is ignored.
   - The effect of the convective term in the fluid motion is very small and thus is ignored.

- The model is concerned with changes about the resting state (equilibrium).
- The fluid is viscous.
- An isentropic fluid assumption is taken so that the navier-stokes equations are given in the velocity-pressure form.

2. Assumptions Tympanic membrane:

   - The tympanic membrane lies perpendicular to the flow of air in the ear canal (typically lies at an angle to the flow).
   - The tympanic membrane is assumed to deflect only in one direction (such that each cross-section remains perpendicular to its equilibrium position), that is, the Euler Bernoulli assumption. The angular motion about and in-line along the equilibrium are assumed to be negligible [79].
   - The motion at the boundary between the air in the ear canal and the tympanic membrane is assumed to be very small so that the boundary is not time varying.
   - The malleus is attached rigidly at the centre of the tympanic membrane.

3. Assumptions Middle Ear:

   - The middle ear bones are assumed to be rigid and thus are modelled as a mass spring damper system [74, 75].
   - The stapes rotational motion is very small and can be approximated as linear [74, 75].
   - The stapes is in direct contact with the fluid in the scala vestibula [74, 75].
   - The round window is in direct contact with the fluid in the scala tympani [74, 75].

4. Assumptions Scala Vestibula and Scala Tympani:

   - The Scala Vestibula and Scala Tympani are modelled as rectangular chambers [80],[81],[82],[83].
   - The effect of the convective term in the fluid motion is very small and thus is ignored [84] .
   - The model is concerned with changes about the resting state (equilibrium).
   - The fluid is viscous.
   - An isentropic fluid assumption is taken so that the navier-stokes equations are given in the velocity-pressure form.

  - There is exchange of fluid between the scala vestibula and scala tympani at the helicotrema.

5. Assumptions Cochlear partition:

  - The membranes in the cochlear partition are assumed to deflect only in one direction (such that each cross-section remains perpendicular to its equilibrium position), that is, the Euler Bernoulli assumption. The angular motion about and in-line along the equilibrium are assumed to be negligible [79],[85].
  - The motion at the boundary between the fluid in the scala vestibula and scala tympani partition and the membranes in the cochlear partition is assumed to be very small so that the boundary is not time varying.
  - The tectorial membrane and the basilar membrane are interconnected by a distributed spring.

6. Assumptions Outer Hair Cells:

  - The Outer Hair Cells can be modelled as an simplified equivalent circuit model [77, 78].

- All boundaries remain constant, that is they do not vary with time. Any displacements at the boundaries of different media are very small and considered negligible.

4.3.3 Outer ear modelling

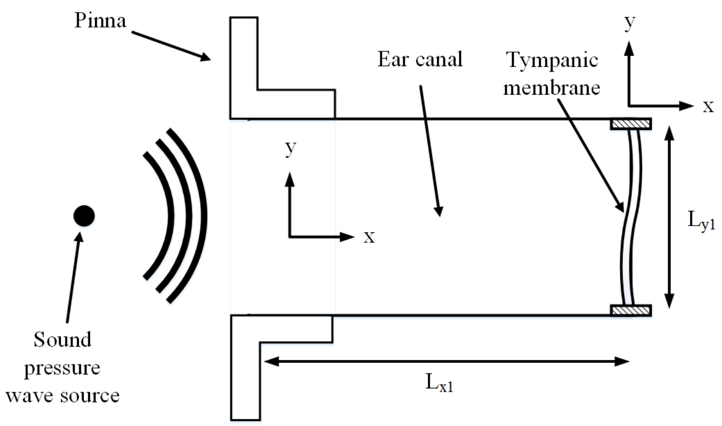

Figure 4.1: Outer ear model

Ear canal

Air in the ear canal is modelled as a non-viscous fluid that obeys the Navier-Stokes (N.S.) equations in which the fluid pressure, $P = P(\rho)$ depends only on the density, ρ, of the fluid (a barometric fluid), under constant entropy (isentropic) conditions. The N.S. equations are expressed as follows:

$$\begin{aligned} P &= P(\rho) \\ \partial_t \rho &= -\nabla \cdot (\rho \boldsymbol{v}) \\ \rho \partial_t \boldsymbol{v} &= -\rho \left(\boldsymbol{v} \cdot \nabla\right) \boldsymbol{v} - \nabla P \end{aligned} \tag{4.20}$$

where $\boldsymbol{v} = \begin{bmatrix} v_x & v_y \end{bmatrix}^T$ is the fluid velocity vector, v_x and v_y are the fluid velocities along the x and y-axis directions, ∂_t is the partial derivative with respect to time and $\nabla = \begin{bmatrix} \partial_x & \partial_y \end{bmatrix}^T$ is the vector gradient operator and $\partial_{(\cdot)}$ is the partial derivative with respect to the spatial coordinates.

$\Omega_1 = \{x \in [0, L_{x1}], y \in [0, L_{y1}]\}$

Assuming that the fluid is initially at rest and the sound pressure waves entering the ear canal disturb the fluid slightly (resulting in small perturbations, in this case only first and second order perturbations are considered). The perturbations are

$$\begin{aligned} \rho &= \rho_a + \rho_b \\ P &= P_a + P_b \\ \boldsymbol{v} &= \boldsymbol{v}_a + \boldsymbol{v}_b \end{aligned} \tag{4.21}$$

where the subscripts a and b indicate whether the parameter is constant or time/spatially varying, respectively. Since the fluid is initially at rest, $v_a = 0$. Under isentropic conditions, speed of sound in air is related to the changes in the air pressure, density as follows

$$C_a^2 = \left(\frac{\partial P}{\partial \rho}\right)_s \tag{4.22}$$

The fluid pressure can now be written as $P = P_a + C_a^2 \rho_b$. The N.S. equations can be simplified by substituting equation 4.21 into 4.20

$$\begin{aligned} P &= P_a + C_a^2 \rho_b \\ \rho_b \partial_t \boldsymbol{v}_b &= -\rho_b \left(\boldsymbol{v}_b \cdot \nabla\right) \boldsymbol{v}_b - \nabla P \\ \partial_t \rho_b &= -\nabla \cdot (\rho_b \boldsymbol{v}_b) \end{aligned} \tag{4.23}$$

It is more appropriate to write the N.S. equations in pressure-velocity form as opposed to the density-velocity form given in equation 4.20, due to the interaction of the air with the tympanic membrane

Considering the interaction

$$\kappa_a = -\frac{1}{V_b}\frac{\partial v_b}{\partial P_b} = -\frac{1}{\rho_a}\frac{\partial \rho}{\partial P} = \frac{1}{\rho_a C_a^2} \tag{4.24}$$

For small perturbations, $(\boldsymbol{v}_b \cdot \nabla)\,\boldsymbol{v}_b \approx \mathbf{0}$ and is neglected. Finally, the N.S. equations in pressure-velocity form are

$$\begin{aligned} \rho_a \partial_t \boldsymbol{v}_a &= -\nabla P_a \\ \kappa_a \partial_t P_a &= -\nabla \cdot \boldsymbol{v}_a \end{aligned} \tag{4.25}$$

Equation 4.25 can now be converted to the Port-Hamiltonian form by defining the state vector

$$x_1 = \begin{bmatrix} \Pi_{x_1} & \Pi_{y_1} & \Psi_1 \end{bmatrix}^T \tag{4.26}$$

where $\Pi_{x_1} = \rho_1 v_{x_1}$ and $\Pi_{y_1} = \rho_1 v_{x_1}$ are the fluid momentum along the x and y-axis directions, respectively, $\Psi_1 = \kappa_1 P_1$ is the fluid "stiffness" and the subscript, 1 is used to identify the ear canal. The total energy, the Hamiltonian, $H_1(x_1)$, is

$$H_1(x_1) = \frac{1}{2}\iint_{\Omega_1} x_1^T \mathcal{L}_1 x_1 \, d\Omega_1 \tag{4.27}$$

where

$$\boldsymbol{L_1} = \begin{bmatrix} 1/\rho_1 & 0 & 0 \\ 0 & 1/\rho_1 & 0 \\ 0 & 0 & 1/\kappa_1 \end{bmatrix}, \quad d\Omega_1 = dx\,dy$$

in expanded form

$$H_1(\boldsymbol{x_1}) = \frac{1}{2}\int_0^{L_{y_1}}\int_0^{L_{x_1}} \left(\frac{(\Pi_{x_1})^2}{\rho_1} + \frac{(\Pi_{y_1})^2}{\rho_1} + \frac{(\Psi_1)^2}{\kappa_1} \right) dx\,dy \tag{4.28}$$

The state equations of the fluid in the ear canal in PH-form are

$$\partial_t x_1 = \left(\mathcal{J}^1 - \mathcal{G}_R^1 \mathcal{S}^1 \mathcal{G}_R^{*1}\right)(\delta_{x_1} H_1) \tag{4.29}$$

where

$$\mathcal{J}^1 = \begin{bmatrix} 0 & 0 & -\partial_x \\ 0 & 0 & -\partial_y \\ -\partial_x & -\partial_y & 0 \end{bmatrix}, \quad \mathcal{G}_R^1 = \begin{bmatrix} \partial_x & \partial_y & 0 \end{bmatrix}, \quad \mathcal{G}_R^{*1} = -(\mathcal{G}_R^1)^T,$$

$$\mathcal{S}^1 = \begin{bmatrix} 0 & 0 & 0 \\ 0 & 0 & 0 \\ 0 & 0 & 0 \end{bmatrix}, \quad e_p^1 = S^1 f_p^1, \quad (\delta_{x_1} H_1) = \mathcal{L}_1 x_1 = \begin{bmatrix} \Pi_{x_1}/\rho_1 \\ \Pi_{y_1}/\rho_1 \\ \Psi_{x_1}/\kappa_1 \end{bmatrix} \tag{4.30}$$

Tympanic membrane

The Tympanic membrane is modelled as an Euler-Bernoulli beam with viscous damping B_2 [79]

$$\rho_2 \partial_t^2 v_2 = -\partial_y^2 \left(EI_2 \partial_y^2 v_2 \right) - B_2 \partial_t v_2 \tag{4.31}$$

where the subscript 2 is used to identify the Tympanic membrane, v_2 is the displacement of the beam from the undisturbed position, ρ_2 and EI_2 are the density per unit length and flexural rigidity, respectively. Defining the momentum and curvature, $\Pi_2 = \rho_2 \partial_t v_2$ and $\Psi_2 = \partial_y^2 v_2$, respectively, the state vector of the P.H. model of the Tympanic membrane, x_2, is

$$x_2 = \begin{bmatrix} \Pi_2 & \Psi_2 \end{bmatrix}^T \tag{4.32}$$

Substituting these states into equation 4.31 and taking the time derivative of x_2, the following equations

$$\begin{aligned} \partial_t \Pi_2 &= -\partial_y^2 EI_2 \Psi_2 - B_2 \frac{\Pi_2}{\rho_2} \\ \partial_t \Psi_2 &= \partial_y^2 \frac{\Pi_2}{\rho_2} \end{aligned} \tag{4.33}$$

are obtained, which can be derived from a Hamiltonian

$$H_2(x_2) = \frac{1}{2} \int_a^b \left(\frac{(\Pi_2)^2}{\rho_2} + EI_2 (\Psi_2)^2 \right) dy \tag{4.34}$$

which can be written as

$$H_2(x_2) = \frac{1}{2} \int_a^b x_2^T \mathcal{L}_2 x_2 \, dy \tag{4.35}$$

where

$$\mathcal{L}_2 = \begin{bmatrix} 1/\rho_2 & 0 \\ 0 & EI_2 \end{bmatrix}$$

The P.H. model of the Tympanic membrane takes the form

$$\begin{aligned} \partial_t x_2 &= \left(\mathcal{J}^2 - G_R^2 S^2 G_R^{*2} \right) (\delta_{x_2} H_2) + G_I^2 u_I^2 + G^2 u^2 \\ y_{2_I} &= G_I^{*2} (\delta_{x_2} H_2) \\ y_2 &= G^{*2} (\delta_{x_2} H_2) \end{aligned} \tag{4.36}$$

where

$$
\begin{aligned}
\mathcal{J}^2 &= P_0^2 + P_1^2\partial_y + P_2^2\partial_y^2,\\
P_0^2 = \begin{bmatrix}0 & 0\\ 0 & 0\end{bmatrix}, \quad P_1^2 &= \begin{bmatrix}0 & 0\\ 0 & 0\end{bmatrix}, \quad P_2^2 = \begin{bmatrix}0 & -1\\ 1 & 0\end{bmatrix},\\
\mathcal{G}_R^2 = \begin{bmatrix}1 & 0\\ 0 & 0\end{bmatrix}, \quad \mathcal{G}_R^{*2} &= -(\mathcal{G}_R^2)^T, \quad \mathcal{S}^2 = \begin{bmatrix}-B_2 & 0\\ 0 & 0\end{bmatrix},\\
, \quad \mathcal{G}_I^2 = \begin{bmatrix}1\\ 0\end{bmatrix}, \quad \mathcal{G}^2 &= \begin{bmatrix}1\\ 0\end{bmatrix}, \qquad (\delta_{x_2}H_2) = \mathcal{L}_2 x_2 = \begin{bmatrix}\Pi_2/\rho_2\\ EI_2\Psi_2\end{bmatrix}
\end{aligned}
\tag{4.37}
$$

The boundary ports are

$$
\begin{bmatrix}f_\partial\\ e_\partial\end{bmatrix} = \frac{1}{\sqrt{2}}\begin{bmatrix}Q_2 & -Q_2\\ I & I\end{bmatrix}\begin{bmatrix}(\delta_{x_2}H_2)(b)\\ (\delta_{x_2}H_2)(a)\end{bmatrix} = \frac{1}{\sqrt{2}}\begin{bmatrix}EI_2\partial_y\Psi_2(a) - EI_2\partial_y\Psi_2(b)\\ \Pi_2\partial_y\rho_2(b) - \Pi_2\partial_y\rho_2(a)\\ \Pi_2\rho_2(a) + \Pi_2\rho_2(b)\\ EI_2\Psi_2(a) + EI_2\Psi_2(b)\end{bmatrix}
\tag{4.38}
$$

where

$$
Q_2 \quad = \quad P_2^2 \tag{4.39}
$$

The Dirac structure is given by:

$$
\begin{aligned}
\left\langle e^1, \mathcal{J}e^2\right\rangle_{L_2,\Omega} &= \int_\Omega (e_2^1)^T \mathcal{J}_2 e_2^2 \, d\Omega\\
&= \int_\Omega \begin{bmatrix}e_1^1 & e_2^1\end{bmatrix}\begin{bmatrix}0 & -\partial_y^2\\ \partial_y^2 & 0\end{bmatrix}\begin{bmatrix}e_1^2\\ e_2^2\end{bmatrix} d\Omega\\
&= \int_\Omega -e_1^1\partial_y^2 e_2^2 + e_2^1\partial_y^2 e_1^2 \, d\Omega\\
&= \left[-e_1^1\partial_y e_2^2 + e_2^1\partial_y e_1^2\right]_a^b\\
&= -e_1^1(b)\partial_y e_2^2(b) + e_2^1(b)\partial_y e_1^2(b) + e_1^1(a)\partial_y e_2^2(a) - e_2^1(a)\partial_y e_1^2(a)
\end{aligned}
$$

The Dirac structure is given by:

$$
\begin{aligned}
\left\langle -\mathcal{J}e^1, e^2\right\rangle_{L_2,\Omega} &= \int_\Omega \left(-\mathcal{J}_2 e_2^1\right)^T e_2^2 \, d\Omega\\
&= \int_\Omega \left(-\begin{bmatrix}0 & -\partial_y^2\\ \partial_y^2 & 0\end{bmatrix}\begin{bmatrix}e_1^1\\ e_2^1\end{bmatrix}\right)^T \begin{bmatrix}e_1^2\\ e_2^2\end{bmatrix} d\Omega\\
&= \left[e_1^2\partial_y e_2^1 - e_2^2\partial_y e_1^1\right]_a^b\\
&= e_1^2(b)\partial_y e_2^1(b) - e_2^2(b)\partial_y e_1^1(b) - e_1^2(a)\partial_y e_2^1(a) + e_2^2(a)\partial_y e_1^1(a)
\end{aligned}
$$

4.3.4 Outer ear results and discussion

Figure 4.2 shows the initial test that was performed on the tympanic membrane. An initial condition (non-zero velocity at the centre of the tympanic membrane) resulted in waves of vibration moving towards the boundaries of the Tympanic membrane as shown in figure 4.2.

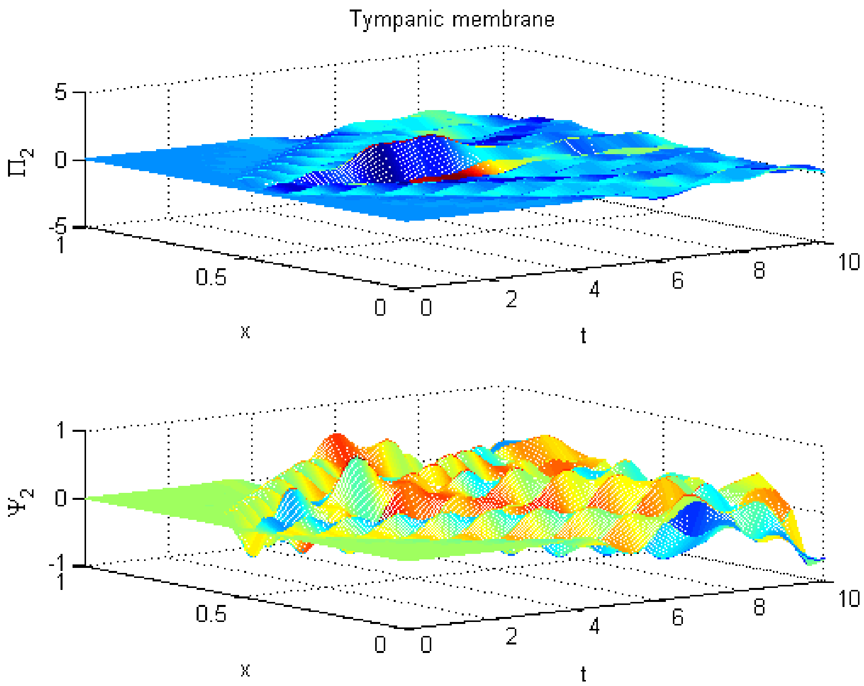

Figure 4.2: Tympanic Membrane

Frequency response of the outer ear

The Port Hamiltonian ear model developed was validated and verified by plotting the transfer function. The magnitude versus frequency curve plotted is comparable to Gan et al's [40] result. Gan et al's [40] result was obtained through a comparison of responses of the middle ear system to harmonic pressure on the lateral side of the tympanic membrane. A consistent pressure of 90dB SPL was exerted on the lateral side of the tympanic membrane and the harmonic analysis was conducted on the model over the frequency range of 200 to 8000 Hz using ANSYS. Figure 4.3 shows the Port Hamiltonian frequency response of the tympanic membrane. The outer ear consists of the ear canal and the tympanic membrane which forms the boarder between the outer and the inner ear. The human ear dynamic behaviour for

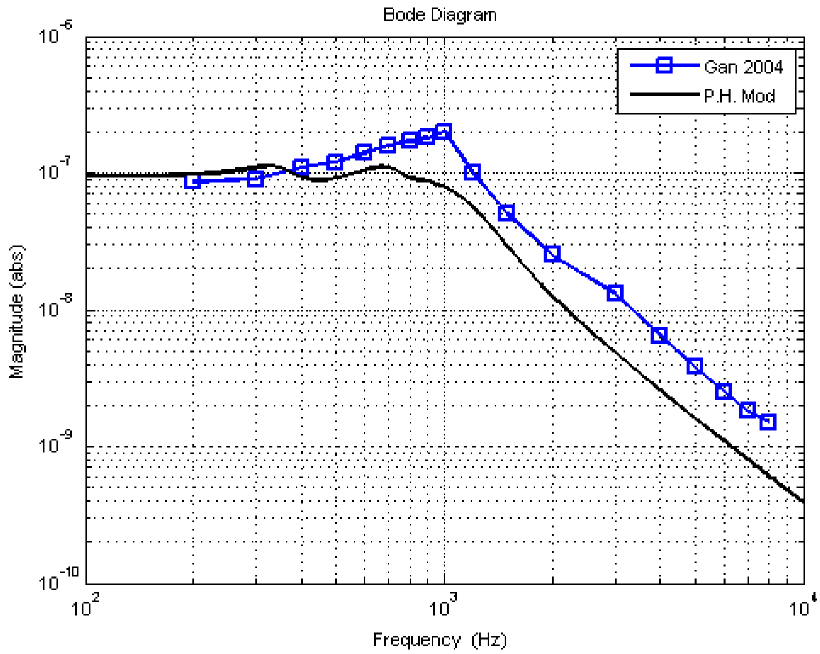

Figure 4.3: Frequency response

sound transmission can be characterized using the ratio of the tympanic membrane displacement to the ear canal sound pressure. This ratio is defined as the transfer function for the middle ear at the tympanic membrane. The tympanic membrane is considered as the input port to the middle ear. The graph in figure 4.3 starts at a magnitude of 1×10^{-7} and starts to roll off at 1 kHz.

4.3.5 Middle ear modelling

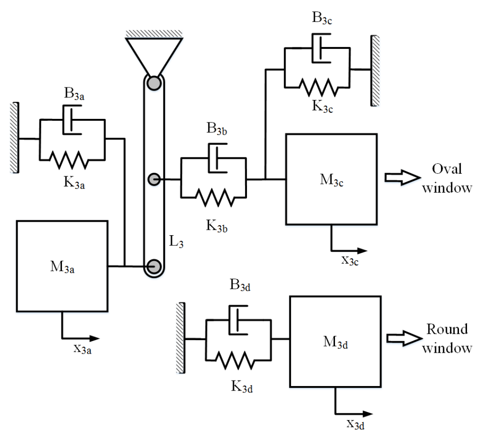

Figure 4.4: Lumped mass model of the middle ear [86]

The middle ear is modelled as a system of coupled masses, springs and dampers as shown in figure 4.4, [86]. The total energy of the system is given by the Hamiltonian function, H_3, which is the sum of the kinetic energy T_3 and the potential energy U_3 given by

$$H_3\left(\boldsymbol{x_3}\right) = T_3 + U_3 \tag{4.40}$$

where

$$\begin{aligned} T_3 &= \frac{1}{2}\left(\frac{\pi_{3_a}^2}{M_{3_a}} + \frac{\pi_{3_c}^2}{M_{3_c}} + \frac{\pi_{3_d}^2}{M_{3_d}}\right) \\ U_3 &= \frac{1}{2}\left(K_{3_a}\psi_{3_a}^2 + K_{3_b}\left(L\psi_{3_a} - \psi_{3_c}\right)^2 + K_{3_c}\psi_{3_c}^2 + K_{3_d}\psi_{3_d}^2\right) \end{aligned}$$

where the subscripts 3_a, 3_b, 3_c and 3_d represent the malleus, incus, stapes window and round window, respectively. $M_{(\cdot)}$ is the mass, $\pi_{(\cdot)}$ is the translational momentum, $\psi_{(\cdot)}$ is the displacement, $K_{(\cdot)}$ is the spring stiffness and G is the ratio of the moment arm due to the Maleus-incus joint. The P.H. model of the middle ear is given by

$$\begin{aligned} \partial_t x_3 &= \left(\mathcal{J}_3 - \mathcal{R}_3\right)\partial_{x_3} H_3 + \mathcal{G}_3 u_3 \\ y_3 &= \mathcal{G}_3^* \partial_{x_3} H_3 \end{aligned} \tag{4.41}$$

where y_3 is the output, the state vector is

$$x_3 = \begin{bmatrix} \pi_{3_a} & \psi_{3_a} & \pi_{3_c} & \psi_{3_c} & \pi_{3_d} & \psi_{3_d} \end{bmatrix}^T \tag{4.42}$$

the skew-symmetric matrix $\mathcal{J}_3 = -\mathcal{J}_3^T$ is

$$\mathcal{J}_3 = \begin{bmatrix} 0 & -1 & 0 & 0 & 0 & 0 \\ 1 & 0 & 0 & 0 & 0 & 0 \\ 0 & 0 & 0 & -1 & 0 & 0 \\ 0 & 0 & 1 & 0 & 0 & 0 \\ 0 & 0 & 0 & 0 & 0 & -1 \\ 0 & 0 & 0 & 0 & 1 & 0 \end{bmatrix} \tag{4.43}$$

the symmetric dissipation matrix, $\mathcal{R}_3 = \mathcal{R}_3^T$, is

$$\mathcal{R}_3 = \begin{bmatrix} B_{3_a} + L_3 B_{3_b} L_3 & 0 & -L_3 B_{3_b} & 0 & 0 & 0 \\ 0 & 0 & 0 & 0 & 0 & 0 \\ -L_3 B_{3_b} & 0 & B_{3_a} + B_{3_c} & 0 & 0 & 0 \\ 0 & 0 & 0 & 0 & 0 & 0 \\ 0 & 0 & 0 & 0 & B_{3_d} & 0 \\ 0 & 0 & 0 & 0 & 0 & 0 \end{bmatrix} \tag{4.44}$$

and the partial derivative of the Hamiltonian with respect to the states is

$$\partial_{x_3} H_3 = \begin{bmatrix} \pi_{3_a}/M_{3_a} \\ K_{3_a}\psi_{3_a} + L_3 K_{3_b}\left(L_3\psi_{3_a} - \psi_{3_c}\right) \\ \pi_{3_c}/M_{3_c} \\ K_{3_b}\psi_{3_c} - K_{3_b}\left(L_3\psi_{3_a} - \psi_{3_c}\right) \\ \pi_{3_d}/M_{3_d} \\ K_{3_d}\psi_{3_d} \end{bmatrix} \tag{4.45}$$

and the control input allocation and control input matrix

$$\mathcal{G}_3 = \begin{bmatrix} 0 & 0 & 0 \\ 1 & 0 & 0 \\ 0 & 0 & 0 \\ 0 & 1 & 0 \\ 0 & 0 & 0 \\ 0 & 0 & 1 \end{bmatrix}, \quad \mathcal{G}_3^* = \begin{bmatrix} 0 & 1 & 0 & 0 & 0 & 0 \\ 0 & 0 & 0 & 1 & 0 & 0 \\ 0 & 0 & 0 & 0 & 0 & 1 \end{bmatrix}, \quad u_3 = \begin{bmatrix} u_{3_a} \\ u_{3_c} \\ u_{3_d} \end{bmatrix} \tag{4.46}$$

4.3.6 Middle ear results and discussion

Figure 4.5 shows the ossilation of the bones in the middle ear.

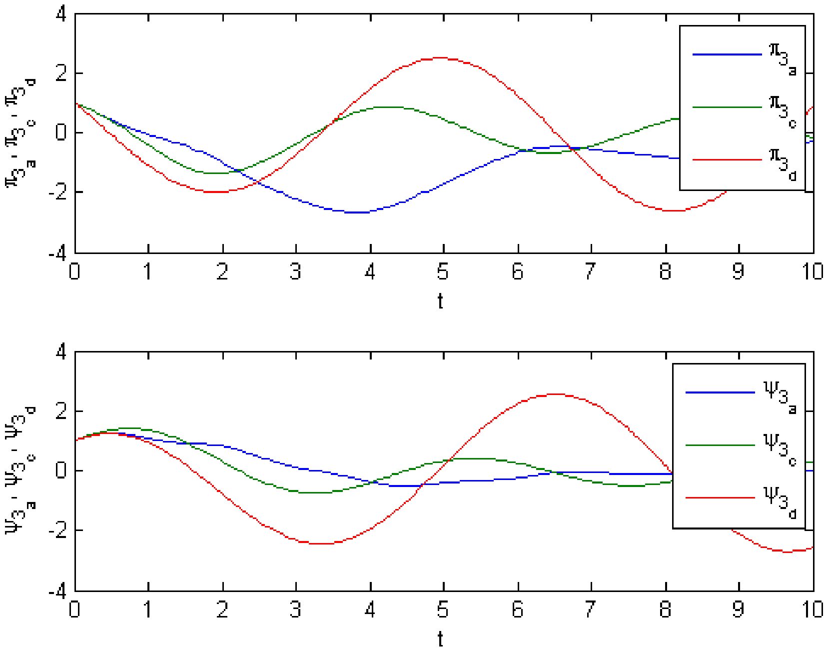

Figure 4.5: Middle ear time response

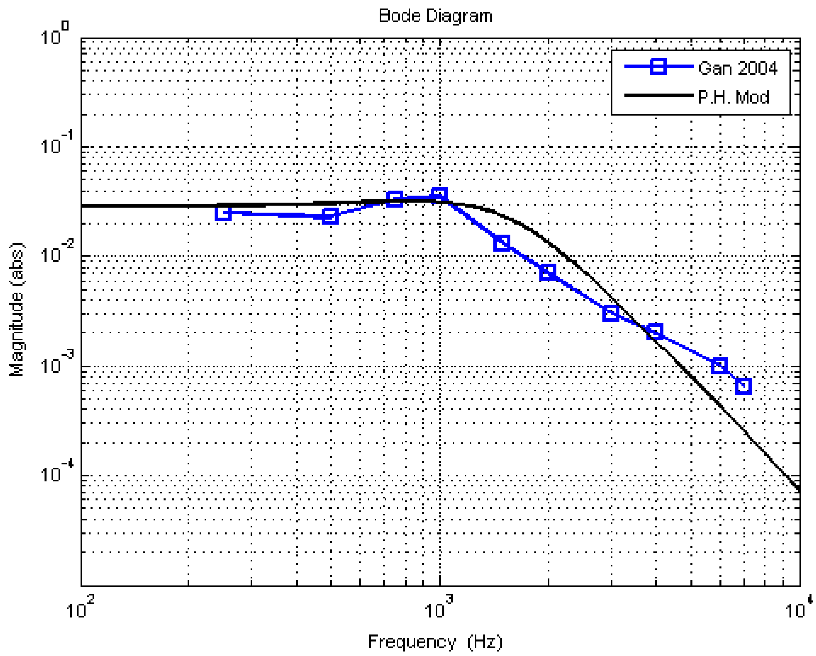

Figure 4.6: Stapes magnitude verses frequency

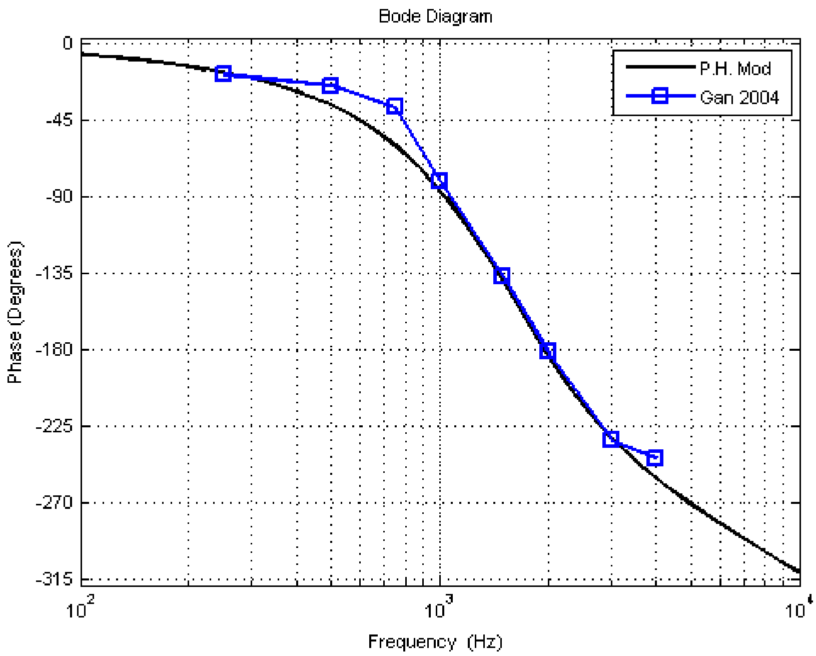

Figure 4.7: Stapes phase verses frequency plots

The mixed Port Hamiltonian system consists of a lumped parameter model of the human middle ear and it is based on anatomical data that is published and temporal bone experimental results. Table 4.2 and 4.3 provides a list of parameters used for connections between the tympanic membrane, the three ossicles and the boundary conditions. To verify and validate the middle ear, bode plots graph of the middle ear were plotted and compared with Gan et al's [40] results as shown in figure 4.6 and 4.7.

The graph starts with a magnitude of 0.023 dB at a frequency of 100 Hz, it proceeds steadily and forms a peak at around 1 kHz. This is consistent with the results obtained by Gan et al [40] whose resonant peak occurs at around 1 kHz. This behaviour confirms the behaviour of the middle ear as a resonant system tuned to the frequency between 700 and 1200 kHz. It is also observed that there is a decay rate of approximately -6dB octave at the higher frequencies. The developed model allows for investigation of ONIHL which is mostly affected by speech frequencies which occur between 3-6 kHz whereas previous studies focused on the behaviour of the middle human ear models at lower frequencies which were less than 1 kHz.

This developed PH model is not just useful for the study of the mechanism of the ear sound transmission but can also be used to provide a theoretical basis of building a physical model of the ear. The developed PH model of the middle ear is capable of simulating the normal and abnormal behaviour of the middle ear.

4.3.7 Inner ear modelling

Scala Vestibula and Scala Tympani fluid

The fluid in the Scala Vestibula (S.V.) and the Scala Tympani (S.T.) are modelled using the same formulation as given in section 4.3.3, that is the pressure-velocity form of the N.S. equations with the addition of fluid viscosity term, $\mu\nabla \cdot \nabla$, to represent the viscous nature of the perilymph fluid in the S.V. and S.T. The N.S. equations with viscosity are [87]

$$\begin{aligned} \rho\partial_t \boldsymbol{v} &= -\nabla P + \mu\nabla \cdot \nabla \boldsymbol{v} \\ \kappa\partial_t P &= -\nabla \cdot \boldsymbol{v} \end{aligned} \tag{4.47}$$

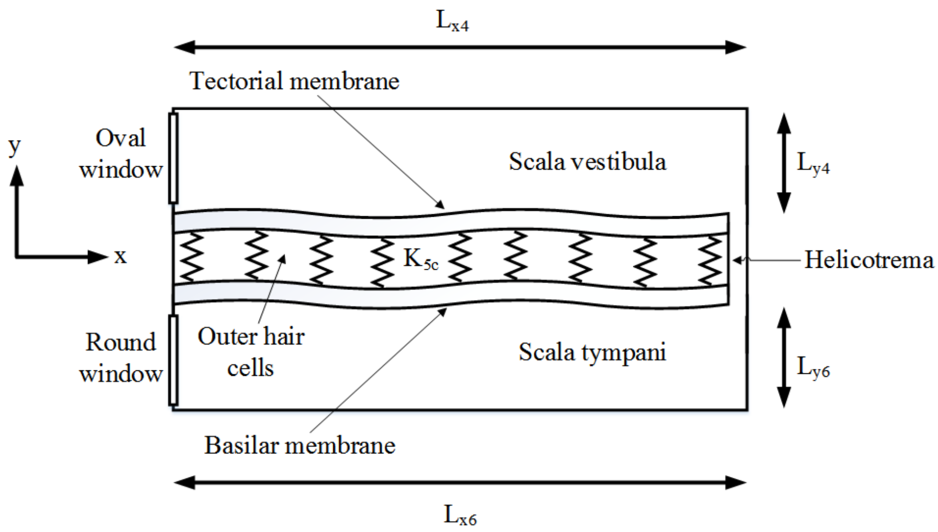

Figure 4.8: Model of the inner ear

The state vector of the P.H. model

$$\boldsymbol{x_i} = \begin{bmatrix} \Pi_{x_i} \\ \Pi_{y_i} \\ \Psi_i \end{bmatrix} = \begin{bmatrix} \rho_i v_{x_i} \\ \rho_i v_{y_i} \\ \kappa_i P_i \end{bmatrix} \tag{4.48}$$

where the subscript $i = 4$ and $i = 6$ represent the S.V. and the S.T., respectively, Π_{x_i} and Π_{y_i} are the fluid momenta along the x and $y-$axis directions, respectively, Ψ_i is the fluid stiffness, ρ_i is the fluid density, v_{x_i} and v_{y_i} are the fluid velocities along the x and $y-$axis directions, respectively and κ_i is the fluid compressibility.

Taking the time derivative of 4.48 making the appropriate substitutions into equation 4.47, the Port-Hamiltonian equations of the fluid in the S.T. and S.V. are given by

$$\partial_t x_i = \left(\mathcal{J}^i - \mathcal{G}_R^i \mathcal{S}^i \mathcal{G}_R^{*i}\right)(\delta_{x_i} H_i) \tag{4.49}$$

where

$$\mathcal{J}^i = \begin{bmatrix} 0 & 0 & -\partial_x \\ 0 & 0 & -\partial_y \\ -\partial_x & -\partial_y & 0 \end{bmatrix}, \quad \mathcal{G}_R^i = \begin{bmatrix} \partial_x & \partial_y & 0 \end{bmatrix}, \quad \mathcal{G}_R^{*i} = -(\mathcal{G}_R^i)^T,$$

$$\mathcal{S}^i = \begin{bmatrix} \mu_i & 0 & 0 \\ 0 & \mu_i & 0 \\ 0 & 0 & \mu_i \end{bmatrix}, \quad e_p^i = S f_p^i, \quad (\delta_{x_i} H_i) = \mathcal{L}_i x_i = \begin{bmatrix} \Pi_{x_i}/\rho_i \\ \Pi_{y_i}/\rho_i \\ \Psi_i/\kappa_i \end{bmatrix} \tag{4.50}$$

where μ_i is the fluid viscosity, δ_{x_i} is the variational derivative with respect to the state vector, x_i. These equations are obtained from a Hamiltonian

$$H_i(x_i) = \frac{1}{2} \iint_{\Omega_i} x_i^T \mathcal{L}_i x_i \, dx \, dy \tag{4.51}$$

where

$$\mathcal{L}_i = \begin{bmatrix} 1/\rho_i & 0 & 0 \\ 0 & 1/\rho_i & 0 \\ 0 & 0 & 1/\kappa_i \end{bmatrix} \tag{4.52}$$

written fully

$$H_i\left(x_i\right) = \frac{1}{2}\int_0^{L_{y_i}}\int_0^{L_{x_i}} \left(\frac{(\Pi_{x_i})^2}{\rho_i} + \frac{(\Pi_{y_i})^2}{\rho_i} + \frac{(\Psi_i)^2}{\kappa_i} \right) dx\, dy \tag{4.53}$$

The Dirac structure is given by:

$$\begin{aligned} \left\langle e^1, \mathcal{J} e^2 \right\rangle_{L_2,\, d\Omega} &= \iint_\Omega (e^1)^T \mathcal{J} e^2 \, d\Omega \\ &= -\iint_\Omega \left[e_1 \partial_x e_3 + e_3 \partial_x e_1 + e_2 \partial_y e_3 + e_3 \partial_y e_2 \right] \, d\Omega \\ &\quad - \int_0^{L_y} \left[e_1 e_3 + e_3 e_1 \right]_0^{L_x} \, dy - \int_0^{L_x} \left[e_2 e_3 + e_3 e_2 \right]_0^{L_y} \, dx \end{aligned} \tag{4.54}$$

The Dirac structure is given by:

$$\begin{aligned} \left\langle -\mathcal{J} e^1, e^2 \right\rangle_{L_2,\, d\Omega} &= \iint_\Omega (-\mathcal{J} e^1)^T e^2 \, d\Omega \\ &= \iint_\Omega \left[e_1 \partial_x e_3 + e_3 \partial_x e_1 + e_2 \partial_y e_3 + e_3 \partial_y e_2 \right] \, d\Omega \\ &\quad + \int_0^{L_y} \left[e_1 e_3 + e_3 e_1 \right]_0^{L_x} \, dy + \int_0^{L_x} \left[e_2 e_3 + e_3 e_2 \right]_0^{L_y} \, dx \end{aligned} \tag{4.55}$$

The time derivative of the Hamiltonian

$$\begin{aligned} \partial_t H_i &= \iint_\Omega x_i^T \mathcal{L} \left(\partial_t x_i \right) \, d\Omega \\ &= \iint_\Omega x_i^T \mathcal{L} \left(\mathcal{J}^i - \mathcal{G}_R^i \mathcal{S}^i \mathcal{G}_R^{*i} \right) \left(\delta_{x_i} H_i \right) \, d\Omega \\ &= \iint_\Omega e_i^T \left(\mathcal{J}^i - \mathcal{G}_R^i \mathcal{S}^i \mathcal{G}_R^{*i} \right) e_i \, d\Omega \\ &= \int_0^{L_y} \left[-e_1 e_3 - e_3 e_1 + e_1 \mu_i \partial_x e_1 + e_2 \mu_i \partial_x e_2 + e_3 \mu_i \partial_x e_3 \right]_0^{L_x} \, dy \\ &\quad + \int_0^{L_x} \left[-e_2 e_3 - e_3 e_2 + e_1 \mu_i \partial_y e_1 + e_2 \mu_i \partial_y e_2 + e_3 \mu_i \partial_y e_3 \right]_0^{L_y} \, dx \\ &\quad + \iint_\Omega \left[-e_1 \partial_x e_3 - e_2 \partial_y e_3 - e_3 \partial_x e_1 - e_3 \partial_y e_2 + e_1 (\mu_i \partial_x^2 + \mu_i \partial_y^2) e_1 \right. \\ &\quad \left. + e_2 (\mu_i \partial_x^2 + \mu_i \partial_y^2) e_2 + e_3 (\mu_i \partial_x^2 + \mu_i \partial_y^2) e_3 \right] \, d\Omega \end{aligned} \tag{4.56}$$

That is

$$\int_0^{L_y} \begin{bmatrix} e_1 \\ e_2 \\ e_3 \end{bmatrix}^T \begin{bmatrix} 0 & 0 & -1 \\ 0 & 0 & 0 \\ -1 & 0 & 0 \end{bmatrix} \begin{bmatrix} e_1 \\ e_2 \\ e_3 \end{bmatrix} + \begin{bmatrix} e_1 \\ e_2 \\ e_3 \end{bmatrix}^T \begin{bmatrix} \mu_i \partial_x & 0 & 0 \\ 0 & \mu_i \partial_x & 0 \\ 0 & 0 & \mu_i \partial_x \end{bmatrix} \begin{bmatrix} e_1 \\ e_2 \\ e_3 \end{bmatrix} dy \quad (4.57)$$

$$+ \int_0^{L_x} \begin{bmatrix} e_1 \\ e_2 \\ e_3 \end{bmatrix}^T \begin{bmatrix} 0 & 0 & 0 \\ 0 & 0 & -1 \\ 0 & -1 & 0 \end{bmatrix} \begin{bmatrix} e_1 \\ e_2 \\ e_3 \end{bmatrix} + \begin{bmatrix} e_1 \\ e_2 \\ e_3 \end{bmatrix}^T \begin{bmatrix} \mu_i \partial_y & 0 & 0 \\ 0 & \mu_i \partial_y & 0 \\ 0 & 0 & \mu_i \partial_y \end{bmatrix} \begin{bmatrix} e_1 \\ e_2 \\ e_3 \end{bmatrix} dx \quad (4.58)$$

Cochlear partition

The Cochlear partition (C.P.) is modelled as a pair of Euler-Bernoulli beams coupled together by a linear massless distributed spring, of stiffness $K_{5_{ab}}$. The C.P.'s equations of motion are expressed as [88, 71, 87, 77]:

$$\begin{aligned} \rho_{5_a} \partial_t^2 v_{5_a} &= -\partial_x^2 \left(EI_{5_a} \partial_x^2 v_{5_a} \right) - B_{5_a} \partial_t v_{5_a} - K_{5_{ab}} \left(v_{5_a} - v_{5_b} \right) \\ \rho_{5_b} \partial_t^2 v_{5_b} &= -\partial_x^2 \left(EI_{5_b} \partial_x^2 v_{5_b} \right) - B_{5_b} \partial_t v_{5_b} + K_{5_{ab}} \left(v_{5_a} - v_{5_b} \right) \end{aligned} \quad (4.59)$$

where $\rho_{(\cdot)}$ is density per unit length, $v_{(\cdot)}$ is the transverse deflection of the beam, $EI_{(\cdot)}$ is flexural rigidity and $B_{(\cdot)}$ is viscous damping. The subscripts 5, 5_a and 5_b are used to indicate the Cochlear partition and the tectorial and basilar membranes, respectively.

The Port-Hamiltonian state vector of the C.P., x_5, is

$$x_5 = \begin{bmatrix} \Pi_{5_a} & \Psi_{5_a} & \Pi_{5_b} & \Psi_{5_b} & \Phi_{5_{ab}} \end{bmatrix}^T \quad (4.60)$$

where $\Pi_{5_{(\cdot)}} = \rho_{5_{(\cdot)}} \partial_t v_{5_{(\cdot)}}$ and $\Psi_{5_{(\cdot)}} = \partial_x^2 v_{5_{(\cdot)}}$ are is the momentum and curvature of the membranes, respectively and $\Phi_{5_{ab}}$ is the relative displacement between the tectorial and basilar membranes. $\Phi_{5_{ab}}$ is calculated by integrating the difference in membrane velocities

$$\partial_t \Phi_{5_{ab}} = \Pi_{5_a} / \rho_{5_a} - \Pi_{5_b} / \rho_{5_b} \quad (4.61)$$

Taking the time derivative of the state vector x_5, making the appropriate substitutions into equation 4.59, the equations of the C.P. in terms of the P.H. states become

$$\begin{aligned} \partial_t \Pi_{5_a} &= -\partial_x^2 EI_{5_a} \Psi_{5_a} - B_{5_a} \Pi_{5_a} / \rho_{5_a} - K_{5_{ab}} \Phi_{5_{ab}} \\ \partial_t \Psi_{5_a} &= \partial_x^2 \Pi_{5_a} / \rho_{5_a} \\ \partial_t \Pi_{5_b} &= -\partial_x^2 EI_{5_b} \Psi_{5_b} - B_{5_b} \Pi_{5_b} / \rho_{5_b} + K_{5_{ab}} \Phi_{5_{ab}} \\ \partial_t \Psi_{5_b} &= \partial_x^2 \Pi_{5_b} / \rho_{5_b} \end{aligned} \quad (4.62)$$

Equation 4.62 can be derived from the Hamiltonian

$$H_5(x_5) = \frac{1}{2}\int_a^b x_5^T \mathcal{L}_5 x_5 \, dx \tag{4.63}$$

where [71]

$$\mathcal{L}_5 = \begin{bmatrix} 1/\rho_{5_a} & 0 & 0 & 0 & 0 \\ 0 & EI_{5_a} & 0 & 0 & 0 \\ 0 & 0 & 1/\rho_{5_b} & 0 & 0 \\ 0 & 0 & 0 & EI_{5_b} & 0 \\ 0 & 0 & 0 & 0 & K_{5_{ab}} \end{bmatrix}$$

written out in full

$$\begin{aligned} H_5(x_5) &= \frac{1}{2}\int_0^{L_{x5}} \left(\frac{(\Pi_{5_a})^2}{\rho_{5_a}} + EI_{5_a}(\Psi_{5_a})^2 + \frac{(\Pi_{5_b})^2}{\rho_{5_b}} + EI_{5_b}(\Psi_{5_b})^2 \right. \\ &\quad \left. + K_{5_{ab}}(\Phi_{5_{ab}})^2 \right) dx \end{aligned} \tag{4.64}$$

The P.H. model of the C.P. is

$$\begin{aligned} \partial_t x_5 &= \left(\mathcal{J}_5 - \mathcal{G}_R^5 \mathcal{S}^5 \mathcal{G}_R^{*5}\right)(\delta_{x_5} H_5) + G_I^5 u_5 \\ y_5 &= G_I^{*5}(\delta_{x_5} H_5) \end{aligned} \tag{4.65}$$

where

$$\mathcal{J}_5 = P_0^5 + P_1^5 \partial_x + P_2^5 \partial_x^2,$$

$$P_0^5 = P_1^5 = \begin{bmatrix} 0&0&0&0&0 \\ 0&0&0&0&0 \\ 0&0&0&0&0 \\ 0&0&0&0&0 \\ 0&0&0&0&0 \end{bmatrix}, \quad P_2^5 = \begin{bmatrix} 0&-1&0&0&0 \\ 1&0&0&0&0 \\ 0&0&0&-1&0 \\ 0&0&1&0&0 \\ 0&0&0&0&0 \end{bmatrix},$$

$$\mathcal{G}_R^5 = \begin{bmatrix} 1&0&0&0&0 \\ 0&0&0&0&0 \\ 0&0&1&0&0 \\ 0&0&0&0&0 \\ 0&0&0&0&0 \end{bmatrix}, \quad \mathcal{G}_R^{*5} = -(\mathcal{G}_R^5)^T, \quad \mathcal{S}_5 = -\begin{bmatrix} B_{5_a}&0&0&0&0 \\ 0&0&0&0&0 \\ 0&0&B_{5_b}&0&0 \\ 0&0&0&0&0 \\ 0&0&0&0&0 \end{bmatrix},$$

$$G_I^5 = \begin{bmatrix} 1&0 \\ 0&0 \\ 0&1 \\ 0&0 \\ 0&0 \end{bmatrix}, \quad u_5 = \begin{bmatrix} u_{5_a} \\ u_{5_b} \end{bmatrix}, \quad (\delta_{x_5} H_5) = \mathcal{L}_5 x_5 = \begin{bmatrix} \Pi_{5_a}/\rho_{5_a} \\ EI_{5_a}\Psi_{5_a} \\ \Pi_{5_b}/\rho_{5_b} \\ EI_{5_b}\Psi_{5_b} \\ K_{5_{ab}}\Phi_{5_{ab}} \end{bmatrix} \tag{4.66}$$

The boundary ports are

$$\begin{bmatrix} f\partial \\ e\partial \end{bmatrix} = \frac{1}{\sqrt{2}} \begin{bmatrix} Q_5 & -Q_5 \\ I & I \end{bmatrix} \begin{bmatrix} \delta_{x_5} H_5(b) \\ \delta_{x_5} H_5(a) \end{bmatrix} = \frac{1}{\sqrt{2}} \begin{bmatrix} EI_{5_a}\Psi_{5_a}(a) - EI_{5_a}\Psi_{5_a}(b) \\ \Pi_{5_a}/\rho_{5_a}(b) - \Pi_{5_a}/\rho_{5_a}(a) \\ EI_{5_b}\Psi_{5_b}(a) - EI_{5_b}\Psi_{5_b}(b) \\ \Pi_{5_b}/\rho_{5_b}(b) - \Pi_{5_b}/\rho_{5_b}(a) \\ \Pi_{5_a}/\rho_{5_a}(a) + \Pi_{5_a}/\rho_{5_a}(b) \\ EI_{5_a}\Psi_{5_a}(a) + EI_{5_a}\Psi_{5_a}(b) \\ \Pi_{5_b}/\rho_{5_b}(a) + \Pi_{5_b}/\rho_{5_b}(b) \\ EI_{5_b}\Psi_{5_b}(a) + EI_{5_b}\Psi_{5_b}(b) \end{bmatrix} \tag{4.67}$$

where

$$Q_5 = P_2^5 \tag{4.68}$$

4.3.8 Inner ear results and discussion

An initial condition (non-zero velocity towards the edges of the Basilar membrane) resulted in waves of vibration moving towards the centre of the Basilar membrane as shown in figure 4.9. This was done to test the coupling between the basilar and tectorial membranes and the fluids in the Scala Vestibula and Scala Tympani. Figure 4.10 shows the response of the fluid in the Scala Vestibula at a point in time due to the movement of the Basilar membrane. The movement of the Basilar membrane causes the fluid to move at its lower boundary and the motion is transmitted to the rest of the fluid. The result of the Scala Tympani is similar and is not shown. Figure 4.11 and 4.12 show that coupling is present, by the relative motion of the Cochlear partition and the motion of the Tectorial, respectively.

The sensitivity of the human ear changes as a function of frequency. Figure 4.13 shows the Sound Pressure Level (SPL) required for the frequencies to be perceived as loud. When sensorineural hearing loss (damage to the cochlea) is present, the perception of loudness is altered. Typically hearing tests are performed over a range of frequencies for instance from 250 to 8000 Hz. The hearing threshold is measured in decibels relative to the normal threshold. Hearing loss is caused by a dip near the 4000 Hz.

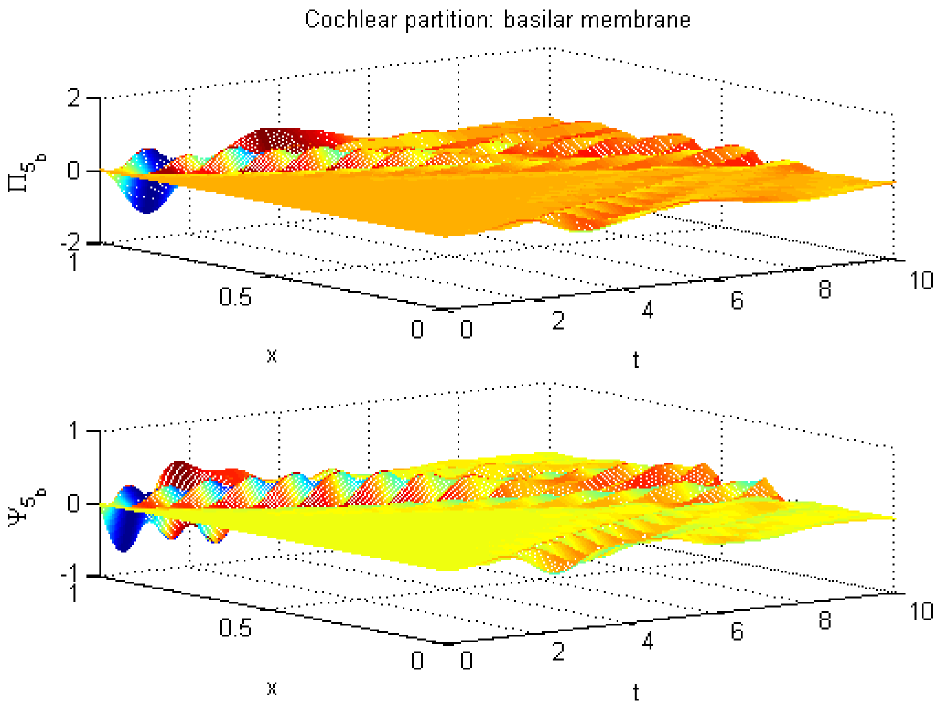

Figure 4.9: Response of the Basilar membrane 10 seconds after application of the disturbance

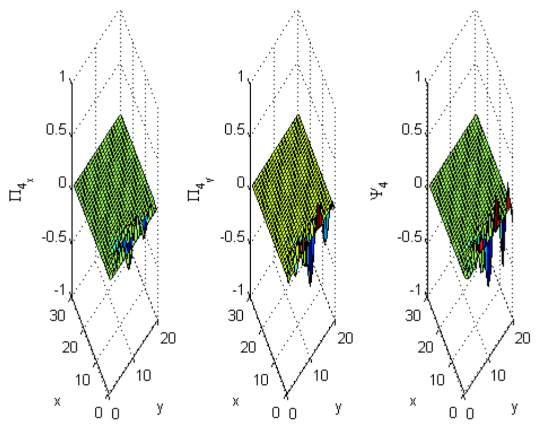

Figure 4.10: Response of the Scala Vestibula at a time instant

4.3.9 Outer Hair Cells modelling

Given the Perilymph has a resting potential $\psi_{5_{d0}}$, the Outer Hair Cells are modelled based on an the equivalent circuit model method as shown in figure 4.14[77, 78].

$$\partial_t \psi_{5_d} = \omega_{5_d}(\psi_{5_d} - \psi_{5_{d0}}) + \eta_{5_d}\phi_{5_{ab}} \tag{4.69}$$

where ψ_{5_d} and ω_{5_d} are the voltage and cut-off frequency of the OHC surface, respectively, η_{5_d} is a constant conversion factor and $\phi_{5_{ab}}$ is the relative displacement of the Basilar and Tectorial membranes. $\phi_{5_{ab}}$ is obtained by integrating $\Phi_{5_{ab}}$.

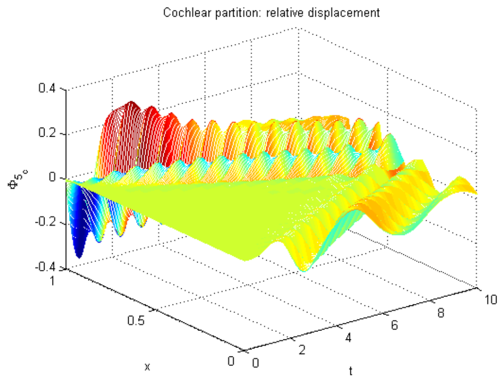

Figure 4.11: Cochlear partition relative velocity

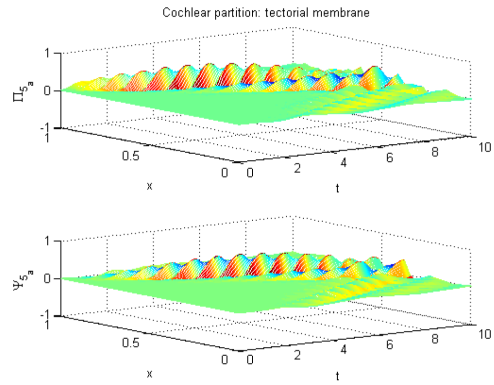

Figure 4.12: Tectorial membrane

The Port-Hamiltonian state vector of the OHC is x_{5_d}

$$x_{5_d} = \begin{bmatrix} \Psi_{5_d} \end{bmatrix} = \begin{bmatrix} \psi_{5_d} \end{bmatrix} \tag{4.70}$$

The Hamiltonian function H_{5_d} is given by

$$H_{5_d} = \frac{1}{2}\omega_{5_d}(\Psi_{5_d} - \Psi_{5_{d0}})^2 \tag{4.71}$$

The P.H. model of the OHC is

$$\partial_t x_{5_d} = \mathcal{J}_{5_d}(\delta_{5_d} H_{5_d}) + G_{5_d} u_{5_d} \tag{4.72}$$

$$y_{5_d} = G_I^{*5_d}(\delta_{5_d} H_{5_d}) \tag{4.73}$$

The pressure applied by the OHC onto the Basilar and Tectorial membranes P_{ohc} is [77, 78]

$$P_{ohc}(x,t) = K_{5_{ab}}(\phi_{5_{ab}} - \Delta_{ohc}) \tag{4.74}$$

where Δ_{ohc} is the deflection of the outer hair cell [77, 78]

$$\Delta_{ohc} = \alpha_s \tanh(-\alpha x_{5_d}) \tag{4.75}$$

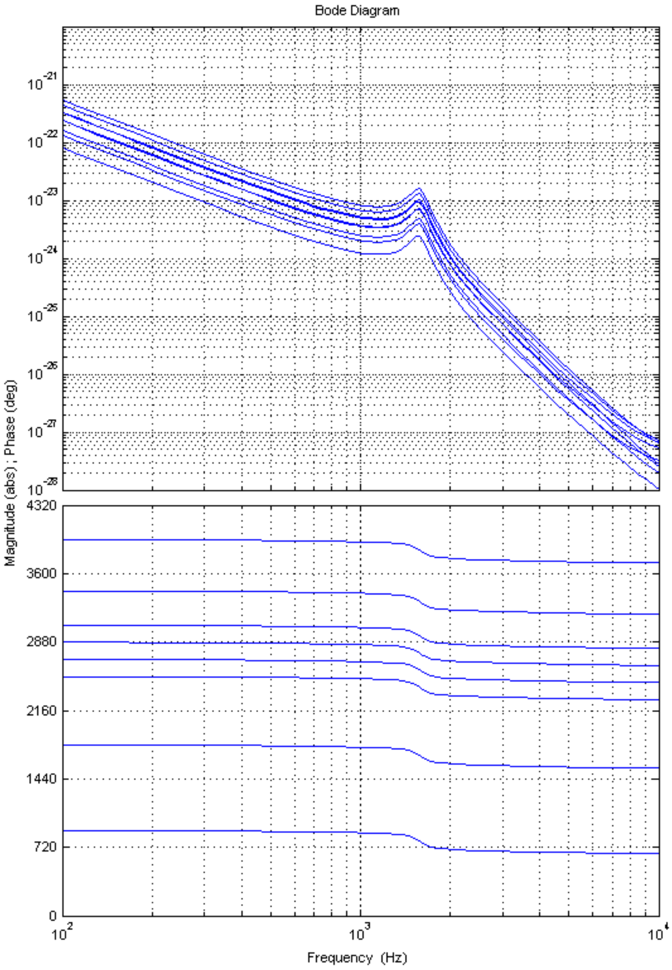

Figure 4.13: Cochlear frequency response

where α_1 and α_s are the reference voltage and peak to peak deflection due to electro-mobility.

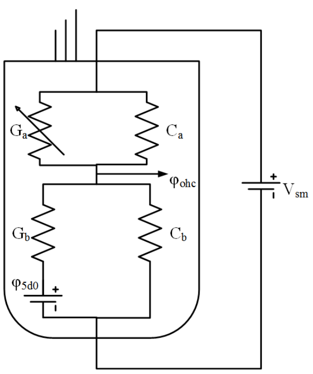

Figure 4.14: Outer Hair Cell electrical circuit model [77, 78]

4.3.10 Outer Hair Cells results and discussion

Figure 4.15 shows the frequency response of the OHC at 0.3889cm, 1.1667cm, 1.9444cm, 2.7222cm and 3.5cm from the base of the Cochlear.

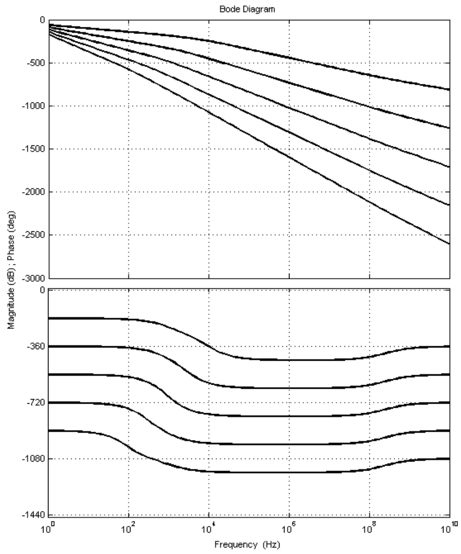

Figure 4.15: Outer Hair Cell frequency response, at the points 0.3889cm, 1.1667cm, 1.9444cm, 2.7222cm and 3.5cm from the base of the Cochlear

The cochlear displacement velocity is mainly enhanced by the OHC activities. For frequencies that are greater than 1 KHz which is the cutoff frequency of the OHCs membrane, the enhancement becomes very significant. The basilar membrane motion is very sensitive to the any change in the gain of the OHCs. ONIHL is traditionally observed by an audiogram whose maximum threshold shift occurs at 4KHz. This model is consistent with the assumption by Furst [77, 78] et al which proposes that the loss of OHCs occurs randomly along the cochlea in humans. This is further supported by current research that indicates that the loss in hearing sensitivity in humans that occurs at 4 KHz is independent of the type of noise exposure [77, 78]. Presbycusis is characterized by hearing loss at high frequencies. The proposed Port-Hamiltonian model only deals with OHC hearing loss. It is therefore assumed that the loss of IHC that usually follows OHC loss is the cause of profound hearing loss. The Port-Hamiltonian results of the OHCs were validated against Furst et al [77, 78] and were found to be comparable and followed a similar pattern of behaviour [77, 78].

4.4 Model discretization

In order for the model to be simulated it is essential to perform discretization. The process used to discretize this model is presented in detail in the subsections that follow.

4.4.1 Ear Canal

The discrete form of $\mathcal{J}$, formally skew symmetric matrix, is given by

$$J = -\begin{bmatrix} O & O & J_\Pi \\ O & O & J_\Theta \\ J_\Pi & J_\Theta & O \end{bmatrix} \tag{4.76}$$

where O is a zero matrix with a diagonal that has $n_x \times n_y$ elements. J_Π and J_Θ are obtained by factorizing the central difference approximations of the fluid momentum in the $x-$ and $y-$ axis directions, respectively. These approximations are given by

$$\partial_x \Pi \approx \bar{J}_\Pi = \frac{\Pi_{i-1}^{j} - \Pi_{i+1}^{j}}{2\Delta_x} \tag{4.77}$$

and

$$\partial_x \Theta \approx \bar{J}_\Theta = \frac{\Theta_i^{j-1} - \Theta_i^{j+1}}{2\Delta_y} \tag{4.78}$$

respectively, where i and j are used to index the discrete fluid cells as shown in figure 4.19, $i = 1, 2, \cdots, n_x - 1, n_x$ and $j = 1, 2, \cdots, n_y - 1, n_y$, for n_x cells along the $x-$axis direction and n_y cells along the $y-$axis direction. The length of an individual cell along the $x-$axis and $y-$axis directions is given by

$$\Delta_x = \frac{L_x}{(n_x - 1)} \tag{4.79}$$

and

$$\Delta_y = \frac{L_y}{(n_y - 1)} \tag{4.80}$$

where L_x and L_y are the lengths of the fluid chamber along the $x-$axis and $y-$axis directions, respectively. The state vector is given by

$$x = \begin{bmatrix} \Pi \\ \Theta \\ \Psi \end{bmatrix} \tag{4.81}$$

where

$$\Pi = \begin{bmatrix} \Pi_1^1 \\ \vdots \\ \Pi_{n_x}^1 \\ \Pi_1^2 \\ \vdots \\ \Pi_{n_x}^2 \\ \Pi_1^{n_y-1} \\ \vdots \\ \Pi_{n_x}^{n_y-1} \\ \Pi_1^{n_y} \\ \vdots \\ \Pi_{n_x}^{n_y} \end{bmatrix}, \quad \Theta = \begin{bmatrix} \Theta_1^1 \\ \vdots \\ \Theta_{n_x}^1 \\ \Theta_1^2 \\ \vdots \\ \Theta_{n_x}^2 \\ \Theta_1^{n_y-1} \\ \vdots \\ \Theta_{n_x}^{n_y-1} \\ \Theta_1^{n_y} \\ \vdots \\ \Theta_{n_x}^{n_y} \end{bmatrix}, \quad \Psi = \begin{bmatrix} \Psi_1^1 \\ \vdots \\ \Psi_{n_x}^1 \\ \Psi_1^2 \\ \vdots \\ \Psi_{n_x}^2 \\ \Psi_1^{n_y-1} \\ \vdots \\ \Psi_{n_x}^{n_y-1} \\ \Psi_1^{n_y} \\ \vdots \\ \Psi_{n_x}^{n_y} \end{bmatrix} \tag{4.82}$$

Factorizing $\bar{J}_\Theta$, the matrix J_Θ of dimension $n_x \times n_y$ along its diagonal is given by

$$J_\Theta = \begin{bmatrix} 0 & -1 & 0 & \cdots & 0 & 0 & 0 & 0 \\ 1 & 0 & -1 & 0 & \ddots & \ddots & 0 & 0 \\ 0 & 1 & 0 & -1 & \ddots & \ddots & \ddots & 0 \\ \vdots & \ddots & 1 & 0 & \ddots & \ddots & \ddots & 0 \\ 0 & \ddots & \ddots & \ddots & \ddots & -1 & \ddots & \vdots \\ 0 & \ddots & \ddots & \ddots & 1 & 0 & -1 & 0 \\ 0 & 0 & \ddots & \ddots & \ddots & 1 & 0 & -1 \\ 0 & 0 & 0 & 0 & \cdots & 0 & 1 & 0 \end{bmatrix} \tag{4.83}$$

The components of the symmetric dissipation matrix R_x and R_y are

$$\bar{R}_x = \nu \left(\frac{\Pi_{i-1}^j - 2\Pi_i^j + \Pi_{i+1}^j}{\Delta_x} \right) + \nu \left(\frac{\Theta_i^{j-1} - 2\Theta_i^j + \Theta_i^{j+1}}{\Delta_y} \right) \tag{4.84}$$

$$\bar{R}_y = \nu \left(\frac{\Pi_{i-1}^j - 2\Pi_i^j + \Pi_{i+1}^j}{\Delta_x} \right) + \nu \left(\frac{\Theta_i^{j-1} - 2\Theta_i^j + \Theta_i^{j+1}}{\Delta_y} \right) \tag{4.85}$$

where ν is the fluid viscosity. Factorizing the matrices $\bar{R}_x$ and $\bar{R}_y$

$$\bar{R}_x = R_x \Pi \tag{4.86}$$

$$\bar{R}_y = R_y \Theta \tag{4.87}$$

for example when $n_x = 4$ and $n_y = 3$, R_x and R_y take the following form

$$R_x = R_y = \left[\begin{array}{cccccccccccc}
* & * & & & * & & & & & & & \\
* & * & * & & & * & & & & & & \\
& * & * & * & & & * & & & & & \\
& & * & * & & & & * & & & & \\
* & & & & * & * & & & * & & & \\
& * & & & * & * & * & & & * & & \\
& & * & & & * & * & * & & & * & \\
& & & * & & & * & * & & & & * \\
& & & & * & & & & * & * & & \\
& & & & & * & & & * & * & * & \\
& & & & & & * & & & * & * & * \\
& & & & & & & * & & & * & *
\end{array}\right] \tag{4.88}$$

where the asterisks $*$ are used for non-zero entries in the matrix whose values are

$$R_x(i,j) = R_y(i,j) = -\nu\frac{2}{\Delta_x} - \nu\frac{2}{\Delta_y}, \qquad \text{for } i = j \tag{4.89}$$

$$\begin{aligned} R_x(i + (j-1)n_x, i + (j-1)n_x + 1) &= \nu\frac{1}{\Delta_x} \\ \text{for } i = 1, \cdots, n_x - 1 \quad j &= 1, \cdots, n_y \end{aligned} \tag{4.90}$$

$$\begin{aligned} R_y(i + (j-1)n_x + 1, i + (j-1)n_x) &= \nu\frac{1}{\Delta_x} \\ \text{for } i = 1, \cdots, n_x \quad j &= 1, \cdots, n_y - 1 \end{aligned} \tag{4.91}$$

The symmetric dissipation matrix R is

$$R = -\begin{bmatrix} R_x & O & O \\ O & R_y & O \\ O & O & O \end{bmatrix} \tag{4.92}$$

where O is a zero matrix that has a diagonal with $n_x \times n_y$ elements. The matrix $\mathcal{L}$ is given by

$$\mathcal{L} = \begin{bmatrix} 1/\rho \times I & O & O \\ O & 1/\rho \times I & O \\ O & O & 1/\kappa \times I \end{bmatrix} \tag{4.93}$$

where I is an identity matrix with a diagonal of $n_x \times n_y$ elements and O is a zero matrix with a diagonal that has $n_x \times n_y$ elements.

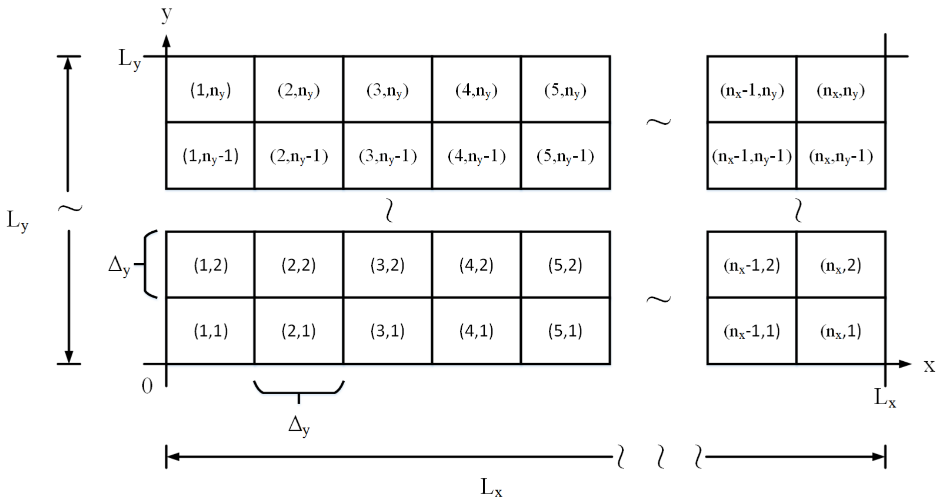

Figure 4.16: Ear canal fluid discretization, where (i, j) is the cell index for $i = 1, 2, \cdots, n_x - 1, n_x$ and $i = 1, 2, \cdots, n_y - 1, n_y$, Δ_x and L_x are the step size and the length along the $x-$axis, respectively and Δ_y and L_y are the step size and the length along the $y-$axis, respectively

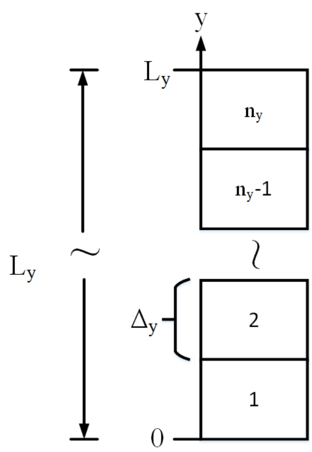

Figure 4.17: Tympanic membrane discretization, where $i = 1, 2, \cdots, n_y - 1, n_y$ is the cell index and Δ_y is the step size and L_y is the length along the $y-$axis

4.4.2 Tympanic membrane

Figure 4.17 shows the discrete Tympanic membrane. It consists of n_y cell elements of length Δ_y given by

$$\Delta_y = \frac{L_y}{(n_y - 1)} \tag{4.94}$$

where $n_y > 1$ is the number of discrete elements and L_y is the length of the membrane. The matrix $\mathcal{L}$ is given by

$$\mathcal{L} = \begin{bmatrix} \mathcal{L}_\rho & O \\ O & \mathcal{L}_{EI} \end{bmatrix} \tag{4.95}$$

where O is a $n_y \times n_y$ zero matrix. The diagonal elements of the matrices $\mathcal{L}_\rho$ and $\mathcal{L}_{EI}$ are given by

$$\mathcal{L}_\rho = \text{diag}\begin{pmatrix} 1/\rho_1 & 1/\rho_2 & \cdots & 1/\rho_{n_y-1} & 1/\rho_{n_y} \end{pmatrix} \tag{4.96}$$

where ρ_i is the density of element i along the length of the membrane and

$$\mathcal{L}_{EI} = \text{diag}\begin{pmatrix} EI_1 & EI_2 & \cdots & EI_{n_y-1} & EI_{n_y} \end{pmatrix} \tag{4.97}$$

where EI_i is the Young's modulus of element i along the length of the membrane. The state vector x is given by

$$x = \begin{bmatrix} \Pi \\ \Theta \end{bmatrix} \tag{4.98}$$

where the momentum, Π, and curvature, Θ, are vectors of dimension $n_y \times 1$ given by

$$\Pi \quad = \quad \begin{bmatrix} \Pi^1 & \Pi^2 & \cdots & \Pi^{n_y-1} & \Pi^{n_y} \end{bmatrix}^T \tag{4.99}$$

and

$$\Theta \quad = \quad \begin{bmatrix} \Theta^1 & \Theta^2 & \cdots & \Theta^{n_y-1} & \Theta^{n_y} \end{bmatrix}^T \tag{4.100}$$

The discretization for of the skew symmetric matrix $\mathcal{J}$ is given by

$$\mathcal{J} = \begin{bmatrix} O & -J_\Theta \\ J_\Pi & O \end{bmatrix} \tag{4.101}$$

where O is a zero matrix of dimension $n_y \times n_y$. J_Θ and J_Π are found by factorizing the discrete second order approximations of the momentum

$$\partial_y^2 \Pi \approx \frac{\Pi^{j-1} - 2\Pi^j + \Pi^{j+1}}{\Delta_y} = \bar{J}_\Pi \tag{4.102}$$

and curvature

$$\partial_y^2 \Theta \approx \frac{\Theta^{j-1} - 2\Theta^j + \Theta^{j+1}}{\Delta_y} = \bar{J}_\Theta \tag{4.103}$$

where $j = 1, 2, \cdots, n_y - 1, n_y$.

$$\bar{J}_\Pi = J_\Pi \Pi = \begin{bmatrix} -2 & 1 & & & & & \\ 1 & -2 & 1 & & & & \\ & 1 & -2 & \ddots & & & \\ & & \ddots & \ddots & \ddots & & \\ & & & \ddots & -2 & 1 & \\ & & & & 1 & -2 & 1 \\ & & & & & 1 & -2 \end{bmatrix} \begin{bmatrix} \Pi_1 \\ \Pi_2 \\ \vdots \\ \vdots \\ \vdots \\ \Pi_{n_y-1} \\ \Pi_{n_y} \end{bmatrix} \tag{4.104}$$

and

$$\bar{J}_\Theta = J_\Theta \Theta = \begin{bmatrix} -2 & 1 & & & & & \\ 1 & -2 & 1 & & & & \\ & 1 & -2 & \ddots & & & \\ & & \ddots & \ddots & \ddots & & \\ & & & \ddots & -2 & 1 & \\ & & & & 1 & -2 & 1 \\ & & & & & 1 & -2 \end{bmatrix} \begin{bmatrix} \Theta_1 \\ \Theta_2 \\ \vdots \\ \vdots \\ \vdots \\ \Theta_{n_y-1} \\ \Theta_{n_y} \end{bmatrix} \tag{4.105}$$

J_Π and J_Θ are matrices with three diagonals (the remaining elements of these matrices are zeroes).

4.4.3 Tectorial and Basilar membranes

The Tectorial and Basilar membranes are discretized into n_x cell elements of equal length Δ_x as shown in figure 4.18. Δ_x is given below

$$\Delta_x = \frac{L_x}{(n_x - 1)} \tag{4.106}$$

where L_x is the length of the membrane and $n_x > 1$ is the number of discrete elements. The state vector x is given by

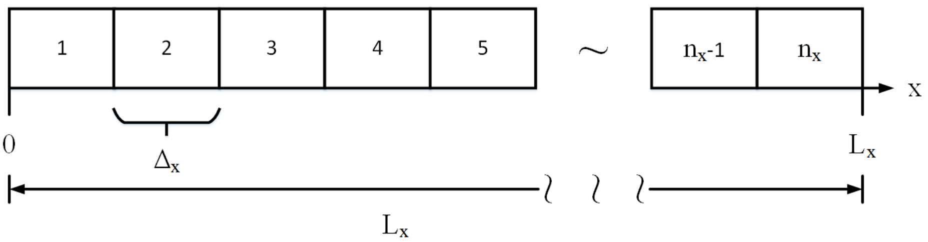

Figure 4.18: Tectorial and Basilar membrane discretization, where $i = 1, 2, \cdots, n_x - 1, n_x$ is the cell index, Δ_x and L_x are the step size and the length along the $x-$axis

$$x = \begin{bmatrix} \Pi \\ \Theta \end{bmatrix} \tag{4.107}$$

where the momentum, Π, and curvature, Θ, are given by n_x discrete elements

$$\Pi = \begin{bmatrix} \Pi_1 & \Pi_2 & \cdots & \Pi_{n_x-1} & \Pi_{n_x} \end{bmatrix}^T \tag{4.108}$$

$$\Theta = \begin{bmatrix} \Theta_1 & \Theta_2 & \cdots & \Theta_{n_x-1} & \Theta_{n_x} \end{bmatrix}^T \tag{4.109}$$

The second order partial derivatives of Π and Θ are approximated as

$$\bar{J}_\Pi = \frac{\Pi_{i-1} - 2\Pi_i + \Pi_{i+1}}{\Delta_x} \approx \partial_x^2 \Pi \tag{4.110}$$

and

$$\bar{J}_\Theta = \frac{\Theta_{i-1} - 2\Theta_i + \Theta_{i+1}}{\Delta_x} \approx \partial_x^2 \Theta \tag{4.111}$$

where $i = 2, 3, \cdots, n_x - 1, n_x$. Factorizing $\bar{J}_\Pi$ and $\bar{J}_\Theta$, the discrete skew symmetric matrix $\mathcal{J}$ is given by

$$\mathcal{J} = \begin{bmatrix} O & J_\Pi \\ J_\Phi & O \end{bmatrix} \tag{4.112}$$

where O is a zero matrix of dimension $n_x \times n_x$,

$$\bar{J}_\Pi = J_\Pi \Pi = \begin{bmatrix} -2 & 1 & & & & & \\ 1 & -2 & 1 & & & & \\ & 1 & -2 & \ddots & & & \\ & & \ddots & \ddots & \ddots & & \\ & & & \ddots & -2 & 1 & \\ & & & & 1 & -2 & 1 \\ & & & & & 1 & -2 \end{bmatrix} \begin{bmatrix} \Pi_1 \\ \Pi_2 \\ \vdots \\ \vdots \\ \vdots \\ \Pi_{n_x-1} \\ \Pi_{n_x} \end{bmatrix} \tag{4.113}$$

and

$$\bar{J}_\Theta = J_\Theta \Theta = \begin{bmatrix} -2 & 1 & & & & & \\ 1 & -2 & 1 & & & & \\ & 1 & -2 & \ddots & & & \\ & & \ddots & \ddots & \ddots & & \\ & & & \ddots & -2 & 1 & \\ & & & & 1 & -2 & 1 \\ & & & & & 1 & -2 \end{bmatrix} \begin{bmatrix} \Theta_1 \\ \Theta_2 \\ \vdots \\ \vdots \\ \vdots \\ \Theta_{n_x-1} \\ \Theta_{n_x} \end{bmatrix} \tag{4.114}$$

J_Π and J_Θ are matrices with three diagonals (the remaining elements of these matrices are zeros). The matrix $\mathcal{L}$ is given by

$$\mathcal{L} = \begin{bmatrix} \mathcal{L}_\rho & O \\ O & \mathcal{L}_{EI} \end{bmatrix} \tag{4.115}$$

where O is a $n_x \times n_x$ zero matrix. The diagonal elements of the matrix $\mathcal{L}_\rho$ and $\mathcal{L}_{EI}$ are given by

$$\mathcal{L}_\rho = \mathrm{diag}\begin{pmatrix} 1/\rho_1 & 1/\rho_2 & \cdots & 1/\rho_{n_x-1} & 1/\rho_{n_x} \end{pmatrix} \tag{4.116}$$

and

$$\mathcal{L}_{EI} = \mathrm{diag}\Big(EI_1 \quad EI_2 \quad \cdots \quad EI_{n_x-1} \quad EI_{n_x}\Big) \tag{4.117}$$

respectively, where ρ_i is the density and EI_i is the Young's modulus of element i along the length of the membrane.

4.4.4 Scala Tympani and Scala Vestibula

The matrix $\mathcal{L}$ is given by

$$\mathcal{L} = \begin{bmatrix} 1/\rho \times I & O & O \\ O & 1/\rho \times I & O \\ O & O & 1/\kappa \times I \end{bmatrix} \tag{4.118}$$

where I is an identity matrix with a diagonal of $n_x \times n_y$ elements and O is a zero matrix with a diagonal that has $n_x \times n_y$ elements. The discrete form of $\mathcal{J}$, formally skew symmetric matrix, is given by

$$J \quad = \quad - \begin{bmatrix} O & O & J_\Pi \\ O & O & J_\Theta \\ J_\Pi & J_\Theta & O \end{bmatrix} \tag{4.119}$$

where O is a zero matrix with a diagonal that has $n_x \times n_y$ elements. J_Π and J_Θ are obtained by factorizing the central difference approximations of the fluid momentum in the $x-$ and $y-$ axis directions, respectively. These approximations are given by

$$\partial_x \Pi \approx \bar{J}_\Pi \quad = \quad \frac{\Pi^j_{i-1} - \Pi^j_{i+1}}{2\Delta_x} \tag{4.120}$$

and

$$\partial_x \Theta \approx \bar{J}_\Theta \quad = \quad \frac{\Theta^{j-1}_i - \Theta^{j+1}_i}{2\Delta_y} \tag{4.121}$$

respectively, where i and j are used to index the discrete fluid cells as shown in figure 4.19, $i = 1, 2, \cdots, n_x - 1, n_x$ and $j = 1, 2, \cdots, n_y - 1, n_y$, for n_x cells along the $x-$axis direction and n_y cells along the $y-$axis direction. The length of an individual cell along the $x-$axis and $y-$axis directions are given by

$$\Delta_x = \frac{L_x}{(n_x - 1)} \tag{4.122}$$

and

$$\Delta_y = \frac{L_y}{(n_y - 1)} \tag{4.123}$$

where L_x and L_y are the lengths of the fluid chamber along the $x-$axis and $y-$axis directions, respectively. The state vector is given by

$$x = \begin{bmatrix} \Pi \\ \Theta \\ \Psi \end{bmatrix} \tag{4.124}$$

where

$$\Pi = \begin{bmatrix} \Pi_1^1 \\ \vdots \\ \Pi_{n_x}^1 \\ \Pi_1^2 \\ \vdots \\ \Pi_{n_x}^2 \\ \Pi_1^{n_y-1} \\ \vdots \\ \Pi_{n_x}^{n_y-1} \\ \Pi_1^{n_y} \\ \vdots \\ \Pi_{n_x}^{n_y} \end{bmatrix}, \quad \Theta = \begin{bmatrix} \Theta_1^1 \\ \vdots \\ \Theta_{n_x}^1 \\ \Theta_1^2 \\ \vdots \\ \Theta_{n_x}^2 \\ \Theta_1^{n_y-1} \\ \vdots \\ \Theta_{n_x}^{n_y-1} \\ \Theta_1^{n_y} \\ \vdots \\ \Theta_{n_x}^{n_y} \end{bmatrix}, \quad \Psi = \begin{bmatrix} \Psi_1^1 \\ \vdots \\ \Psi_{n_x}^1 \\ \Psi_1^2 \\ \vdots \\ \Psi_{n_x}^2 \\ \Psi_1^{n_y-1} \\ \vdots \\ \Psi_{n_x}^{n_y-1} \\ \Psi_1^{n_y} \\ \vdots \\ \Psi_{n_x}^{n_y} \end{bmatrix} \tag{4.125}$$

Factorizing $\bar{J}_\Theta$, the matrix J_Θ of dimension $n_x \times n_y$ along its diagonal is given by

$$J_\Theta = \begin{bmatrix} 0 & -1 & 0 & \cdots & 0 & 0 & 0 & 0 \\ 1 & 0 & -1 & 0 & \ddots & \ddots & 0 & 0 \\ 0 & 1 & 0 & -1 & \ddots & \ddots & \ddots & 0 \\ \vdots & \ddots & 1 & 0 & \ddots & \ddots & \ddots & 0 \\ 0 & \ddots & \ddots & \ddots & \ddots & -1 & \ddots & \vdots \\ 0 & \ddots & \ddots & \ddots & 1 & 0 & -1 & 0 \\ 0 & 0 & \ddots & \ddots & \ddots & 1 & 0 & -1 \\ 0 & 0 & 0 & 0 & \cdots & 0 & 1 & 0 \end{bmatrix} \tag{4.126}$$

The components of the symmetric dissipation matrix R_x and R_y are

$$\bar{R}_x = \nu \left(\frac{\Pi_{i-1}^j - 2\Pi_i^j + \Pi_{i+1}^j}{\Delta_x} \right) + \nu \left(\frac{\Theta_i^{j-1} - 2\Theta_i^j + \Theta_i^{j+1}}{\Delta_y} \right) \tag{4.127}$$

$$\bar{R}_y = \nu \left(\frac{\Pi_{i-1}^j - 2\Pi_i^j + \Pi_{i+1}^j}{\Delta_x} \right) + \nu \left(\frac{\Theta_i^{j-1} - 2\Theta_i^j + \Theta_i^{j+1}}{\Delta_y} \right) \tag{4.128}$$

where ν is the fluid viscosity. Factorizing the matrices $\bar{R}_x$ and $\bar{R}_y$

$$\bar{R}_x = R_x \Pi \tag{4.129}$$

$$\bar{R}_y = R_y \Theta \tag{4.130}$$

for example when $n_x = 4$ and $n_y = 3$, R_x and R_y take the following form

$$R_x = R_y = \begin{bmatrix}
* & * & & & * & & & & & & & \\
* & * & * & & & * & & & & & & \\
& * & * & * & & & * & & & & & \\
& & * & * & & & & * & & & & \\
* & & & & * & * & & & * & & & \\
& * & & & * & * & * & & & * & & \\
& & * & & & * & * & * & & & * & \\
& & & * & & & * & * & & & & * \\
& & & & * & & & & * & * & & \\
& & & & & * & & & * & * & * & \\
& & & & & & * & & & * & * & * \\
& & & & & & & * & & & * & *
\end{bmatrix} \tag{4.131}$$

where the asterisks $*$ are used for non-zero entries in the matrix whose values are

$$R_x(i,j) = R_y(i,j) = -\nu \frac{2}{\Delta_x} - \nu \frac{2}{\Delta_y}, \qquad \text{for } i = j \tag{4.132}$$

$$\begin{aligned} R_x(i + (j-1)n_x, i + (j-1)n_x + 1) &= \nu \frac{1}{\Delta_x} \\ \text{for } i = 1, \cdots, n_x - 1 \quad j &= 1, \cdots, n_y \end{aligned} \tag{4.133}$$

$$\begin{aligned} R_y(i + (j-1)n_x + 1, i + (j-1)n_x) &= \nu \frac{1}{\Delta_x} \\ \text{for } i = 1, \cdots, n_x \quad j &= 1, \cdots, n_y - 1 \end{aligned} \tag{4.134}$$

The symmetric dissipation matrix R is

$$R = -\begin{bmatrix} R_x & O & O \\ O & R_y & O \\ O & O & O \end{bmatrix} \tag{4.135}$$

where O is a zero matrix that has a diagonal with $n_x \times n_y$ elements.

4.5 Model interconnection/Coupling

The individual Port-Hamiltonian model sub-systems were coupled by considering the following boundary conditions:

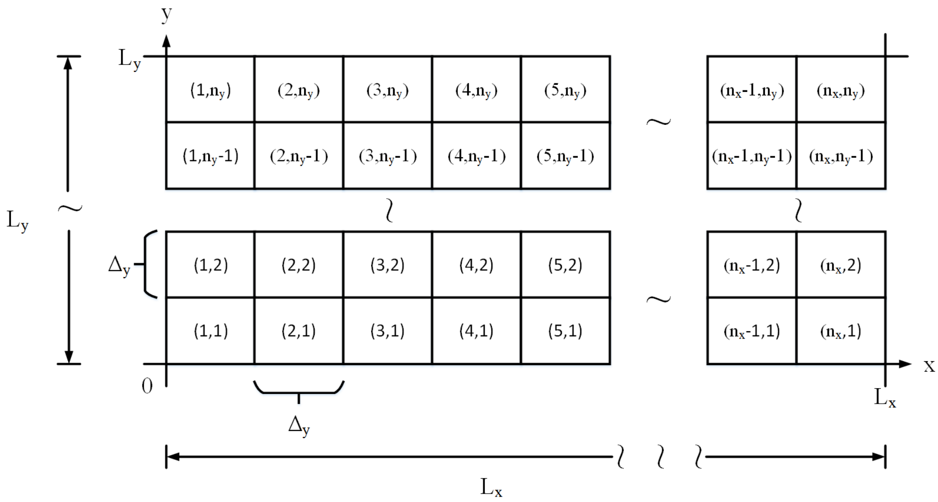

Figure 4.19: Scala Tympani and Scala Vestibula fluid discretization, where (i, j) is the cell index for $i = 1, 2, \cdots, n_x - 1, n_x$ and $i = 1, 2, \cdots, n_y - 1, n_y$, Δ_x and L_x are the step size and the length along the $x-$axis, respectively and Δ_y and L_y are the step size and the length along the $y-$axis, respectively

1. Sound Source/Ear canal interconnection:

   - Sound pressure at the source is equal to the pressure at the entrance of the ear canal

$$P_{source}(t) = \frac{\Psi_1(t, 0, y)}{\kappa} \tag{4.136}$$

2. Ear canal/Tympanic membrane interconnection:

   - At their interface, the Ear Canal's air momentum component along the $x-$axis direction, Π_1, is equal to the momentum of the Tympanic membrane:

$$\Pi_1(t, L_x, y) = \Pi_2(t, y) \tag{4.137}$$

   - At their interface, air pressure of the Ear Canal, Ψ_1, is equal to the force per unit area of Tympanic membrane:

$$\frac{\Psi_1(t, L_x, y)}{\kappa_1} = \frac{F_2(t, y)}{A_2} \tag{4.138}$$

   assuming the area of contact remains constant.

3. Tympanic membrane/Middle Ear interconnection:

- The momentum of the Tympanic membrane, Π_2, is equal to the momentum of the Malleus at their interface:

$$\Pi_2(t, L_x, \frac{L_y}{2}) = \Pi_{3_a}(t) \tag{4.139}$$

4. Middle Ear/Cochlear Partition interconnection:

- The momentum of the Stapes, Π_{3_c}, is equal to the momentum of the fluid in the Scala Vestibula at their interface:

$$\Pi_{3_c}(t) = \Pi_4(t, 0, y) \tag{4.140}$$

- The force of the Stapes, F_{3_c}, is equal to the fluid pressure per unit area applied by the Scala Vestibula at their interface:

$$F_{3_c}(t) = \frac{\Psi_4(t, 0, y)}{A_{3_c}} \tag{4.141}$$

assuming the area of contact remains constant.

- The momentum of the round window, Π_{3_d}, is equal to the momentum of the fluid in the Scala Tympani at their interface:

$$\Pi_{3_d}(t) = \Pi_6(t, 0, y) \tag{4.142}$$

- The force of the round window, F_{3_d}, is equal to the fluid pressure per unit area applied by the Scala Tympani at their interface:

$$F_{3_c}(t) = \frac{\Psi_6(t, 0, y)}{A_{3_d}} \tag{4.143}$$

assuming the area of contact remains constant.

5. Scala Vestibula and Tectorial Membrane:

- The momentum of the Scala Vestibula fluid, Θ_4, is equal to the momentum of the Tectorial membrane at their interface:

$$\Theta_4(t, x, 0) = \Pi_{5_a}(t, x) \tag{4.144}$$

- The force of the Tectorial membrane, F_{5_a}, is equal to the fluid pressure per unit area applied by the Scala Vestibula at their interface:

$$F_{5_a}(t, x) = \frac{\Psi_4(t, 0, y)}{A_{5_a}} \tag{4.145}$$

assuming the area of contact remains constant.

6. Scala Tympani and Basilar Membrane:

- The momentum of the Scala Tympani fluid, Θ_6, is equal to the momentum of the Basilar membrane at their interface:

$$\Theta_6(t, x, L_y) = \Pi_{5_b}(t, x) \tag{4.146}$$

- The force of the Basilar membrane, F_{5_b}, is equal to the fluid pressure per unit area applied by the Scala Tympani at their interface:

$$F_{5_b}(t, x) = \frac{\Psi_6(t, L_x, y)}{A_{5_b}} \tag{4.147}$$

  assuming the area of contact remains constant.

7. Helicotrema

- The fluid momentum and pressure of the Scala Vestibula and Scala Tympani are equal at the helicotrema.

$$\Theta_4(t, L_x, 0) = \Theta_6(t, L_x, L_y) \tag{4.148}$$

$$\Psi_4(t, L_x, 0) = \Psi_6(t, L_x, L_y) \tag{4.149}$$

4.5.1 Integrated Port Hamiltonian outer, middle and inner ear results

To display the full range of actual values, the graph (Refer to figure 4.70) is plotted on a logarithmic scale as opposed to a linear scale. As frequency is varied from 0 kHz to 1000 kHZ, three peaks are observed. These peaks occur at around 1.3 kHz,3 kHz and 4kHz respectively. The frequency response curve indicates how an individual's ability to hear varies with an increase in noise intensity and frequency. The distinctive regions appear on the frequency response curve. These regions correspond to the normal, mild, moderate, severe and profound hearing loss. The integrated Port Hamiltonian model of the human ear reported in this study provides a computational tool to predict the outer, middle and inner ear functions for assessment of ONIHL. Compared to other models published in the literature, this model has unique features including an accurate anatomic structure of the middle ear. This model is capable of predicting the travelling wave pattern along the basilar membrane.

4.6 Conclusion

A comprehensive integrated Port-Hamiltonian model of the outer, middle and inner ear has been presented. This model is based mainly based on the Dirac structure. The

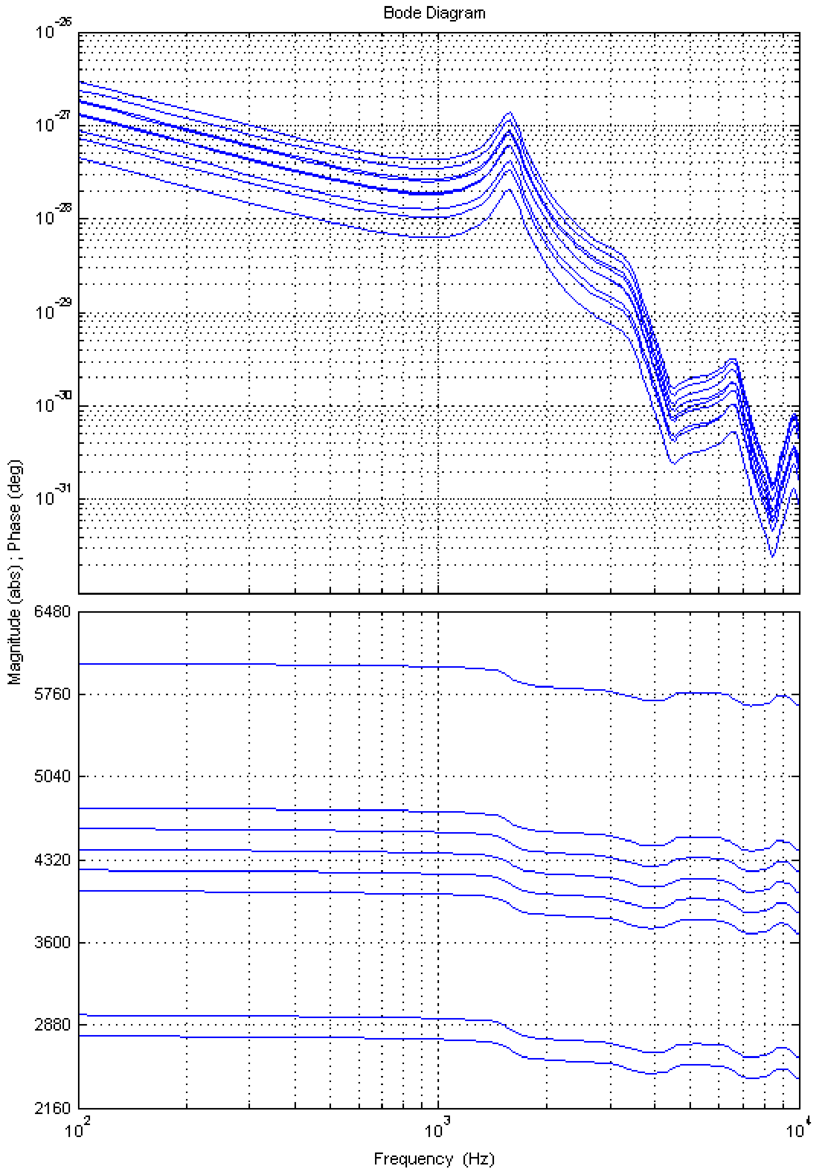

Figure 4.20: Complete model frequency response

assumptions taken to simplify the system are also provided. A detailed explanations of the system discretization and coupling is also given. In chapter 5, the model will be used as a plant in the noise policy management model.

Chapter 5

Noise policy management model

5.1 Chapter overview

The noise management model is developed by firstly considering the risk management matrix which is mainly used in the military to rank tasks in order of priority. The risk management matrix is converted to a noise management matrix and finally a feedback based policy management model is developed. The static model has statistical equations that represents the ear. The dynamic model uses the Port-Hamiltonian model of the ear developed in chapter 4 of this research work. Both the static model using ISO:1999 standard and a dynamic model are used in estimation of the hearing threshold shift which may be used as an indicator of ONIHL.

5.2 Background

5.2.1 The matrix

Loud noise is one of the risks an individual is exposed to in the mine. There are numerous ways in which this noise can be monitored and managed. Moroe [5] proposes a noise management matrix to assist administrators in noise identification and management. In order to understand the functioning of a noise management matrix, a risk management matrix is presented.

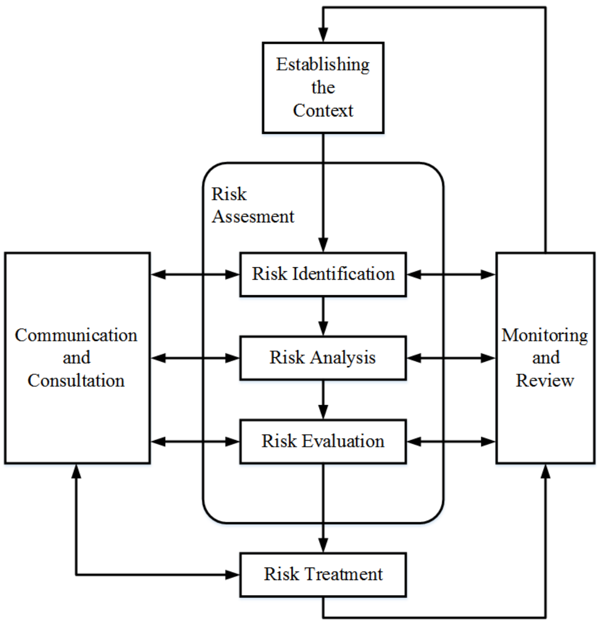

Figure 5.1: Defining noise as a risk [91]

Risk management matrix

Risk is defined [89] as the probability of an event exposing one to danger occurring or not occurring. It may also be defined as the statistical expectation value of unwanted events which may occur or not occur [89]. A risk matrix is used in periods of evaluation to define the intensity of risk by considering the category of an outcome against the category of probability or likelihood [89]. Risk matrices have previously been used by the military in the United States of America (USA) to grade tasks in order of significance and urgency [90]. According to Donoghue [90], risk management has become an important topic and practice being explored by the academics, business community and medical practitioners. Complete risk mitigation is impossible, therefore the dilemma faced is estimating the measure to which risk is allowed and how can it be efficiently managed [90]. Risk management may be defined as the reduction of risk to acceptable levels by society with the guarantee of control and monitoring [90]. Risk assessment entails precise definition of modules in numerical terms which enables one to calculate the chances of wanted and unwanted outcomes. These modules are then averaged by multiplying the chances by the impact effect [90]. The risk management matrix constitutes establishing goals and context, hazard identification, risk assessment and risk control [90].

The noise management matrix

The risk management matrix in the preceding section is used to create a noise management matrix. The noise management matrix has hazard identification in which the environment and the risk are identified. For this case, the environment is the mine and the risk is noise. Establishing goals and context in a mine entails clearly understanding the policies which make up the regulatory requirements, codes of conduct and standards for the mining industry. The perception of risk criteria in the mine and the interpretation is important. Risk assessment in the mine involves evaluating the risk or injury resulting from ONIHL. Determination of source of noise, the consequences and quantifying the chances of unprotected exposure to noise without controls in place [90]. The controls used have to be identified and their effectiveness should be measured in quantifiable amounts. The risk control for the noise management matrix is used as a risk assessment tool. It guides and assists in identifying and implementing control measures that will eliminate or reduce the risks and ensure that adequate monitoring is practised [90]. From this noise management

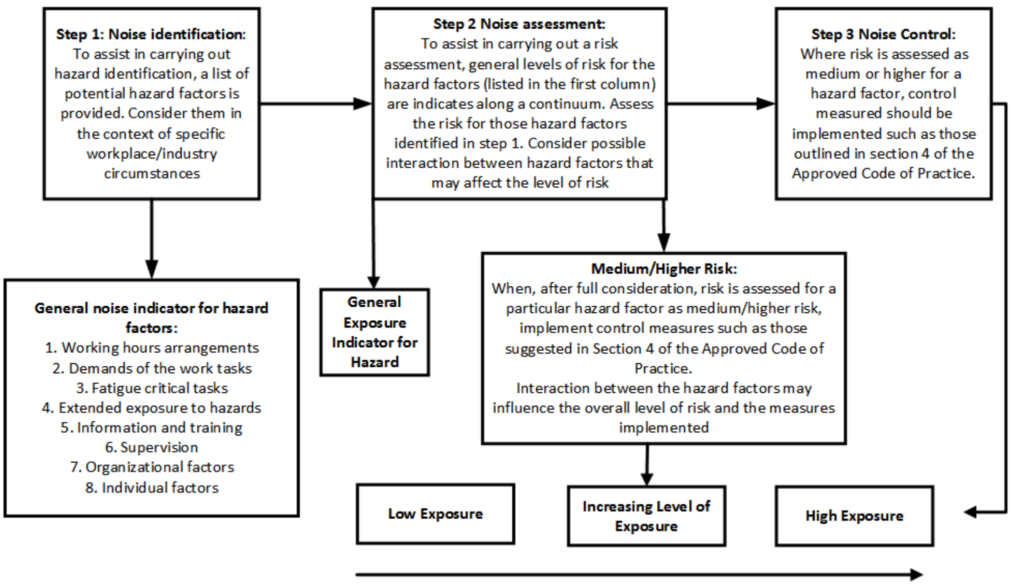

Figure 5.2: Noise management matrix [5].

matrix, a feedback based measurement system is designed.

Current noise measurement systems

The International Standard Organization (ISO) [69] provides statistical equations that allows for predictions of the threshold shift for individuals according to gender, age, exposure level and duration. The data, procedures and prediction method presented in the standard have their basis on predetermined simplifications of experimental data where the daily sound exposure period is not greater than 12 hours. The standard is useful in predicting the threshold shift; however it is limited in its inability to include the policies and intervention that may exist in the mine. Software tools based on the ISO standard that can provide guidance in assigning workers to jobs based on the noise levels to which they will be exposed have also been developed [69].

5.3 System modelling

The static and dynamic models are presented in the later sections of this research report. The static model does not include the human ear. The ISO:1999 standard statistical equations are used in estimation of the threshold shift of an individual. The dynamic model includes a subsystem represented with a Port Hamiltonian model of the human ear and a demonstration of how threshold shift of a mine worker is measured within the feedback loop is demonstrated. For both the static and dynamic models, case scenarios in the mine simulated from open source literature are used to demonstrate how the models works.

5.3.1 Static feedback model

The static feedback model is developed from the noise matrix and risk matrix. It acts as an initial stage to the development of the dynamic feedback model with an actual ear. An engineering control approach is applied resulting in modelling the system as a feedback based system. The practical application of this system would be: To estimate, monitor and provide quantitative information that can aid the miners, mining administrators or policy makers in decision making thus reducing the impact of occupational noise in the mine on the workers. This therefore forms part of an early intervention and management of ONIHL in the mine. The input to these systems is the noise that a person not exposed to occupational noise, experiences in their life time. The occupational noise exposure is the disturbance to the system. The estimated ONIHL is the output. These system may therefore be defined as a feedback based Single Input Single Output (SISO) nonlinear stochastic system. Shown in 5.3 is the static feedback based noise policy management model that is developed from the noise management matrix in 5.2.

Overall system diagram for the static feedback based model for ONIHL monitoring

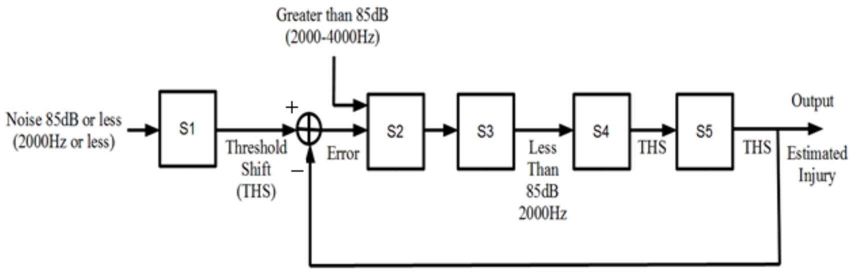

Figure 5.3: Overall system diagram for a feedback based model for ONIHL monitoring.

Threshold shift for an individual not exposed to occupational noise

In 5.3, S1 represents the threshold shift of an individual who has not been exposed to occupational noise. Equation 5.1 is used to determine the effects of age on the hearing ability of this individual. The input to this system is exposure which is less than 85 dB at 2000 Hz. At this level of exposure and frequency in the absence of any other factors, for instance being exposed to a sudden explosion [92], then the only loss that would occur is ONIHL due to presbycusis. The output to this system is the threshold shift. The hearing threshold level associated with age (HTLA) [69] is calculated as shown by equation 5.1 The formulae applicable for the hearing threshold, H, as a function of age Y (years), for the different ranges of the percentage, Q, having hearing threshold level exceeding the value H_Q are [69]: For $Q = 50\%$

$$H_{md,Y} = a(Y - 18)^2 + H_{md;18} \tag{5.1}$$

For $5\% \leq Q < 50\%$

$$H_Q = H_{md,Y} + K_{S_u} \tag{5.2}$$

For $50\% < Q \leq 95\%$

$$H_Q = H_{md,Y} - K_{S_1} \tag{5.3}$$

Where S_u, is the standard deviation of the upper half of the distribution, S_1, is the standard deviation of the lower half of the distribution and $H_{md,18}$, is the median value of the hearing threshold of ontologically normal persons of the same sex aged 18 years, which for practical purposes is taken as zero, as specified in the ISO 389 series. Hence, H_Q is the hearing threshold level associated with age.

The values for the co-efficient a and the multiplier are presented in table A.4 of this research report [69].

$$S_u = b_u + 0.445 H_{md,Y} \tag{5.4}$$

$$S_1 = b_1 + 0.356H_{md,y} \tag{5.5}$$

The values of bu and b1 are listed in table A5 of the appendix A.

Policy and Intervention

S2 is the system that represents the mandatory code of conduct imposed in a mine for both surface and underground employees and anyone on site [93]. S2 is simplified by lumping the policies and the intervention together. Depending on the policy implemented by the mine, occupation noise is attenuated or increased. The system is therefore represented with an equation used by manufacturers in the industry in design of noise reduction protective gear [94]. Shown by equation 5.6.

$$d = -20log_{10}(1 - C) \tag{5.6}$$

where d =decibel drop with the material at the given frequency, and C = coefficient provided by the manufacturer.

Sensors

S3 is the sensing unit of this system. The sensor used in this unit is the NIOSH Sound Level Meter mobile application tool [95]. This sensor is used to measure sound levels in the mine; it outputs the noise intensity and the frequency. The subunits within the subsystem constitute a sound level meter. The transfer function of this unit is used to provide information on the behaviour of the subsystem.

Threshold shift for an individual exposed to occupational noise

S4 is defined by 5.7 and it represents an individual who has been exposed to occupational noise and at the same time affected by presbycusis.

$$H^{'} = H + N - \frac{H \times N}{120} \tag{5.7}$$

$H^{'}$ = Hearing threshold level, in decibels, associated with age and noise (HTLAN), H = Hearing threshold level, expressed in decibels, associated with age (HTLA) and N = Actual or potential noise induced permanent threshold shift (NIPTS), expressed in decibels.

N is calculated using equations:

$$N_{50} = \left[u + vlg(\frac{t}{t_0})\right](L_{EX,8h} - L_0)^2 \tag{5.8}$$

$$N_{50,t<10} = \frac{lg(t+1)}{lg(11)} N_{50,t=10} \tag{5.9}$$

where $L_{ex,8h}$ = is the noise exposure level normalized to a nominal $8h$ working day, expressed in decibels, L_o = is the sound pressure level, defined as a function of frequency, expressed in decibels, below which the effect on hearing is negligible, t = is the exposure duration, expressed in years t_o = is 1 year, u and v are given as a function of frequency.

This formula applies to $L_{ex,8h}$ greater than L_o. In cases where $L_{ex,8h}$ is less than L_o, it shall be deemed equal to L_o so that N_{50} is zero.

Check up

S5 represents the check subsystem. This can be daily, weekly or monthly monitoring of the threshold shifts. For annual and biannual check-ups, an audiogram is used to establish if threshold temporal threshold shift has resulted in permanent threshold shift, thus damage to hearing, resulting in ONIHL. Temporal check-up can be performed on a weekly or monthly basis to establish the integrity of the inner ear hair cells.

5.3.2 Results and discussion

Case scenarios will be used to demonstrate the use of the static feedback noise policy management model. The graphs (Figure 5.4 -5.9) shows 6 mine workers, 3 female and 3 male who started employment at the age of 50, 40 and 25 respectively. They work in a deep level mine with highest noise intensity of 107 dB at a frequency of 4000 HZ. The results show what is to be expected under such exposures if the workers were unmonitored for 15 years. The existing baseline of the mine workers is ignored and hence all of them are assumed to have perfect hearing with no previous exposure to occupational noise prior to employment.

There is a steady increase in the threshold shift of the mine workers over the years. Both male and Female when left unmonitored, implying that they are not wearing

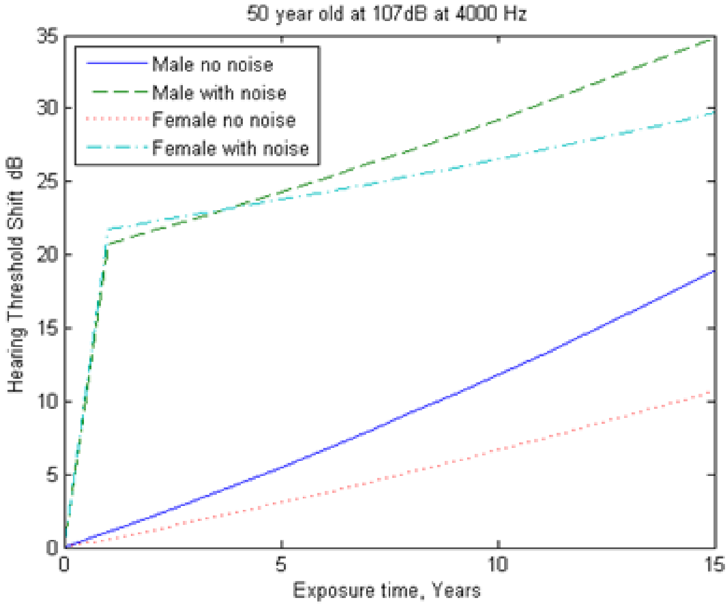

Figure 5.4: Threshold shift of a 50 year old unmonitored mine worker.

any ear protection for 15 years with an exposure of 107 dB at 4000 Hz. The Men experience this shift in 6.25 years while women experience the shift after 7.5 years. On the same graph (Figure 5.4), we observe that for men and women who were only affected by presbycusis, the threshold shift on the 15th year is approximately 15 dB for men and 9dB for women.

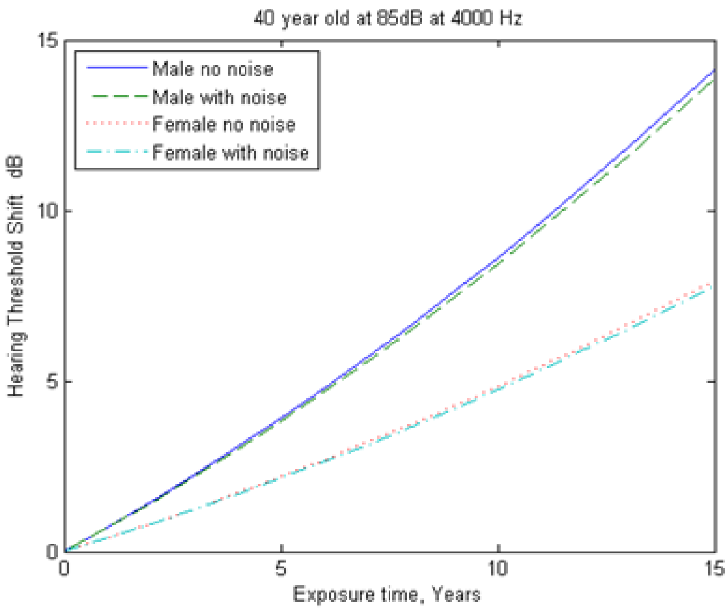

Figure 5.5: Threshold shift monitored 50 year old mine worker.

In this graph (Figure 5.5),the mine workers are given ear protection and they remain monitored to ensure that they wear the ear protection at all times. There is a significant decrease in the threshold shift for the curves for men and women who were exposed to occupational noise and given sufficient protection with monitoring . This shows that monitoring of the mine workers results in preservation of their hearing ability.

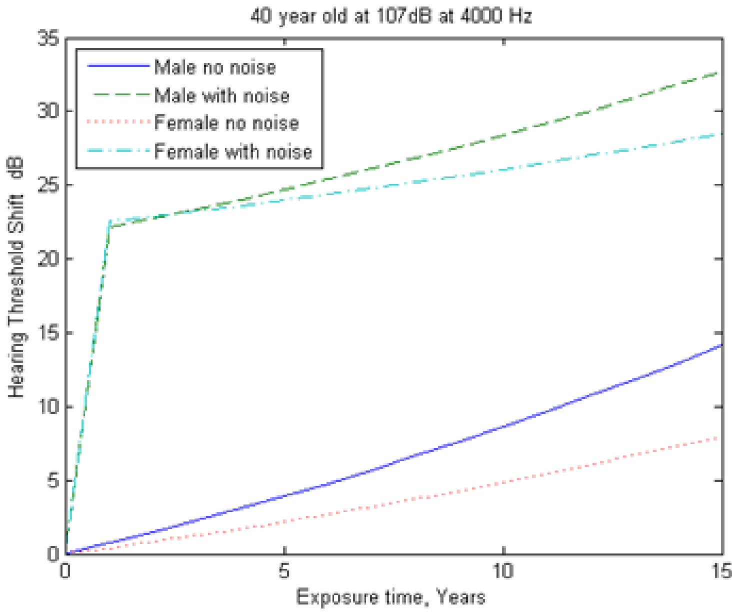

Figure 5.6: Threshold shift of an unmonitored 40 year old mine worker.

For a man and woman who started working at the age of 40, the threshold shift of 25 dB occurs after 7 years for men and after 10 for women. Compared to the graphs of those who were employed at 50, the increase in time before the 25 dB shift occurs is possibly due to the employees being affected less by prebycusis

When monitored, the mine workers have almost the same threshold shift as the male and female who have not been exposed to occupational noise.

The workers who were employed at 25 years old, do experience a threshold shift of 25dB, which occurs approximately on the 12th year of exposure. The delay in the shift is also attributed to the effects of presbycusis not having started to have an effect.

The monitored group is consistent with the results obtained for the 50 and 40 year old where no significant shift is observed.

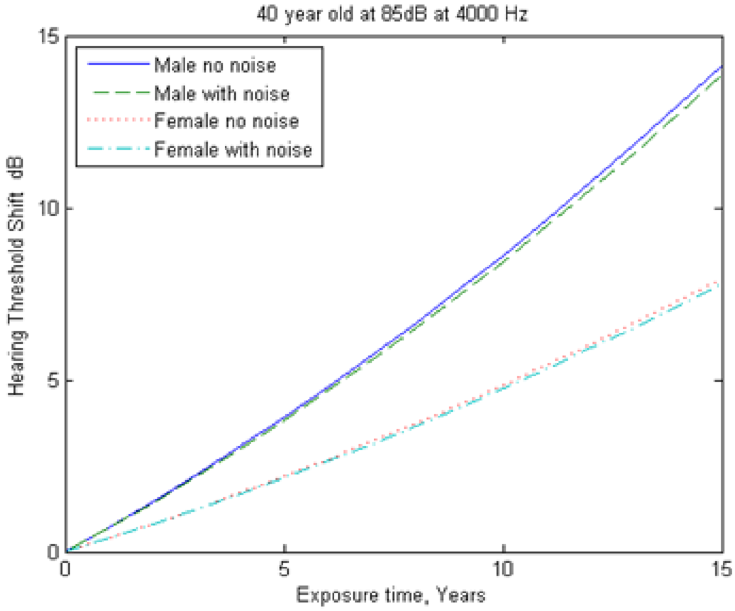

Figure 5.7: Threshold shift of a monitored 40 year old mine worker.

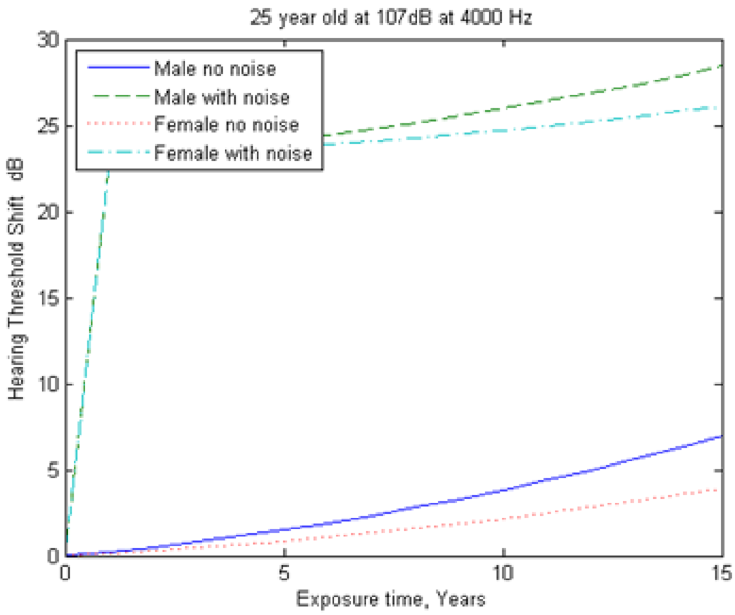

Figure 5.8: Threshold shift unmonitored 25 year old mine worker.

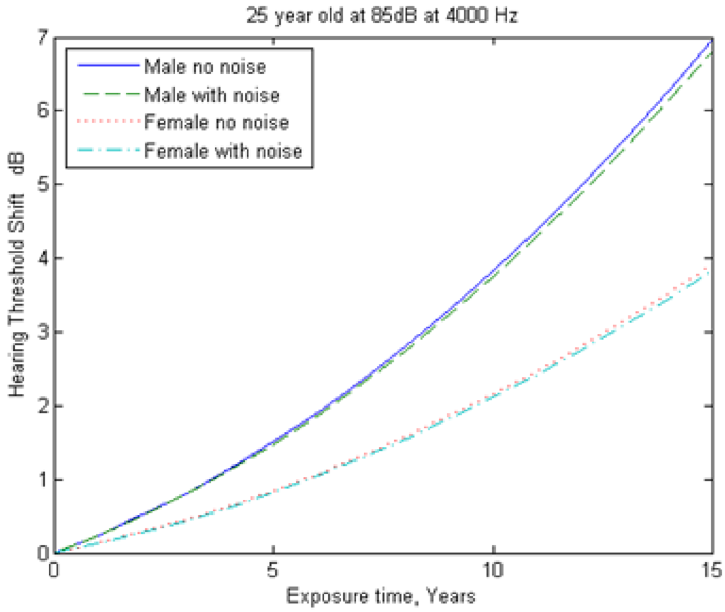

Figure 5.9: Threshold shift monitored 25 year old mine workers.

From the graphs, it is quite evident that if left unmonitored all three mine workers irrespective of their age, in less than 10 years, will have experienced a threshold shift of more than 25 dB from their given base line. The designed system currently offers a predictive model to the mine administrators who should now take measures to monitor the mine workers frequently to ensure that the threshold does not shift with more than 25 dBs, which is one of the MHSC requirements.

All the results presented were consistent with results previously presented by [5]

The presented static model has the following limitations:

- It is static and excludes the dynamic aspects of the system, for instance, it does not include the ear model.
- It does not include controllers.
- It was not validated using real data from a mine.

The dynamic model is presented in section 5.3.3 attempts to address the limitations of the static model by including the dynamic aspects in the system, incorporating controllers, interpreting mining policies as controllers and validating the model using open source data from a mine. The dynamic feedback model presents an example of a noise monitoring model contextualized for drill operators who work in a deep gold

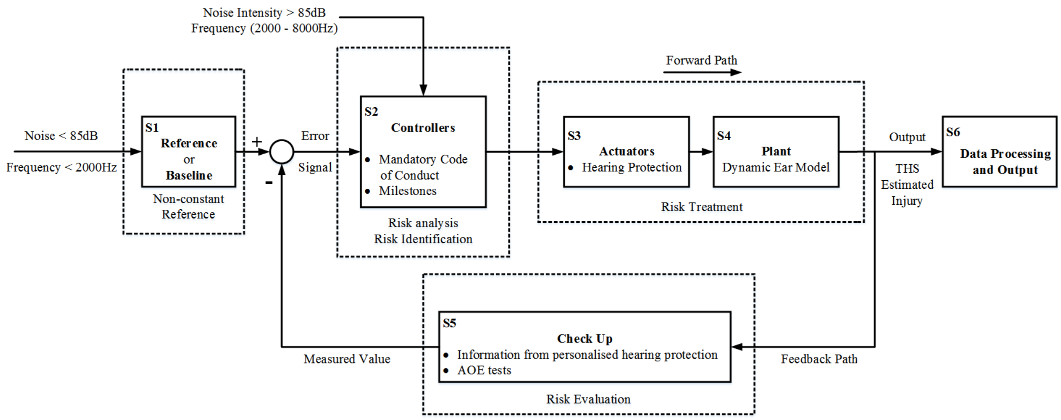

Figure 5.10: Smart automated noise policy monitoring and feedback control system for mine workers

mine in South Africa. This model can be used generically in the mines. It can also be occupational specific to target the most affected career occupation in the mine for instance drillers.

5.3.3 Dynamic Feedback model

The static model is refined by inclusion of dynamic aspects for example the Port Hamiltonian model of the ear. Figure 5.10 shows a smart automated noise policy monitoring feedback control system for mine workers. A mining employee represented by (S4) working in an environment with noise intensity equal or greater than 85 dB is expected to adhere to the mandatory code of conduct, summed up by the noise policy in the mines as shown in (S2). One of the policies requires the employees to wear hearing protection (S3). The employee undergoes a periodic hearing check up (S5) conducted annually or biannually. For this system, it is proposed that the check up should be done at a much shorter interval, for instance daily. The information obtained from the check up is compared to the base line or reference (S1). If the employee has experienced significant threshold shift from the baseline, then, the mining administrators should apply other policies and the whole process repeats again. For effective communication to happen between the employees and the administrators, the information on the current state of hearing (daily threshold shift), is sent to the administrator via a data processing unit (S6)

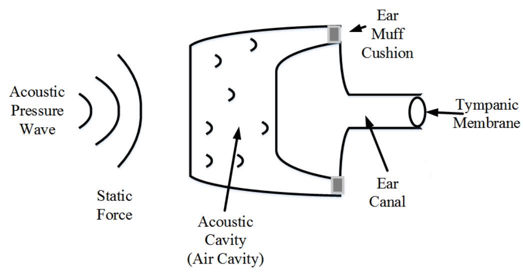

Figure 5.11: The ear muff being used as an attenuator

5.3.4 Sub systems description

S1: Reference or baseline

This unit represents an individual who has not been exposed to occupational noise. However, they are still affected by presbycusis represented by equation 5.1 . The input to this system is noise at less than 85 decibels. The reference may be termed as a moving reference since each year the individual grows older. The reference may also be viewed as a Standard Threshold Shift (STS) of a mine worker when they are first employed in that particular mining company [96].

S2: Controllers

Several controllers from basic to intelligent controllers may be used in the system and when policy is changed, it is interpreted as change of a controller. Basic controllers that may be used is the Proportional Integral Derivative controller (PID). Optimal and robust controller for example LQR and $H\infty$ may also be used. Intelligent controllers for instance fuzzy logic and Artificial Neural Networks may be used to effectively demonstrate how the correct choice of policy results in preservation of hearing of a mine worker [96].

S3: Actuators

Hearing protection worn by the mine worker is interpreted as the attenuator. This hearing protection could be the ear muffs or ear plugs. In the context of this research, the ear muffs will be used as shown in figure 5.11 [96].

To further understand the actuator subsystem as represented by the ear muff in figure 5.11, details of the materials that the ear muff is made up of are provided.

Ear muff cup (Protector Shell): Solid material (Density $1200kgm^{-3}$, $1500ms^{-2}$ sound velocity and $2mm$ thickness)

Air cavity: Homogeneous medium ($1.21kgm^{-3}$ density, $34.3m\ s$ sound velocity.

Attenuation of hearing protection is represented by the following equation 5.10 [1], [93]:

$$A_{tt} = 20Log\left(\frac{P_{ff}}{P_w}\right), \tag{5.10}$$

where A_{tt} is the attenuation (Measured in decibels), P_{ff} is the sound pressure in free field without the muff and P_w is an ear muff.

S4: Plant

This is represented by a dynamic ear model. It could be probabilistic or a dynamic ear model for example: Electrical circuit model, non-lumped parameter model and finite element ear models. For this research, it is represented by an intergrated Port-Hamiltonian model of the human outer, middle and inner ear.

S5: Check up

Most mine workers are checked annually or biannually. With this system the state of hearing of mine work is done per second and the information sent to a data processing and output unit. This output information is used to monitor the state of hearing of a mine worker [97], [98].

S6: Data processing and Output system

The input to this unit is the mine workers' currently measured threshold shift. S6 is the output unit for the whole system. It is a measure of estimated hearing injury or how far an individual has shifted from the baseline or reference. This output measurement is further processed using the Internet Of things (IoT) to facilitate

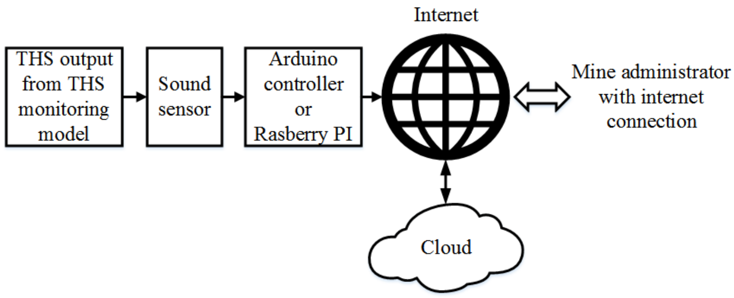

Figure 5.12: Noise monitoring data processing unit

effective communication between the mine workers and the mine administrators. This is the unit that obtains the output from the main monitoring system and sends the information to the administrator. All the data from the output is stored for future reference and analysis. The system then groups the information for the mine administrator based on the level of importance. For a miner worker experiencing a significant THS for an extended period of time, for instance a week, the next step is taken to ensure their hearing is preserved. This subsystem uses the IoT to ensure immediate and rapid response to significant hearing threshold shifts. If a team of mine workers is collectively being affected, an early intervention can be implemented to ensure no further loss of hearing occurs, therefore illustrating the necessity of IoT in the systems. The output information is constantly compared to the reference. This ensures that the mine workers state of hearing is tracking the reference or the baseline. Previously developed data processing and output system similar to the one presented include [99], [100].

5.4 Results and discussion

Illustration of how the model works

A case scenario is used to illustrate how the model works. Consider three subjects employed by a deep level mine as drillers. They are approximately the same age, work under the same conditions of frequency and are exposed to the same noise intensity. They work for eight hours a day. They have similar Standard Threshold shift approximated to be the same. All subjects are provided with hearing protection at the beginning of their career. Figure 5.15 shows how the threshold shifts of the subjects vary over a period of two weeks. Details of a,b,c,d and e are provide in the interpretation of the mining policies using control laws subsection.

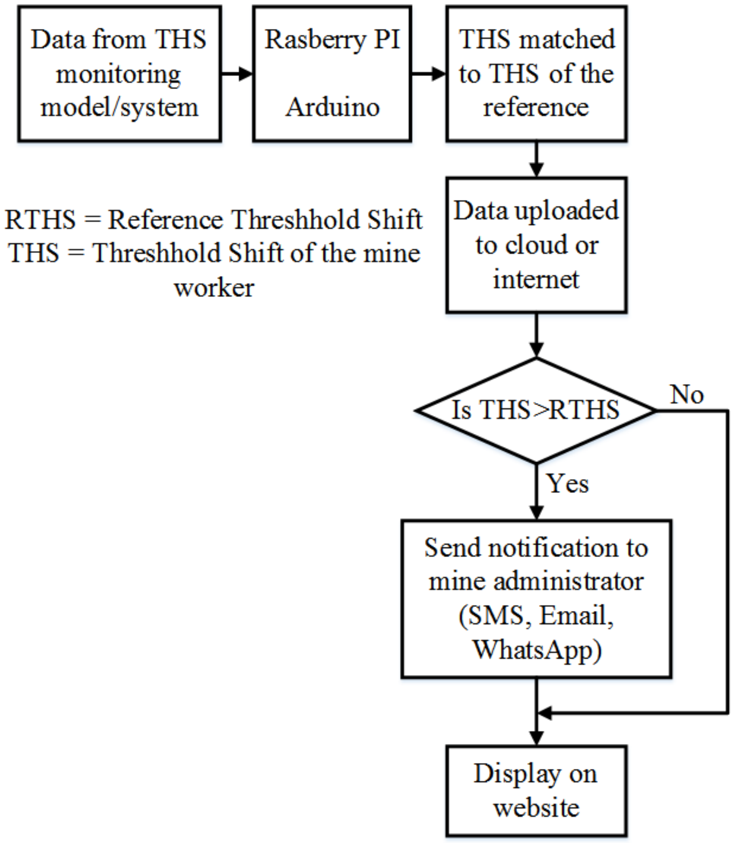

Figure 5.13: Flow diagram showing the flow of information, [99], [100]

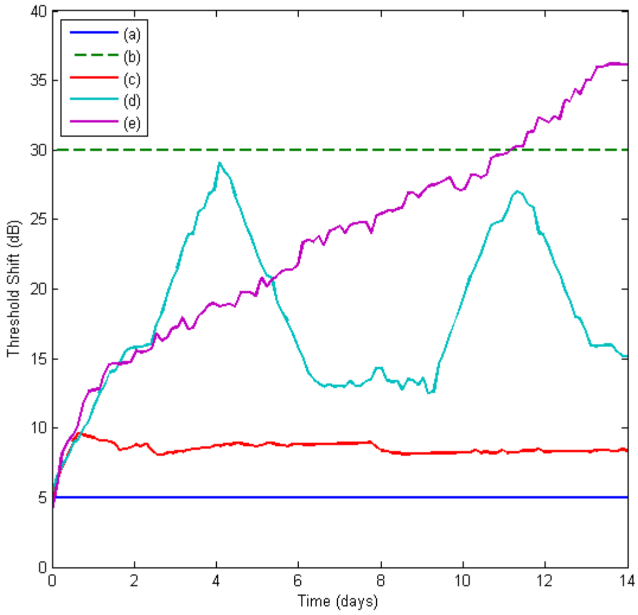

Figure 5.14: Two week monitoring of threshold shift for three mine workers

MSHC expects when the subjects threshold shift is measured and compared to the milestone baseline, there should be no average change of hearing of 10 dB at the speech frequencies [97]. From figure 5.15, subject 1 needs no further hearing management as long as there is continuous adherence to the rules and regulations pertaining to noise policy and wearing of Hearing Protection Devices (HPD). Subject 2 when compared to the milestone baseline, their hearing threshold shifts progressively. It increases and overshoots to above 25 dB, therefore violating the 2014 MHSC milestones targets. This employee has to be called by management to establish if the hearing loss is work related. If it is, then a thorough check up is to be conducted by the medical personnel. The employer also has the opportunity to investigate if the worker's hearing protection is functioning properly and provides sufficient noise attenuation. The hierarchy of controls to limit exposure to significant levels of noise in the work environment is employed [97].

Subject 3, has Significant Threshold shift occurring in two peaks, then experiences a recovery. It is established that the subject's threshold shift is not work related. The employee is to undergo counselling and training to understand the danger of exposure to continuous noise that is equal to or greater than 85 dB without wearing hearing protection or sufficient protection. This is aimed at encouraging the employee to take responsibility for his hearing health.

The three employees are used to demonstrate how the feedback based dynamic model can be used to inform the administrators early on the state of hearing of each employee, therefore resulting in an early intervention. The three employees, had not experienced a permanent threshold shift during the two weeks. Thus, close monitoring plays a role in flagging the issues related to noise induce hearing loss that they were already experiencing. The model allows for an early intervention to be conducted on the employees hence it results in preservation of their hearing while saving the mining company from future law suits [101]. When subjects are working in an environment of noise intensity that is greater than 85 dB, then the mandatory code of practices, agreed milestones from MHSC and STS have to be observed. Constant monitoring of their employees would ensure adherence to set governmental rules and regulations.

Explanation of how the controllers work

From figure 5.15, the mining policies from the mandatory code of conduct and set milestones can be interpreted using a control law. (a) corresponds to the STS,

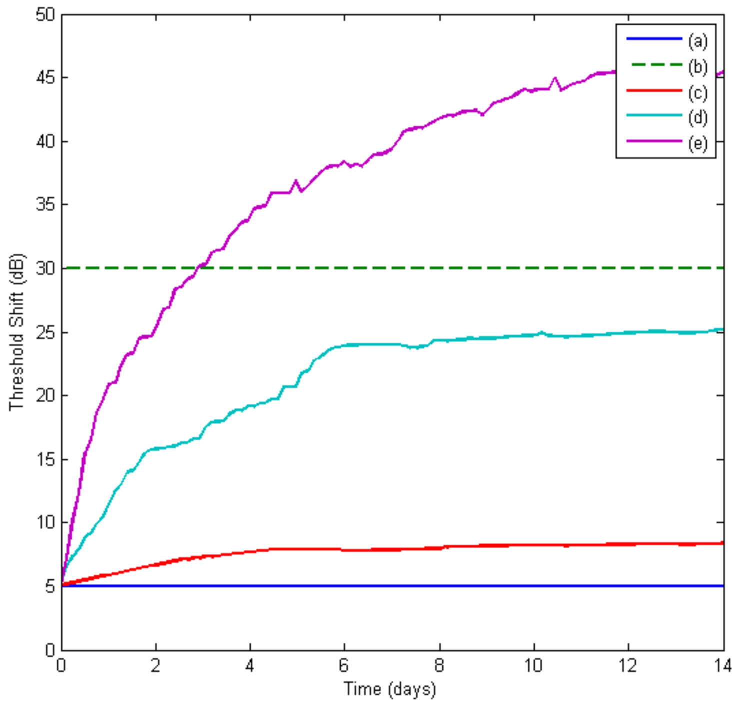

Figure 5.15: Interpretation of different controllers as policy

measured when a mine worker is employed as required by the regulations [97]. For this particular subject, their threshold had shifted by 5 dB when they started to work as drill operators. (b) indicates the 25 dB milestone target for the mine workers. MHCS. The target is to ensure that no worker experiences a threshold shift of more than 25 dB. When intelligent controllers like fuzzy logic are used to control the system, the baseline or the reference is closely tracked. This corresponds to a mine worker who has several noise policies imposed on them to ensure that their threshold shift is not significant. This mine worker wears personalised hearing protection and is constantly monitored to ensure that they are wearing their hearing protection constantly. (c) Is mine worker with sufficient hearing protection and his threshold shift closely follows the baseline (d) shows a mine worker who has basic policy applied of wearing the hearing protection provided by the mine. Their Threshold shift is far off from the base line and an intervention will soon have to be made. This corresponds to the LQR controller. (e) corresponds to a mine worker who is currently not using their hearing protection, hence their threshold shift continues to increase without recovering. This mine worker is likely to experience permanent threshold shift resulting in permanent hearing loss. This corresponds to the PID controller.

5.5 Machine learning techniques for noise policy management model

Machine learning techniques which include clustering and classification of a new employee can be used to further improve the use of data obtained from the noise policy management model. The mine workers can be clustered using K - means to determine their hearing properties. Logistic regression, support vector machines, decision trees and random forest classification techniques can be applied to classify the mine workers. Depending on the classification of a mine worker which is based on the base line and future threshold shift,recommendations to suitable mining tasks would be made by the administrator. This would act as one way of using the model to administer early intervention.

5.6 Conclusion

A novel smart automated noise policy monitoring and feedback control system for mine workers has been presented. The key contribution to this uniqueness is the dynamic feedback noise policy formulation as a feedback controller. A further novelty is a smart processing web based display of results using the IoT paradigm. This model includes a demonstration of how the Port-Hamiltonian model of the human outer, middle and inner ear can be used within a feedback system in measurement of ONIHL.

Chapter 6

Recommendations and conclusions

6.1 Chapter overview

This chapter provides the conclusion to the work done in the development of a Port Hamiltonian model of the outer, middle and inner ear and its applications. It concludes and summarizes the main findings of the study. The summarised findings from this work are provided in section 6.1. The summarised contribution in section 6.2 and the proposed future work is suggested in section 6.3

6.2 Summary of findings

This study confirmed that the Port Hamiltonian method is a valid technique for modelling the human outer, middle and inner ear. It was also shown that threshold shift of a mine worker can be estimated using a feedback system which includes the hearing protection for the mine worker and the policies that govern the allowed frequencies, noise intensity and duration of exposure.

6.3 Summary of contributions

The main contributions to knowledge in this research are:

- Development of a comprehensive integrated Port - Hamiltonian model of the human Outer, middle and inner ear that can be used for estimation and assessment of noise induced hearing loss.

- Unique application of this Port-Hamiltonian model as a noise policy management feedback model.

  The significance of the developed Port - Hamiltonian model is that it may be used for monitoring and providing early intervention for Noise Induced Hearing Loss for the mines.

6.4 Future research

The following are the recommendations to improving this work in future:

6.4.1 Port Hamiltonian model of the human outer, middle and inner ear

- The pinna has the behaviour similar to a reflecting dish and directs sound towards the ear canal. This work can be remodelled to include the effects of the pinna at the speech frequencies
- The ear drum or tympanic membrane can be modelled as concave shape and terminating at the ear canal at approximately 40 degrees slanted angle
- pressure of the sound wave on the tympanic membrane which is boosted by a factor of thirty by the incus, malleus and stapes can be considered
- The cochlea can be modelled as a fluid filled, snail shaped cavern

6.4.2 Noise policy feedback management model

In future, a working prototype will be built and tested in a mine set-up to monitor occupational noise induced hearing loss and provide early intervention.

6.5 Conclusions

A Port Hamiltonian Model of the human outer, middle and inner ear has been presented. The built model is based on a dirac stucture and has the advantage of being capable of producing simulation results in a shorter period of time for complex systems. The integrated human ear model's application is demonstrated by the development of a noise policy management model for mine workers in South Africa. The data obtained from the data processing and output unit of the noise policy model is further processed using machine learning techniques resulting in a unique system that can be used to monitor mine workers in the mine and provide early intervention.

Bibliography

[1] M. M. Metidieri, H. F. S. Rodrigues, F. J. M. B. d. O. Filho, D. P. Ferraz, A. F. d. A. Neto, and S. Torres, "Noise-Induced Hearing Loss (NIHL): literature review with a focus on occupational medicine," *International Archives of Otorhinolaryngology*, vol. 2, no. 17, pp. 208–212, 2013.

[2] S. Strauss, D. W. Swanepoel, P. Becker, Z. Eloff, and J. W. Hall, "Prevalence and degree of noise-induced hearing loss in South African gold miners," *Occupational Health Southern Africa*, vol. 18, no. 6, pp. 20–25, 2012.

[3] D. of Minerals and Energy, "Presidential mine health and safety audit," Available at:http://www.dmr.gov.za/other-reports/summary/130-other-reports/485-presidential-audit-report.html., 2008.

[4] NIOSH, "Occupational noise exposure," NIOSH, Cincinnati, Tech. Rep. 98-126, 06 1998.

[5] N. Moroe, "Occupational noise induced hearing loss in the mining industry: Exploring the benefits of using a noise management matrix in South African mines," Ph.D. dissertation, University of the Witwatersrand, Johannesburg, South Africa, 10 2017.

[6] O. S. Hong, M. J. Kerr, G. L. Poling, and S. Dhar, "Understanding and preventing noise-induced hearing loss," *Disease-a-Month*, vol. 59, no. 4, pp. 110–118, 2013, clinical Issues in Hearing Loss.

[7] W. Babisch, A. Davis, M. Brink, C. C., J. S., and S. S., "Auditory and non-auditory effects of noise on health," *pubmed*, vol. 9925, no. 383, pp. 1325 – 1332, 2014.

[8] K. S. Nanda, "Noise impact assessment and prediction in mines using soft computing techniques," Ph.D. dissertation, National Institute of Technology Rourkela, Odisha, India, 07 2012.

[9] C. O. M. O. South Africa Intergrated Annual Review, "Stakeholder engagement and communication," http://chamberofmines.org.za/reports/2016/, 2016.

[10] A. L. Edwards, "Noise-induced hearing loss: Prevalence, degree and impairment criteria in south african gold miners," Ph.D. dissertation, University of Pretoria, Pretoria, South Africa, 2012.

[11] B. Witt, "Dispelling hearing protection myths," https://ohsonline.com/articles/2012/10/01/dispelling-hearing-protection-myths.aspx., 2012.

[12] S. G. Kujawa and M. C. Liberman, "Adding insult to injury: Cochlear nerve degeneration after 'temporary' noise-induced hearing loss," *The Journal of neuroscience: the official journal of the Society for Neuroscience*, vol. 29, no. 45, pp. 14 077–14 085, 2009.

[13] A. H. Suter and A. Suter, "Engineering controls for occupational noise exposure: The best way to save hearing," *Sound and Vibration*, no. 45, pp. 24–31, 01 2012.

[14] P. Sun, J. Qin, and K. Campbell, "Fatigue modeling via mammalian auditory system for prediction of noise induced hearing loss," *Computational and Mathematical Methods in Medicine*, vol. 2015, p. 13, 2015.

[15] A. De Paolis, M. Bikson, J. T. Nelson, J. A. De Ru, M. Packer, and L. Cardoso, "Analytical and numerical modeling of the hearing system: Advances towards the assessment of hearing damage," *Hearing Research*, vol. 349, pp. 111 – 128, 2017, noise in the Military.

[16] R. Z. Gan, B. P. Reeves, and X. Wang, "Modelling of sound transmission from ear canal to cochlea," *Annals of Biomedical Engineering*, vol. 35, pp. 2180–2195, 2007.

[17] T. Thejane, "A comprehensive electrical model of the human auditory periphery for otoacoustic emissions study," Ph.D. dissertation, University of Johannesburg, 2013.

[18] W. R. Zemlin, *Speech and hearing science: anatomy and physiology*, 2nd ed. publisher Englewood Cliffs, N.J. : Prentice-Hall, 1981.

[19] A. G. Reeves and R. S. Swenson, "Disorders of the nervous system," 2008. [Online]. Available: http://www.dartmouth.edu/dons/part-1/chapter-6.html

[20] A. L. Edwards and D. Kritzinger, *The noise-induced hearing loss milestones: past and future.* Johannesburg, South Africa: CSIR, Centre for Mining Innovation, 2012.

[21] F. Rossing, T. Moore and P. Wheeler, *The Science of Sound.* Boston, USA: Addison Wesley, 2000.

[22] F. Everest, *Master Handbook of Acoustics.* New York, USA: MCGrawHill, 2001.

[23] S. L. Alvord and L. B. Farmer, “Anatomy and orientation of the human external ear,” *Journal of the American Academy of Audiology*, no. 6, pp. 383–390, 12 I997.

[24] F. Xue, G. Fang, P. Yang, E. I. Zhao, S. E. Brauth, and Y. Tang, “The biological significance of acoustic stimuli determines ear preference in the music frog,” *Journal of Experimental Biology*, vol. 218, no. 5, pp. 740–747, 2015.

[25] S. E. Voss, J. J. Rosowski, S. N. Merchant, and W. T. Peake, “Acoustic responses of the human middle ear,” *Hearing Research*, vol. 150, no. 1, pp. 43 – 69, 2000.

[26] E. G. Ekdale, “Form and function of the mammalian inner ear,” *Journal of Anatomy*, vol. 228, no. 2, pp. 324–337.

[27] J. K. Moore and F. H. Linthicum Jr., “The human auditory system: A timeline of development,” *International Journal of Audiology*, vol. 46, no. 9, pp. 460–478, 2007.

[28] R. T. Sataloff and J. Sataloff, *Occupational Hearing Loss*, 3rd ed. Boca Raton, FL: CRCPress: Taylor and Francis Group, 2006.

[29] A. C. of Occupational and E. M. (ACOEM), “Occupational noise-induced hearing loss: Acoem task force on occupational hearing loss,” *Journal of Occupational and Environmental Medicine*, vol. 54, no. 1, pp. 106–108, 2012.

[30] J. J. Walker, M. C. Cleaveland, L. J. Davis, and S. S. Seales, “Audiometry screening and interpretation,” *American Family Physician*, vol. 87, no. 1, pp. 41–47, 2013.

[31] W. J. Song, *Study on Human Auditory System Models and Risk Assessment of Noise Induced Hearing Loss.* Cincinnati, Ohio, USA: University of Cincinnati, 2010.

[32] S. J. Daniels, "Finite element model of the human eardrum and middle ear," Ph.D. dissertation, Mc Gill University, 2002.

[33] H. Wada and T. Kobayashi, "Dynamical behavior of middle ear: Theoretical study corresponding to measurement results obtained by a newly developed apparatus," *The Journal of the Acoustical Society of America*, vol. 87, pp. 1–10, 1990.

[34] J. Zwislocki, "Some impedance measurements on normal and pathological ears," *The Journal of the Acoustical Society of America,*, vol. 29, p. 1312, 1957.

[35] Y. Onchi, "Mechanism of the middle ear," *The Journal of the Acoustical Society of America,*, vol. 33, pp. 794–805, 1961.

[36] F. M. Wiener and D. A. Ross, "The pressure distribution in the auditory canal in a progressive sound field," *The Journal of the Acoustical Society of America*, vol. 33, pp. 794–805, 1946.

[37] S. M. Khanna and M. R. Stinson, "Specification of the acoustical input to the ear at high frequencies," *The Journal of the Acoustical Society of America,*, vol. 77, pp. 794–805, 1985.

[38] M. Hiipaka, M. Tikander, and M. Karjalainen, "Modeling of external ear acoustics for insert headphone usage," 2009, presented at the 126th Convention 2009 May 710 Munich, Germany.

[39] C. Gigure and P. C. Woodland, "A computational model of the auditory periphery for speech and hearing research. i. ascending path," *The Journal of the Acoustical Society of America*, vol. 33, pp. 794–805, 1993.

[40] R. Z. Gan, B. Feng, and Q. Sun, "Three-dimensional finite element modeling of human ear for sound transmission," *Annals of Biomedical Engineering*, vol. 32, pp. 847 – 859, 2004.

[41] M. Naghibolhosseini, "estimation of outer-middle ear transmission using dpoaes and fractional-order modeling of human middle ear," Ph.D. dissertation, The city University of New York, 2015.

[42] K. M. Lim and R. C. Steele, "A three-dimensional nonlinear active cochlear model analyzed by the wkb-numeric method," *Hearing Research*, vol. 170, no. 1, pp. 190 – 205, 2002, special Issue on the 38th Workshop on Inner Ear Biology, and regular research papers.

[43] S. Ramamoorthy, N. V. Deo, and K. Grosh, "mechano-electro-acoustical model for the cochlea: Response to acoustic stimuli," *Annals of Biomedical Engineering*, vol. 121, pp. 2758 – 2773, 2007.

[44] X. Zhang and R. Z. Gan, "Finite element modeling of energy absorbance in normal and disordered human ears," *Hearing Research*, vol. 301, pp. 146 – 155, 2013, mEMRO 2012 Middle-Ear Bridge between Science and Otology.

[45] J. S. Elliott, N. I. Guangjian, R. B. Mace, and B. Lineton, "Wave finite element analysis of the passive cochlea," *The Journal of the Acoustical Society of America*, vol. 133, pp. 1535 – 1545, 2013.

[46] T. Reichenbach and A. J. Hudspeth, "The physics of hearing: fluid mechanics and the active process of the inner ear," *Reports on progress in Physics, Physical society*, vol. 777, p. 076601, 2014.

[47] J. Tonndorf, "Beats in cochlear models," *The Journal of the Acoustical Society of America*, vol. 31, p. 124, 1959.

[48] J. Jang, J. Lee, S. Woo, D. J. Sly, L. J. Campbell, J.-H. Cho, S. J. O'Leary, M.-H. Park, S. Han, J.-W. Choi, J. H. Jang, and H. Choi, "A microelectromechanical system artificial basilar membrane based on a piezoelectric cantilever array and its characterization using an animal model," *Scientific reports*, vol. 5, p. 12447, 2015.

[49] H. Y. Lee, P. D. Raphael, A. Xia, J. Kim, N. Grillet, B. E. Applegate, A. K. E. Bowden, and J. S. Oghalai, "Two-dimensional cochlear micromechanics measured in vivo demonstrate radial tuning within the mouse organ of corti," *Journal of Neuroscience*, vol. 36, pp. 8160–8173, 08 2016.

[50] M. Kringlebotn, "Network model for the human middle ear," *Scandinavian Audiology*, vol. 17, no. 2, pp. 75–85, 1988.

[51] X. Zhang and R. Z. Gan, "A comprehensive model of human ear for analysis of implantable hearing devices," *IEEE transactions on Biomedical Engineering*, vol. 58, pp. 3024 – 3027, 2011.

[52] R. Z. Gan, Q. Suna, B. Feng, and M. W. Wood, "Acoustic-structural coupled finite element analysis for sound transmission in human earpressure distributions," *Medical Engineering and Physics*, vol. 28, pp. 3024 – 3027, 2005.

[53] N. Kim, K. Homa, S. Puria, and R. C. Steele, "Bone conduction hearing: Three-dimensional finite element model of the human middle and inner ear," *American Institute of Physics*, vol. 28, pp. 340– 345, 2011.

[54] R. Z. Gan, B. Feng, and Q. Sun, "Three-dimensional finite element modeling of human ear for sound transmission," *Annals of Biomedical Engineering*, vol. 32, no. 6, pp. 847–859, 06 2004.

[55] X. Zhang and Z. R. Gan, "Finite element modeling of energy absorbance in normal and disordered human ears," *Hearing Research*, vol. 301, pp. 146 – 155, 2013, mEMRO 2012 - Middle-Ear Bridge between Science and Otology.

[56] R. Z. Gan, C. Tao, D. Chenkai, and F. Yang, "Finite element modeling of sound transmission with perforations of tympanic membrane," *The Journal of the Acoustical Society of America*, vol. 126, pp. 243–253, 2011.

[57] X. Wang, L. Wang, J. Zhou, and Y. Hu, "Finite element modelling of human auditory periphery including a feed-forward amplification of the cochlea," *Computer Methods in Biomechanics and Biomedical Engineering*, vol. 17, pp. 1096–1102, 2014.

[58] R. Z. Gan, P. B. Reeves, and X. Wang, "Modeling of sound transmission from ear canal to cochlea," *Annals of Biomedical Engineering*, vol. 35, pp. 2180 – 2195, 2007.

[59] S. Shen, Y. Liu, X. Sun, W. Zhao, and Y. Su, "A biomechanical model of the inner ear: Numerical simulation of the caloric test," *Annals of Biomedical Engineering*, vol. 2013, pp. 1–9, 2013.

[60] Y. Yoon, S. Puria, and C. R. Steele, "A cochlear model using the time-averaged lagrangian and the push-pull mechanism in the organ of corti," *Journal of mechanics of materials and structures*, vol. 4, pp. 977–986, 2009.

[61] J. M. Hernandez, "Solution using lagrange equations to the model of cochlear micromechanics," *Journal of mechanics of materials and structures*, vol. 37, pp. 29 –37, 2016.

[62] Y. Onchi, "A study of the mechanism of the middle ear," *The journal of acoustical society of America*, vol. 21, pp. 404 – 410, 1949.

[63] A. van der Schaft, "Port-hamiltonian systems: an introductory survey," no. suppl 2. European Mathematical Society Publishing House (EMS Ph), 2006, pp. 1339–1365.

[64] L. A. Mora, J. I. Yuz, H. Ramirez, and Y. Le Gorrec, "A port-hamiltonian fluid-structure interaction model for the vocal," *IFAC-PapersOnLine*, vol. 51, no. 3, pp. 62 – 67, 2018.

[65] M. Angerer, S. Musić, and S. Hirche, "Port-hamiltonian based control for human-robot team interaction," in *2017 IEEE International Conference on Robotics and Automation (ICRA)*, 2017, pp. 2292–2299.

[66] M. Seslija, A. van der Schaft, and J. M. A. Scherpen, "Reaction-diffusion systems in the port-hamiltonian framework," *IFAC Proceedings Volumes*, vol. 43, no. 14, pp. 837 – 842, 2010, 8th IFAC Symposium on Nonlinear Control Systems.

[67] F. Ficuciello, R. Carloni, L. C. Visser, and S. Stramigioli, "Port-hamiltonian modeling for soft-finger manipulation," in *2010 IEEE/RSJ International Conference on Intelligent Robots and Systems*, 2010, pp. 4281–4286.

[68] V. Duindam, "Port-based modeling and control for efficient bipedal walking robots," Ph.D. dissertation, University of Twente, 2006.

[69] ISO, *Acoustics Estimation of noise induced hearing loss*, 3rd ed., ISO, Geneva, 10 2013.

[70] J. Phillips, S. Heyns, and G. Nelson, "Rock drills used in south african mines: a comparative study of noise and vibration levels," *The Annals of occupational hygiene*, vol. 51, pp. 305–10, 05 2007.

[71] J. A. Villegas, "A Port-Hamiltonian approach to distributed parameter systems," Ph.D. dissertation, Department of Applied Mathematics, Faculty EWI, Universiteit Twente, Enschede, Twente, Enschede, Netherlands, 2007.

[72] Y. Le Gorrec, H. Zwart, and B. Maschke, "Dirac structures and boundary control systems associated with skew-symmetric differential operators," *SIAM Journal on Control and Optimization*, vol. 44, no. 5, pp. 1864–1892, 2005.

[73] J. C. Crittenden, R. R. Trussell, D. W. Hand, K. J. Howe, and G. Tchobanoglous, *MWH's Water Treatment: Principles and Design*, 3rd ed. John Wiley and Sons, Inc., 2012.

[74] R. Z. Gan, Q. Sun, F. B., and M. W. Wood, "Acousticstructural coupled finite element analysis for sound transmission in human ear-pressure distributions," *Medical Engineering and Physics*, vol. 28, no. 5, pp. 395–404, 2006.

[75] R. Z. Gan, B. Feng, and Q. Sun, "Three-dimensional finite element modeling of human ear for sound transmission," *Annals of Biomedical Engineering*, vol. 32, no. 6, pp. 847–859, Jun 2004.

[76] B. Feng and R. Z. Gan, “Lumped parametric model of the human ear for sound transmission,” *Biomechanics and Modeling in Mechanobiology*, vol. 3, no. 1, pp. 33–47, Sep 2004.

[77] M. Furst, “Cochlear model for hearing loss,” in *Update On Hearing Loss*, F. Bahmad Jr., Ed. Rijeka: IntechOpen, 2015, ch. 1.

[78] A. Cohen and M. Furst, “Integration of Outer Hair Cell activity in a one-dimensional Cochlear model,” *The Journal of the Acoustical Society of America*, vol. 115, no. 5, pp. 2185–2192, 2004.

[79] E. Goll and E. Dalhoff, “Modeling the eardrum as a string with distributed force,” *Journal of the Acoustical Society of America*, vol. 130, pp. 1452–1462, September 2011.

[80] G. Ni, L. Sun, and S. J. Elliott, “A linearly tapered box model of the cochlea,” *The Journal of the Acoustical Society of America*, vol. 141, no. 3, pp. 1793–1803, 2017.

[81] T. Reichenbach and A. J. Hudspeth, “The physics of hearing: fluid mechanics and the active process of the inner ear,” *Reports on Progress in Physics*, vol. 77, no. 7, p. 076601, jul 2014.

[82] E. Edom, D. Obrist, and L. Kleiser, “Steady streaming in a two-dimensional box model of a passive cochlea,” *Journal of Fluid Mechanics*, vol. 753, pp. 254–278, 2014.

[83] R. P. Beyer, “A computational model of the cochlea using the immersed boundary method,” *Journal of Computational Physics*, vol. 98, no. 1, pp. 145–162, 1992.

[84] L. D. Landau and E. M. Lidshitz, *Fluid Mechanics*, 2nd ed. Oxford, England: Pergamon Press, 1987.

[85] A. Inselberg and R. S. Chadwick, “Mathematical model of the Cochlea I: Formulation and solution,” *SIAM Journal on Applied Mathematics*, vol. 30, no. 1, pp. 149–163, 1976.

[86] Y.-W. Liu and S. T. Neely, “Distortion product emissions from a cochlear model with nonlinear mechanoelectrical transduction in outer hair cells,” *Journal of the Acoustical Society of America*, vol. 127, pp. 2420–2432, April 2010.

[87] V. Trenchant, Y. Fares, H. Ramirez, Y. Le Gorrec, and M. Ouisse, “A port-hamiltonian formulation of a 2d boundary controlled acoustic system,” *IFAC-PapersOnLine*, vol. 48, no. 13, p. 235240, 2015.

[88] F. L. Cardoso-Ribeiro, D. Matignon, , and V. Pommier-Budinger, "Modeling of a fluid-structure coupled system using Port-Hamiltonian formulation," *IFAC-PapersOnLine*, vol. 48, no. 13, pp. 217–222, 2015.

[89] M. Elmontsri, "Review of the strengths and weaknesses of risk matrices," *Journal of Risk Analysis and Crisis Response*, vol. 4, no. 1, pp. 49–57, 2014.

[90] A. M. Donoghue, "The design of hazard risk assessment matrices for ranking occupational health risks and their application in mining and minerals processing," *Occupational Medicine*, vol. 51, no. 2, pp. 118–123, 2001.

[91] F. M. Moroe, K. K. Shangase, M. C. I. Madahana, and N. O. T. C, "Feedback based model in action," *South African Journal of Communication Disorders*, vol. 130, pp. 1–25, September 2019.

[92] D. W. Robinson and W. Burns, *Hearing and Noise in Industry*, 1st ed. Belfast: crown, 1970, no. 101-117.

[93] P. W. Alberti, "The anatomy and physiology of the ear and hearing," in *Occupational exposure to noise: Evaluation, exposure and control*, Geneva, Switzerland, 07 1995, pp. 53–62.

[94] J. Benesty, J. Chen, and Y. Huang, "On the importance of the pearson correlation coefficient in noise reduction," *IEEE Transactions on Audio, Speech, and Language Processing*, vol. 16, no. 4, pp. 757–765, 2008.

[95] NIOSH, *Noise and hearing loss prevention*, 1st ed., NIOSH, Atlanta, G A, USA, 08 2017.

[96] F. M. Moroe, K. K. Shangase, M. C. I. Madahana, and N. O. T. C, "A proposed preliminary model for use to monitor hearing conservation programmes in the mining sector in south africa," *Journal of the Southern African Institute of Mining and Metallurgy*, vol. 130, pp. 1–25, January 2019.

[97] Department of Mineral resources, "Mine health and safety inspectorate guidance notes for the implementation of standard threshold shift in the medical surveillance of noise induced hearing loss," South Africa Department of Minerals and resources, Johannesburg, Tech. Rep. 1, 09 2016.

[98] Mine Health and Safety Inspectorate, "Guideline for the compilation of a mandatory code of practice for an occupational health programme for noise," South Africa Department of Minerals and resources, Johannesburg, Tech. Rep. 1, 09 2003.

[99] L. Ezhilarasi, K. Sripriya, A. Suganya, and K. Vinodhini, "A system for monitoring air and sound pollution using arduino controller with iot technology," *International Research Journal in Advanced Engineering and Technology,*, vol. 3, pp. 1781 – 1785, 2017.

[100] I. Mohannad, E. Abdelghafor, B. Sharief, and M. Ahmed, "Internet of things based smart environmental monitoring using the raspberry-pi computer," 10 2015, pp. 159 –164.

[101] A. L. Edwards and D. Kritzinger, *The noise-induced hearing loss milestones: past and future.* Johannesburg, South Africa: CSIR, Centre for Mining Innovation, 2012.

[102] A. J. van der Schaft, *Port-Hamiltonian Systems: Network Modeling and Control of Nonlinear Physical Systems.* Vienna: Springer Vienna, 2004, pp. 127–167.

[103] A. J. van der Schaft and D. Jeltsema, "Port-hamiltonian systems theory: An introductory overview," *Foundations and Trends in Systems and Control*, vol. 1, no. 2-3, pp. 173–378, 2014.

Appendix A

Appendix

A.1 Introduction

This Appendix provides the ethical clearance that grants this research the permission to publish results obtained from the investigation

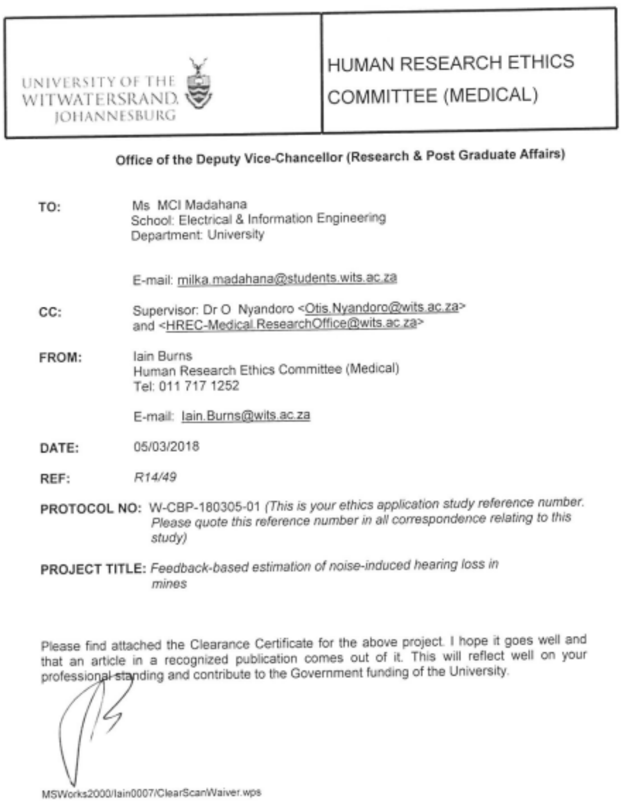

UNIVERSITY OF THE WITWATERSRAND, JOHANNESBURG

HUMAN RESEARCH ETHICS COMMITTEE (MEDICAL)

Office of the Deputy Vice-Chancellor (Research & Post Graduate Affairs)

TO: Ms MCI Madahana
School: Electrical & Information Engineering
Department: University

E-mail: milka.madahana@students.wits.ac.za

CC: Supervisor: Dr O Nyandoro <Otis.Nyandoro@wits.ac.za>
and <HREC-Medical.ResearchOffice@wits.ac.za>

FROM: Iain Burns
Human Research Ethics Committee (Medical)
Tel: 011 717 1252

E-mail: Iain.Burns@wits.ac.za

DATE: 05/03/2018

REF: *R14/49*

PROTOCOL NO: W-CBP-180305-01 *(This is your ethics application study reference number. Please quote this reference number in all correspondence relating to this study)*

PROJECT TITLE: *Feedback-based estimation of noise-induced hearing loss in mines*

Please find attached the Clearance Certificate for the above project. I hope it goes well and that an article in a recognized publication comes out of it. This will reflect well on your professional standing and contribute to the Government funding of the University.

MSWorks2000/Iain0007/ClearScanWaiver.wps

Figure A.1: Ethical clearance certificate.

Table A.1: U, V, L_0, and Y_l

Frequency ($\mathbf{H_z}$)	**U**	**v**	$\mathbf{L_0}$
500	-0.033	0.110	93
1000	-0.020	0.070	89
2000	-0.045	0.066	80
3000	0.012	0.037	77
4000	0.025	0.025	75
6000	0.019	0.024	77

Table A.2: K values

K	**Q**	**K**	**Q**
5	1.645	50	0
10	1.282	95	1.645
15	1.036	90	1.282
20	0.842	85	1.036
25	0.675	80	0.842
30	0.524	75	0.675
35	0.385	70	0.524
40	0.253	65	0.385
45	0.126	60	0.253
		55	0.126

Table A.3: X_u, Y_u, X_l, and Y_l

Frequency	$\mathbf{X_u}$	$\mathbf{Y_u}$	$\mathbf{X_l}$	$\mathbf{Y_l}$
500	0.044	0.016	0.033	0.002
1000	0.022	0.016	0.020	0.000
2000	0.031	0.016	0.016	0.000
3000	0.007	-0.002	0.029	-0.010
4000	0.005	0.009	0.016	-0.002
6000	0.013	0.008	0.028	-0.007

Table A.4: Coefficient of ”a” values

Frequency Hz	**a(dB/year^2) Males**	**a(dB/year^2) Females**
125	0.0030	0.0030
250	0.0030	0.0030
500	0.0035	0.0035
1000	0.0040	0.0040
1500	0.0055	0.0050
2000	0.0070	0.0060
3000	0.155	0.0075
4000	0.0160	0.0090
6000	0.0180	0.0120
8000	0.0220	0.0150

Table A.5: b_u and b_l values

Frequency Hz	**Males B_u**	**Females B_u**	**Males B_l**	**Females B_l**
125	7.23	6.67	5.78	5.34
250	6.67	6.12	5.34	4.89
500	6.12	6.12	4.89	4.89
1000	6.12	6.12	4.89	4.89
1500	6.67	6.67	5.34	5.33
2000	7.23	6.67	5.78	5.34
3000	7.78	7.23	6.23	5.78
4000	8.34	7.78	6.67	6.23
6000	9.45	8.90	7.56	7.12
8000	10.56	10.56	8.45	8.45

A.2 Conclusion

This research has resulted in a total 10 journal papers being published from the presented work. 7 Journals are extracted directly from the presented work and 3 journal papers were published from the related work.

Appendix B

Port-Hamiltonian systems

B.1 Introduction

This appendix provides a summary of the Port-Hamiltonian approach. The Port-Hamiltonian frame work permits for systems to be defined by the interconnection of components from different physical domains [102, 103].

B.2 Importance of the pH system theory

It is always desirable in control to be able to reach at a physical interpretable control law for a given nonlinear problem. The Port-Hamiltonian framework provides controllers that dissipate or even store energy (energy shaping) [102, 103].

B.3 Port-Hamiltonian methodology

The work constitutes of three important theories [102, 103]:

- Port based modelling
- Geometric mechanics
- Systems and control theories

B.3.1 Port-based modelling

Port-Hamiltonian approach provides a unified framework for modelling systems from different physical domains. Energy which is universal can be stored, dissipated or routed through ports in the system. Bond graphs are used to provide a graphical representation of these physical systems [102, 103].

B.3.2 Geometric mechanics

Port-Hamiltonian model is coordinate independent. Hamiltonian systems can be represented without using coordinates. A Dirac structure is the geometric object used represent the interconnection. An interconnected Dirac structure is also a Dirac structure. Using geometric mechanics core attributes of the complex system can be analysed [102, 103].

B.3.3 Systems and control theory

Systems can interact with the environment and are affected/interact with controllers [102, 103].

B.4 Fundamental structure of Port-Hamiltonian systems

B.4.1 Dirac structures

Informal definition of a Dirac structure

Given a Hamiltonian $\mathcal{H}(x) = \mathcal{K}(x) + \mathcal{U}(x)$, where $\mathcal{K}$, $\mathcal{U}$ and x are the kinetic energy, potential energy and state variables, respectively, the flows f and efforts e are defined as [102, 103]

$$f = \dot{x}, \qquad e = \nabla_x \mathcal{H} \tag{B.1}$$

where ∇_x is the gradient of the Hamiltonian along the state x. The power is the product of the flows with their respective efforts, for example. For example, in electric circuits, power, $P = VI$, that is, the product of voltage, V with current I. The state variable (flow) is current and the effort is voltage. These elements are interconnected by the Dirac structure.

Formal definition of a Dirac structure

Definition 6. *The subspace $\mathcal{D} \subset \mathcal{F} \times \mathcal{E}$ is a Dirac structure provided that [103]*

- *for all $(f, e) \in \mathcal{D}$, $\langle e|f \rangle = 0$*
- *$dim\mathcal{D} = dim\mathcal{F}$*

where $\mathcal{F}$ is a linear space and $\mathcal{E} = \mathcal{F}^*$, $\mathcal{F}$ is a linear space that is finite in dimension.

Given matrices F and E each having dimension $n \times n$ so that [103]

$$EF^T + FE^T = 0 \tag{B.2}$$

$$\text{rank}(F|E) = n \tag{B.3}$$

The image and kernel representations of a Dirac structure are [103]

$$\mathcal{D} = \left\{(f, e) \in \mathcal{F} \times \mathcal{E} | \lambda \in \mathbb{R}^n, f - E^T\lambda, e = F^T\lambda = 0\right\} \tag{B.4}$$

and

$$\mathcal{D} = \{(f, e) \in \mathcal{F} \times \mathcal{E} | Ff + Ee = 0\} \tag{B.5}$$

respectively, where $(e, f) = e^T f$.

B.5 Example

This example illustrates the application of the Port-Hamiltonian technique and interconnection of the Dirac structure. Consider the simple LC circuit diagram given in figure B.1[103]. Assuming the inductor and all capacitors are linear, their dynamics are expressed as [103]

$$\dot{\varphi} = -V_L,$$

$$\dot{q}_1 = -I_1 \tag{B.6}$$

and

$$\dot{q}_1 = -I_1 \tag{B.7}$$

where φ is the magnetic-flux, V_L is the voltage across the inductor, q_1 and q_2 are the charges stored and I_1 and I_2 are the currents flowing through capacitors 1 and 2, respectively.

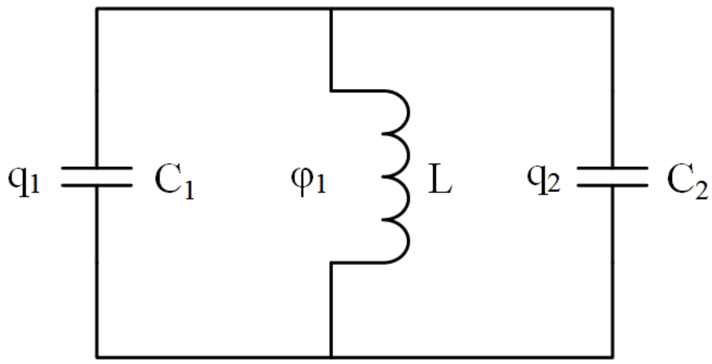

Figure B.1: Simple LC circuit diagram

Applying Kirchhoffs laws (These are the interconnection equations), one obtains [103],

$$\begin{aligned} I_L + I_1 + I_2 &= 0 \\ V_L = V_1 &= V_2 \end{aligned} \tag{B.8}$$

where V_1 and V_2 are the voltages across the capacitors. which can be written in terms of charge and capacitance [103]

$$\begin{aligned} V_1 &= q_1/C_1 \\ V_2 &= q_2/C_2 \end{aligned} \tag{B.9}$$

Since voltage is equal across capacitors in parallel ($V_1 = V_2$) [103]

$$q_1/C_1 = q_2/C_2 \tag{B.10}$$

the state equations are [103]

$$\begin{aligned} \begin{bmatrix} \dot{q}_1 \\ \dot{q}_2 \\ \dot{\varphi} \end{bmatrix} &= \begin{bmatrix} 0 & 0 & 0 \\ 0 & 0 & 1 \\ 0 & -1 & 0 \end{bmatrix} \begin{bmatrix} q_1/C_1 \\ q_2/C_2 \\ \varphi/L \end{bmatrix} + \begin{bmatrix} -1 \\ 1 \\ 0 \end{bmatrix} \lambda \\ 0 &= \begin{bmatrix} -1 & 1 & 0 \end{bmatrix} \begin{bmatrix} q_1/C_1 \\ q_2/C_2 \\ \varphi/L \end{bmatrix} \end{aligned} \tag{B.11}$$

where λ is a Lagrange multiplier.

This system can be expressed in the image representation of the Dirac structure [103]

$$\begin{aligned} \mathcal{D} = \quad & \Big\{ (f,e) \in \mathbb{R}^3 \times \mathbb{R}^3 | f = \begin{bmatrix} f_1 & f_2 & f_3 \end{bmatrix}^T, e = \begin{bmatrix} e_1 & e_2 & e_3 \end{bmatrix}^T, \\ & -f = \begin{bmatrix} 0 & 0 & 0 \\ 0 & 0 & -1 \\ 0 & 1 & 0 \end{bmatrix} e + \begin{bmatrix} 1 \\ -1 \\ 0 \end{bmatrix} \lambda, \quad 0 = \begin{bmatrix} -1 & 1 & 0 \end{bmatrix} e \Big\} \end{aligned} \tag{B.12}$$

or the kernel representation by eliminating the Lagrange multiplier [103]

$$\mathcal{D} = \left\{ (f,e) \in \mathbb{R}^3 \times \mathbb{R}^3 | f = \begin{bmatrix} f_1 & f_2 & f_3 \end{bmatrix}^T, e = \begin{bmatrix} e_1 & e_2 & e_3 \end{bmatrix}^T, \right.$$
$$\left. \begin{bmatrix} 1 & 1 & 0 \\ 0 & 0 & 1 \\ 0 & 0 & 0 \end{bmatrix} f + \begin{bmatrix} 0 & 0 & -1 \\ 0 & 1 & 0 \\ 1 & -1 & 0 \end{bmatrix} e = \begin{bmatrix} 0 \\ 0 \\ 0 \end{bmatrix} \right\} \tag{B.13}$$

B.6 Modelling Port-Hamiltonian systems

This is presented in chapter 4 of this dissertation starting with mathematical preliminaries then followed with a systematic modelling of the outer, middle and inner human ear.